UCLA/Arisaka-GG-S2-Conformal
v23.4 — September 11, 2026 — *Preprint*

Four Observations, One Exponent

Conformality and Scaling Laws, Lévy Flights, Fractality, and $1/f$ Spectra with Two Knees: the Measured Record, Audited

Katsushi Arisaka

Department of Physics and Astronomy, Electrical and Computer Engineering, University of California, Los Angeles, Los Angeles, CA 90095, USA

Contact: arisaka@physics.ucla.edu

Abstract

GG-Theory derives the laws of open systems from a fixed six-dimensional geometry with no adjustable parameter — a program whose record in particle physics and cosmology is stated with its falsifiers named in advance. This paper extends that program to the phenomena that sit closest to life. Its claim, inherited from the Qi-4 pillars of the boundary law and named Qi-CON: any persisting open system, observed through the finite window every real observation has, carries an effective dynamics with one geometric exponent and no intrinsic scale — and that single exponent forces four signatures at once: power-law scaling, heavy-tailed Lévy steps, fractal geometry, and $1/f$ spectra bounded by two knees at derivable places.

The claim is put on trial three ways. First, the record: 245 measurements compiled from four literatures that rarely read one another — allometry, movement ecology, fractal geometry, and $1/f$ noise — every row graded and verified against its primary source, skeptics printed at full size. Second, the arithmetic: on every system where two or more signatures were measured independently, the exponents must satisfy parameter-free lock relations; the cross-consistency audit runs that test across the whole record — seventeen pairs, one identity line, no free parameters. Third, the failure theory: four named modes in which the signatures must degrade, three already exhibited by the record itself.

The verdict is stated at its earned strength: the relations fail nowhere, hold exactly where the physics is exactly understood, hold loosely at honest error bars everywhere else — interesting, and not proof — and the paper closes with the measurements that could kill it, and with why scale-free dynamics is what the geometry of openness offers a world that must explore, adapt, and persist.

Executive Summary

The program, and the extension. GG-Theory is built as a constitution: four axioms, seven postulates, one six-dimensional geometry whose two extra directions are not places but *scale* and *phase* — and no adjustable continuous parameter anywhere. Where it can be checked hardest, the program has put its record in writing with the falsifiers attached: the fine-structure constant from the integer ledger, the twenty-eight Standard Model parameters as observations, the cosmic fractions in powers of $1/\pi$, a derived expansion rate awaiting the standard-siren referee, a dark-matter tone at a named frequency, a new mass scale in collider data already on tape. This paper carries the same constitution toward living systems. The bridge is the boundary law's information pillars: a budget denominating energy, matter, and information in one unit; a selector fixing which branch an observer's record samples; and the third pillar — Qi-CON, the subject of this paper — which says what any selected, persisting branch must look like through a finite window: scale-free, with one exponent, in four signatures, between two knees.

The four records, audited. The evidence base is deliberately the four literatures with the longest skeptical traditions: metabolic and urban scaling, Lévy foraging, fractal geometry, and $1/f$ noise. The compilation — 245 rows, every number traced, graded, and verified against primary sources, twelve corrections printed — shows all four phenomena to be real, windowed, and less clean than their tellings: the founding albatross data retracted, the median claimed fractal spanning barely over a decade, the most famous biological spectral knee unsourced in any primary.

The trial. Three instruments, in rising order of sharpness. The four signatures, audited separately, prove nothing — every signature has rival explanations. The *arithmetic between them* is where the claim lives: one exponent forces closed relations among the step exponent, the fractal dimension, the dynamic exponent, and the spectral slope, so any system with two measured signatures is a parameter-free test. Exactly seventeen such pairs exist — their rarity is itself a finding — and on the identity plot they fail nowhere. Sharpest of all is the failure theory: the derivation forces four named failure modes — window collapse, tempered tails, branch switching, sector domination — and the record already exhibits three of them, in the places the theorems put them.

What is claimed, and what is not. Derived: the generator, the four signatures, the lock relations, the two knees as window edges, the failure modes — every step graded. Open, at full size: the numerical exponent of any named organism, and the hertz of its knees; until the program computes those, its empirical content here is relational — and the whole of it. Not claimed: that every power law in nature is Qi-CON (the climate rows are the lawful counterexample), or that seventeen pairs are proof. The paper closes with six numbered falsifiers, any one of which can put a point far off the line, and with the reading the physics permits: open systems that inherit scale-freedom are equipped for the exploration, adaptation, and persistence life requires.

Keywords: scaling laws; allometry; critical exponents; Lévy flights; heavy tails; fractal dimension; $1/f$ noise; spectral knees; conformal invariance; GDOS; Qi-4; Qi-CON; falsifiability

Four Literatures Keep Measuring the Same Number

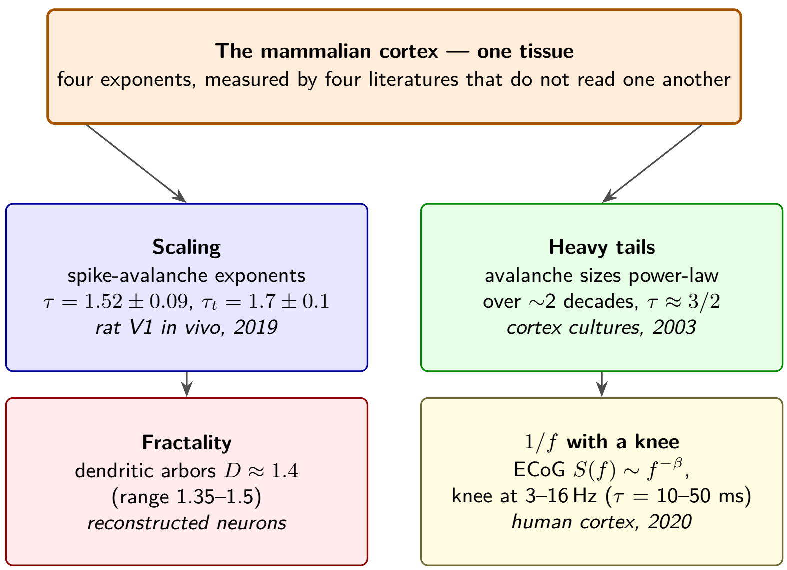

measured on different *preparations, windows, and species — no experiment has measured all four at once.*
Whether the four numbers must *agree is the question this supplement compiles the record to ask.*

The whole supplement in one picture. One tissue — the mammalian cortex — carries all four of the regularities this supplement audits, each measured by a different community in a different decade on a different preparation. Spike avalanches obey power-law scaling with exponents that satisfy a crackling-noise relation; the avalanche sizes themselves are the heavy tail; the neurons' dendritic arbors are fractal; and the cortical field potential carries a $1/f$-type spectrum that bends at a knee corresponding to a 10–50 ms timescale. The four literatures that made these measurements — statistical physics, neuroscience, computational anatomy, electrophysiology — rarely cite one another, and no experiment has measured all four exponents on one preparation. The program's boundary law (GG-A7-Qi4, Part V) claims the four numbers are not independent: one generator exponent fixes them all, so the records must satisfy arithmetic relations across literatures. Parts IV–VII of this supplement audit each record at scale, 245 graded rows in all; Part VIII runs the arithmetic on every system where two or more exponents were independently measured. In full: Figure 1, p. 22.

Overview of Contents

List of Figures

List of Tables

Contents

Part I
Introduction: Scale-Free Phenomena and the Question of Life

What is seen, why it matters for living systems, what a century of modeling has and has not explained, and the claim of this paper

Physics has a peculiar blind spot, and it is shaped like a living thing.

The theories that predict an electron's magnetism to one part in ten trillion have almost nothing quantitative to say about a cell. Not because cells break physical law — nothing does — but because the tools of fundamental physics were built for systems that can be isolated, prepared, and repeated, and a living system is none of these. It is open by construction, historical by nature, and different every time you look. The prevailing accommodation has been a division of labor: physics keeps the exponents and the theorems, biology keeps the mechanisms and the diversity, and the border is patrolled by the word "complexity."

This paper is part of a program that declines the accommodation. The GG-Theory program (Part II) derives the laws of *open* systems from a fixed six-dimensional geometry, and its ambition — stated in the constitutional papers and repeated here without embarrassment — is to bring the science of living systems to the same quantitative standard as particle physics: universality classes instead of case studies, locked exponents instead of fitted curves, and falsifiers named in advance instead of explanations supplied afterward. That ambition would be empty rhetoric if nature had not already left a trail. It has. The trail is the subject of this paper: four families of *scale-free* phenomena that recur across physics, geophysics, and biology — measured for a century, modeled for half of one, and never yet brought under a single quantitative law.

1 Scale-free phenomena in space and time: what is actually seen

Call a phenomenon *scale-free* over a window when its statistics carry no characteristic scale between two cutoffs: doubling the ruler, the step, the patch, or the observation time multiplies the measured quantity by a fixed factor, so that the record is a power law between its edges. Four operationally distinct versions of this statement are measured in nature, stated here in the observer's language before any theory touches them.

In size. Across species spanning more than five decades of body mass, metabolic rate rises as a power of mass — Kleiber's line — and dozens of other biological rates and structures follow their own powers; cities do the same over their populations; earthquakes and river basins do the same over their extents. One number, the exponent, summarizes an entire allometry.

In step. Foraging albatrosses, hunting T cells, migrating metastatic cancer cells, circulating bank notes, and photons in hot vapors take displacement steps whose lengths have no mean scale —

heavy-tailed distributions falling as a power of the step, so that rare long flights carry a finite share of all transport no matter how long the record.

In space. Coastlines, clouds, river networks, bronchial trees, vascular systems, chromatin, and the interstellar medium occupy geometries whose measured content grows as a non-integer power of resolution — fractal dimensions strictly between the topological and embedding integers.

In time. An enormous class of fluctuating signals — semiconductor noise, nerve-membrane potentials, heartbeat intervals, cortical field potentials, river discharge, magnetic-disk-to-galaxy accretion — carries power spectra close to $1/f$ across every decade anyone has measured, a phenomenon old enough that its founding paper predates the transistor.

Each of the four is introduced at full depth, with its complete measured record, in Parts IV–VII; the four landscape figures there (Figures 2–6) are this paper's evidence spine, and a reader who wants to see the phenomena before reading another word of theory should leaf to them now. Two facts about the record deserve to stand in the introduction, because they shape everything downstream. First, *the four families are measured in the same systems*: a single cortex exhibits power-law avalanches, heavy-tailed event sizes, fractal arbors, and a $1/f$ field spectrum (Figure 1); a single marine predator's dive record carries a step exponent, a long-memory exponent, and a spectral slope at once. Second, *every one of the four records is windowed*: real scale-freedom always lives between a lower and an upper cutoff, and — as the audits will show — the cutoffs are usually unmeasured, occasionally measured, and almost never explained.

2 Why this matters for life: emergence, evolution, and the failure of scale-bound description

A physicist can study $1/f$ noise in a resistor for a career without asking what it is *for*. A biologist does not have that luxury, because in living systems the four scale-free signatures sit suspiciously close to function.

The suspicion has three layers, in ascending order of depth. The shallowest is ubiquity: the signatures appear in metabolic networks, foraging tracks, neural avalanches, heartbeat records, gait, gene expression, chromatin folding, vasculature, and bronchial trees — across kingdoms, scales, and substrates that share no mechanism. One level deeper is performance: where the signatures can be perturbed, their loss tracks dysfunction — heartbeat spectra whiten in disease, gait long-memory degrades with age and neurodegeneration, and the migration statistics of a cancer line shift with its invasiveness. Deepest, and least settled, is the evolutionary question: whether scale-freedom is something selection *finds* because it pays — in search efficiency, in adaptability, in robustness — or something open driven matter *does* regardless, which selection then exploits. The four literatures gesture at all three layers; none can compute any of them.

What is missing is not data — the audits below assemble 245 measurements — but a law-level account: something that says *why* these four shapes, *why* together, *why* in windows, and *what arithmetic* their exponents must obey. That is precisely the kind of question particle physics learned to answer in the 1970s, when the renormalization group turned a zoo of critical exponents into computable properties of fixed points. The wager of this paper is that the same maturation is available to the science of living systems — and that the geometry which fixed the Standard Model's constants (Part II) is the instrument.

3 A century of modeling, and three standing limitations

The four literatures have never lacked theories; Parts IV–VII review each record's own, and Part IX examines the cross-cutting frameworks — self-organized criticality, the neural criticality hypothesis, optimal-foraging theory, scale-free network growth, highly optimized tolerance — at full strength. Here it is enough to name the arc and its residue.

The arc: Rubner's surface law (1883) and Kleiber's revision (1932) made biological scaling quantitative; Hurst's Nile studies (1951) and the electronic $1/f$ literature (from 1925) made long memory and scale-free spectra empirical facts; Mandelbrot (1963–1982) unified heavy tails, self-similarity, and fractional dimension into one vocabulary; Wilson's renormalization group (1971) made scale invariance *derivable* at critical points; and the late 1980s and 1990s produced the great mechanistic proposals — Bak's self-organized criticality, West–Brown–Enquist's transport networks, Viswanathan's Lévy foraging optimality, Barabási's preferential attachment — each explaining one signature in one domain with real success.

The residue — the three limitations every one of these frameworks shares, argued in detail in Part IX:

1. **No exponent origins.** Each framework either tunes to a critical point, postulates a growth rule, or optimizes a design; none derives its exponent from anything deeper than the mechanism it assumed, and none explains why *different* mechanisms keep landing on the *same* exponents.

2. **No window theory.** Real records are scale-free between cutoffs. No framework predicts where the cutoffs sit; most treat truncation as a nuisance to be apologized for rather than a quantity to be computed.

3. **No cross-signature law.** The frameworks are single-signature by construction — SOC owns avalanches, foraging theory owns steps, network growth owns degree distributions — and none requires the four signatures of one system to satisfy any relation at all. Yet the mathematics linking them (stable laws, path dimensions, spectral dictionaries) has been standard for decades.

4 Open questions taken as this paper's charge

Five questions, each answerable in principle by measurement, none answered by the existing frameworks:

1. Why do the same four statistical shapes recur across systems that share no mechanism, substrate, or scale? 2. What fixes the numerical value of a given system's exponents — and are the four exponents of one system independent, or four readings of one number? 3. Why is empirical scale-freedom always windowed, and what physics sets the two edges? 4. When the signatures fail — truncated tails, drifting exponents, mimicry by composite processes — do they fail lawfully, in

ways a theory could have predicted? 5. And the question behind the others: is the prevalence of scale-freedom in living matter a coincidence, a selection product, or a theorem about open systems?

5 The claim of this paper, stated once

The GG-Theory answer, developed from Part II onward and audited against the record in between, is a single claim with four consequences. *Any persisting open system, observed through the finite window every real observation has, inherits from the underlying six-dimensional geometry an effective dynamics with no intrinsic scale — one fractional generator with one exponent — and that single exponent forces all four signatures at once: power-law scaling, heavy-tailed steps, fractal support, and a* $1/f$ *band bounded by two knees at derivable places.* The four literatures are, on this claim, four instrument panels wired to one dial.

The claim is constitutional in GG-A7-Qi4 Part V, where it carries the name Qi-CON — the third of the Qi-4 information pillars of the boundary law — and this paper is its extended treatment: the record compiled and audited (Parts III–VIII), the rival accounts examined (Part IX), the exact theory nearest to it disclosed (Part X), the derivation run at full depth with its lock theorem and failure theorem (Parts XI–XII), the laboratory walked through (Part XIII), and the significance and the philosophy priced honestly at the end (Parts XIV–XV).

One constitutional obligation governs the whole. The program's seventh postulate — POS-7, Maximal Falsifiability — requires that every central claim name, in advance, the measurement that would kill it (Arisaka, 2026, A1-Constitution). This paper honors it in kind: the audit of Part VIII is built as a falsification instrument, the derivation closes with six numbered falsifiers, and the sentence *what would refute it* is attached to every worked case. A theory of living systems that cannot be killed by a measurement is not yet science; the one offered here can be, and says where.

6 Outline, and how to read

The paper runs top-down. Part II states the program: the geometry, the boundary law, the engine, the achievements in particle physics and cosmology that earn it a hearing, and the Qi-CON claim in constitutional form. Part III states the four signatures exactly and fixes the rules of the audit — the compilation protocol every number downstream obeys. Parts IV–VII audit the four records at scale; Part VIII runs the cross-consistency arithmetic that no single literature can run. Part IX gives the existing approaches at full strength; Part X draws the line between this program and conformal field theory and AdS/CFT, in a table, in the open. Parts XI and XII are the theory core — the framework at depth, then the derivation of all four signatures from one generator, with the lock theorem, failure theorem, and falsifier list. Part XIII reads nine systems through the theorems; Part XIV states what has been gained and what must still be earned; Part XV closes with the question the whole subject points at — why scale-free nature, and what it has to do with the persistence of living things. Parts XVI–XVIII close the paper: appendices, objections, references.

Three reading paths. *The empiricist*: Parts III–VIII. *The theorist*: Parts II and X–XII. *The life scientist*: Parts VIII, XIII, and the close of Part XV.

Part II
Overview of GG-Theory: Six-Dimensional Geometry Projected on 4D

The constitution, the bulk, the boundary law, the engine, the record in particle physics and cosmology, and the pillar this paper puts on trial

This paper extends a program, and a reader deserves the program whole before being asked to audit its newest claim. This Part is that statement, written for a reader from the life sciences or from statistical physics who has not opened the companion papers: what GG-Theory is, what it has already done where it can be checked hardest — particle physics and cosmology — and how the chain of custody runs from a six-dimensional geometry down to the Qi-CON claim about foraging sharks and cortical noise. Everything here is review; every claim is cited to the companion paper that owns it, and nothing below is needed to *use* the audits of Parts IV–VIII, which stand on the published record alone.

7 What GG-Theory is: a constitution, not a model

GG-Theory is built the way Euclid built geometry: a short list of founding statements, and everything else as theorem. The constitution (Arisaka, 2026, A1-Constitution) fixes four axioms — among them AX-2 GGEP, which *geometrizes* the two structures no local, causal, interacting quantum theory can avoid (a renormalization scale and a gauge phase), and AX-3 OGGEP, which makes the observer's partial view constitutional rather than an afterthought — and seven postulates that discipline everything downstream. Two of the postulates matter constantly in this paper. POS-6 OGN requires that the numbers left over be integers and simple ratios rather than free decimals: the program carries *no adjustable continuous parameter anywhere.* And POS-7 MF — Maximal Falsifiability — requires that every central claim name, in advance, the measurement that would kill it; in the constitution's own words, a filter that lets everything through is not a filter. The posture of the present paper — the audit built as a falsification instrument, the failure theorem, the numbered falsifier list — is POS-7 applied to living systems.

8 The six-dimensional bulk: scale and phase as geometry

The construction (Arisaka, 2026, A2-GG6) adds two directions to the familiar four, and neither is a place. One is *scale* — a dial saying at what energy, or resolution, the world is being examined, carried as the radial coordinate

$$r = \ln\left(\frac{E_{\mathrm{GUT}}}{\mu}\right), \tag{1}$$

so that moving inward along r *is* coarse-graining. The other is a compact *phase* — the angle that electric charge and its relatives already turn. Both are pure numbers carrying no length. On this six-dimensional stage the four forces of the textbook become faces of one geometric object, locked by a single topological identity whose consistency certificate is proved in Arisaka (2026, A3-BI6); six forces follow rather than four, one of them an information force that sets an exchange rate between energy and what a system knows. What the locking identity leaves free is startlingly little: every pure number collapses into five whole numbers — the OGN-5 ledger[1]

$$(M, N, L;\ J, K) \ = \ (1, 3, 5;\ 7, 35), \tag{2}$$

satisfying two independent arithmetic conditions at once and at no other values. Nothing is left to choose except the units.

The full-page plate on the facing page — carried byte-identically by six companion papers and imported here unchanged — draws the whole structure with the scale axis carrying numbers: the bulk as a fiber bundle over the four-dimensional world, the throat tapering as e^{-r}, the lock scale, and the OGN-5 depth at $r = K = 35$.

For this paper one feature of the bulk outranks all others: **scale is a place**. A geometry that stores the renormalization structure in a coordinate hands every projection of itself a scale-covariant kernel — that single fact, run through the projection of the next section, is where the exponent α of Parts XI–XII comes from, and it is the structural idea this program shares with holography (Part X) while claiming none of holography's dualities.

[1] Notation, kept uniform across the cohort: N is the OGN-5 ledger's second entry, and every ledger identity is written with it. $N_c = 3$ is the color triplicity, the three colors of $\mathrm{SU}(3)_C$ — what that entry counts, named where the color reading is the point. $N_g = 3$ is the generation (family) count; it is *not* a ledger entry and is not fixed by the ledger (GG-P2-N3). $N_f = 2N_g = 6$ is the quark-flavor count of a beta function at high scale. Three of these are three and one is six, and they are three different quantities.

A Six-Dimensional Bulk Whose Fifth Dimension Is Scale and Whose Sixth Is Phase

The whole program in one diagram, with the scale axis carrying numbers. The bulk $\mathcal{M}_4 \times I_r \times S^1_\theta$ is a fiber bundle: over every point of the Lorentzian stage sit the two *non-spatial* fibers, scale and phase. AX-2 (GGEP) acts *upward* and builds them; AX-3 (OGGEP) acts *downward*, and registration is the projection that erases (r, θ) — the origin of quantum behavior. The vertical axis is calibrated: $E_{\mathrm{GUT}} = E_{\mathrm{Pl}} e^{-2\pi}$ at $r = 0$, the OGN-5 depth $r = K = 35$ at the infrared boundary, and the lock at $r = 29.41$, which is $K - 2\pi + \ln 2$ exactly.

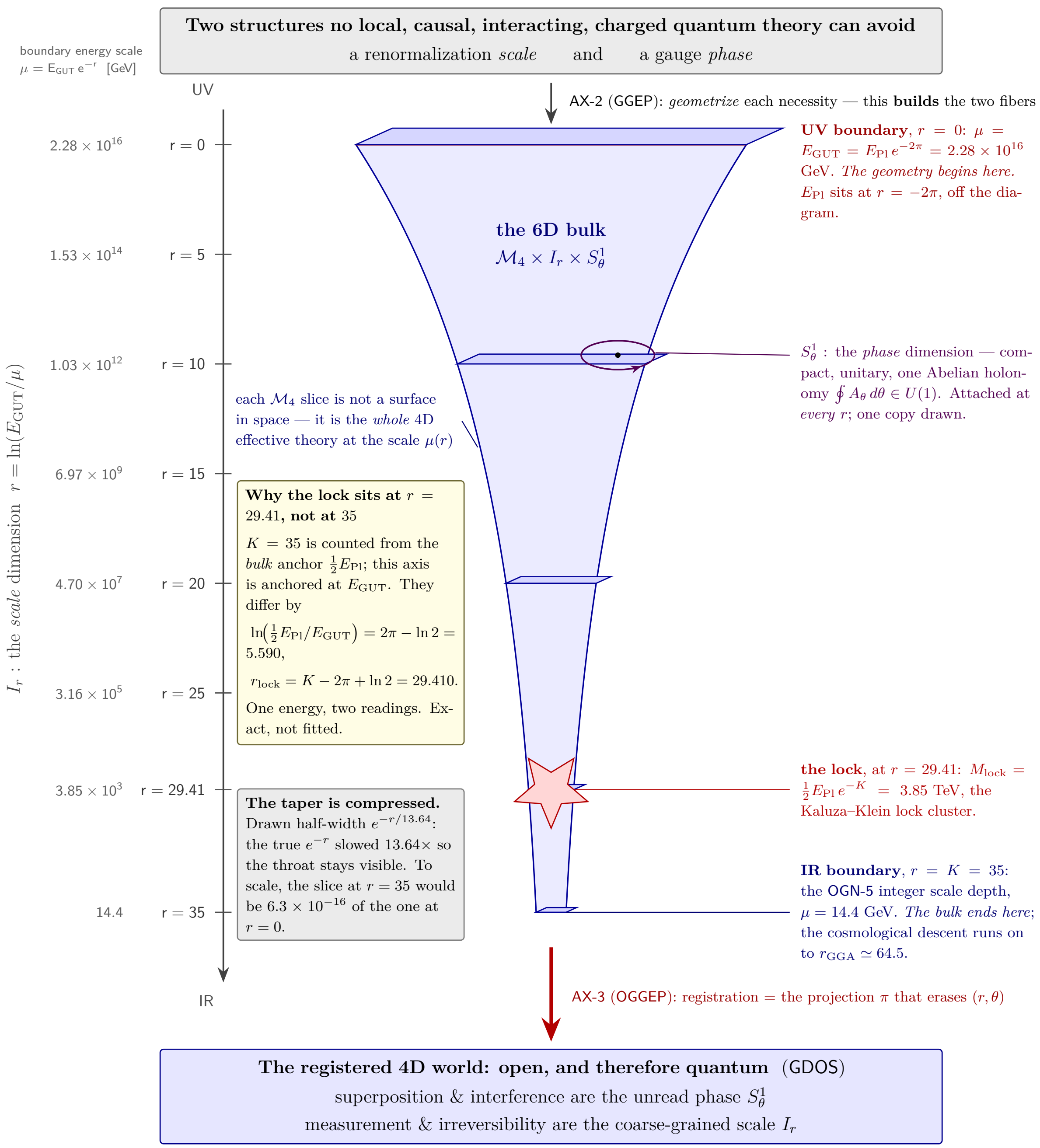

9 GDOS: the boundary law of the partial view

Every system in nature is open; no real system has ever been isolated; the very act of observation already couples observer and observed. Arisaka (2026, A5-GDOS) takes that as the starting point — not a nuisance but the constitutional situation (AX-3) — and derives GDOS, the Geometric Dynamics of Open Systems: the single law any open system must obey, obtained by projecting the six-dimensional bulk through the finite window a real observer has. From this one law, the paper shows, the textbook rules of quantum mechanics, general relativity, and quantum field theory emerge as theorems rather than separate assumptions; the companion Arisaka (2026, A8-QM) carries the quantum-mechanical reading in full, where the century-old measurement problem becomes three precise questions each answered by a theorem, with the Born-rule dynamics closed at the relaxation level as a stated conditional result.

The operational content this paper uses constantly: the projected description of any tracked system is a density $\rho(z, t)$ on the observer's coordinates obeying a continuity law with a four-sector current — gradient, curl, noise, gauge — and the projection retains a *finite range of scales*, bounded by what the instrument resolves and what the system's persistence maintains. Part XI displays the law; here the sentence that matters is structural: *openness and windowedness are not approximations in this program — they are the axioms* — which is why, when the audits of Parts IV–VII keep finding scale-freedom that lives in bounded windows, the finding lands on prepared ground.

10 GRIP and the Gi-4 pillars: the engine and the budget

Arisaka (2026, A6-GRIP) organizes the boundary law from the geometric side into four pillars, of which two act in this paper. The scalar budget $F_{\mathsf{GFF}} = F_{\mathrm{GEP}} + F_{\mathrm{CEP}}$ — an energetic–geometric term plus an information term — is the single ledger all four current sectors descend from. And GRIP, the recursive runtime engine, is what makes *persistence* physical: a selected structure endures by completing cycles of intake, processing, and export against the budget, and a structure that persists maintains an attractor with a slowest relaxation time. That timescale — the attractor time — will reappear in Part XII as the address of the infrared knee, and in the cortex (Part XIII) as a number the neuroscientists have already measured without calling it that.

11 The record where it can be checked hardest: particle physics and cosmology

A program that intends to bring particle-physics standards to biology must first show its standing in particle physics. Table 1 collects the headline results of the companion papers — each row read from the owning paper's own text, each carrying that paper's own grade discipline (derived; conditional on a named step; open). Three rows deserve sentences.

The fine-structure constant emerges in Arisaka (2026, A9-SM) as $\alpha^{-1}(0) = 2^J + N^2 = 128 + 9 = 137$ at first order from the same dyadic-plus-color integers as everything else, matching CODATA's 137.036 after the paper's quantum-dressing completion — one line of the twenty-eight: the Standard

Model's parameters read not as dials but as *observations* that the fixed geometry must return, with the paper stating which it has earned outright, which rest on a single named step, and which remain open. In cosmology (Arisaka, 2026, A10-Cosmos), the present-epoch shape of the universe falls into coupled powers of one number — $\Omega_m = 1/\pi$, $\Omega_\Lambda = 1 - 1/\pi$, $\Omega_b = 1/(2\pi^2)$ — with the tilt and tensor ratio computed, not fitted ($n_s = 0.962$, $r = 0.004$), and the geometry's corridor switch at redshift e^7, the exponential of a single whole number. And the program's exposure to near-term experiment is deliberate: the derived expansion rate $H_0 = 66.6 \pm 0.2$ with gravitational-wave standard sirens named as the referee (Arisaka, 2026, C2-Hubble); the Kaxion dark-matter tone at 1.95 GHz with its paired-tone fingerprint, aimed at by experiments now being built (Arisaka, 2026, C1-Kaxion); the lock cluster at $M_{\text{lock}} = \frac{1}{2} M_{\text{Pl}} e^{-35} \simeq 3.85$ TeV, reachable in collider data already on tape (Arisaka, 2026, P1-KK). Every one of these can fail in public, and each paper names its own executioner — POS-7 in operation, and the standard this paper must now meet on softer ground.

12 The Qi-4 pillars: from geometry toward living organisms

Arisaka (2026, A7-Qi4) builds the information side of the boundary law — the Qi-4 pillars, the program's staircase from projected geometry toward the systems this paper cares about. Qi-QUA denominates the boundary currents in one common unit through the Arisaka equation ($J_E/\mathsf{Q}_\mathsf{B} = J_e = J_B = J_{Qi}$), so that energy, matter, and information flows are one bookkeeping. Qi-EP is the selector: the boundary extremal principle whose three gauges — derived at full length in the companion supplement S1-EP — return the three classical extremal principles of the open-systems literature (least time; the flux–force law with minimum and maximum entropy production as dual readings; the free-energy inference rule), and whose job in any application is to fix *which branch of the dynamics the observer's record samples*. Qi-CON, the third pillar, is the subject of this paper. Qi-HAL, the fourth, carries the inner-hologram construction toward perception and memory, and waits downstream.

The pillar order is load-bearing, not decorative: the budget (Qi-QUA) must exist before a selector (Qi-EP) can extremize it, and only a selected, persisting branch has the stable statistics that Qi-CON diagnoses. That chain — budget, selector, diagnostic — is the precise sense in which the scale-free phenomenology of Parts IV–VII is, on this program's account, the *geometric signature of selected open-system branches*, inherited from the bulk's scale coordinate through the projection: the geometric origin of Qi-CON inside the pillar stack, located exactly.

13 Qi-CON: the central theme of this paper, and how it will be put on trial

Stated constitutionally (GG-A7-Qi4 Part V; restated with full proofs in Part XII): a system on a Qi-EP-selected branch, observed inside an operational window, has an effective generator that is asymptotically homogeneous — the fractional form $\mathcal{L}_{\text{eff}} = -D_\alpha(-\Delta_g)^{\alpha/2}$ with one exponent $0 < \alpha \leq 2$ inherited from the bulk-to-boundary kernel — and therefore *must* display four signatures at once: power-law correlations, α-stable heavy-tailed increments, fractal support of dimension

Table 1: The program's record where it can be checked hardest, one row per headline result. Each row is read from the owning companion's own text and carries its status in that paper's grading. The table's purpose in *this* paper is calibration, in both directions: these results earn the program a hearing when it now claims a law for living systems, and they set the standard of falsifiability — a named number, a named experiment, a named failure condition — that the Qi-CON claim must be held to on biological ground.

Result	Statement	Owner; check
The OGN-5 ledger	all pure numbers collapse to $(1, 3, 5; 7, 35)$, two arithmetic locks, no other values	Arisaka, 2026, A2-GG6; ten falsifiers declared
Anomaly freedom	the six-force bulk is quantum-consistent (the BI-6 certificate)	Arisaka, 2026, A3-BI6
Fine structure	$\alpha^{-1}(0) = 2^J + N^2 = 137$ at first order; CODATA 137.036 after dressing	Arisaka, 2026, A9-SM
28 SM parameters	masses, couplings, mixings as observations of the geometry; graded derived / one-step / open	Arisaka, 2026, A9-SM
Cosmic fractions	$\Omega_m = 1/\pi$, $\Omega_b = 1/(2\pi^2)$, $w = -1$; $n_s = 0.962$, $r = 0.004$ computed	Arisaka, 2026, A10-Cosmos
Expansion rate	$H_0 = 66.6 \pm 0.2$ derived; standard sirens the named referee, $\sim$21 events	Arisaka, 2026, C2-Hubble
Dark matter	the Kaxion near 8.1 μeV; listen at 1.95 GHz; one line, and no partner tone at any spacing	Arisaka, 2026, C1-Kaxion
New mass scale	lock cluster at $M_{\rm lock} = \frac{1}{2} M_{\rm Pl} e^{-35} \simeq 3.85$ TeV; $v = M_{\rm lock}(2/5)^3 \approx 246$ GeV	Arisaka, 2026, P1-KK
Quantum foundations	measurement problem to three theorems; Born rule closed at relaxation level (conditional, one named step)	Arisaka, 2026, A8-QM

$\min(d, \alpha)$, and a $1/f^\beta$ spectral band bounded by two knees at the window's edges.

The trial this paper conducts, in POS-7's spirit, has three instruments, in rising order of sharpness. The *records*: four literatures audited at scale, skeptics included, every number graded (Parts IV–VII). The *arithmetic*: the cross-consistency audit, where independently measured exponents of one system must satisfy the lock relations — a parameter-free test no single literature can run (Part VIII). And the *failure theory*: four named modes in which the signatures must degrade, three of them already exhibited by the record, so that even the claim's failures are predictions (Part XII). The verdict this paper reaches — stated now so the reader can hold the Parts to it — is deliberately bounded: *consistent wherever testable, exactly right wherever the physics is exactly understood, nowhere yet confirmed at the level the program demands of itself, and falsifiable tomorrow by any laboratory with a tracking dataset.*

14 Closing remarks: what a skeptical reader should carry into the audits

Four sentences. The program is a fixed geometry with no dials, whose record in particle physics and cosmology is real, graded, and exposed to near-term experiment — that is what buys it the right to be heard on biology, and nothing more. The chain from bulk to organism runs: scale as a coordinate → projection through a finite window (GDOS) → budget and selector (Qi-QUA, Qi-EP) → the Qi-CON diagnostic — each link a companion paper, each graded. The claim on trial here is narrow and structural: one exponent, four signatures, bounded windows, lawful failures — not a theory of any particular organism. And the reader is asked for exactly one concession while auditing: that openness and partial view be treated as fundamental rather than as noise — because that single inversion, the program's founding move, is where all four of the century's orphan regularities stop being orphans.

Part III
The Four Signatures, Exactly, and the Rules of the Audit

The one-generator claim in operational form, the quartet figure, and the compilation protocol every number downstream obeys

Parts I and II stated the question and the program. This short Part fixes the two things the audits cannot start without: the *exact* operational content of the one-generator claim — what, concretely, the four records would have to show — and the rules under which the record was compiled, so that every number in Parts IV–VIII can be traced, graded, and, where necessary, distrusted for stated reasons.

15 The four signatures, exactly

The four regularities are the four operational signatures of one mathematical object — the homogeneous generator whose constitutional statement is GG-A7-Qi4 Part V's and whose geometric pedigree Part II traced (Arisaka, 2026, A7-Qi4). Here it is stated in the observer's units, because the audits test consequences, not provenance.

Consider a dynamical system observed through a window of scales — every real observation has one — and suppose that, inside the window, the effective generator of its coarse dynamics is *homogeneous*: scale-covariant, with no built-in length. The canonical such generator is fractional,

$$\mathcal{L}_{\text{eff}} = -\,D_\alpha\,(-\Delta)^{\alpha/2}, \qquad 0 < \alpha \le 2, \tag{3}$$

the fractional Laplacian with one exponent α and one rate D_α. Four consequences follow by computation, not by analogy; the derivations are in GG-A7-Qi4 Part V and are rerun at full depth in Part XII of this supplement.

1. **Scaling.** Correlators of the dynamics generated by (3) are homogeneous: $C(\lambda z, \lambda^\alpha t) = \lambda^{-2\Delta}\,C(z,t)$. Observables built on them obey power laws, and ratios of their exponents are fixed.

2. **Lévy statistics.** The propagator of (3) is the α-stable law: $\widehat{p}(k,t) = \exp[-D_\alpha t\,|k|^\alpha]$. Coarse increments are heavy-tailed with stable index $\alpha_{\text{s}} = \alpha$; a step-length survival function measured in the window falls as $P(\ell > L) \sim L^{-\alpha}$, so the density exponent is $\mu = 1 + \alpha$.

3. **Fractality.** Sample paths of an α-stable process in embedding dimension d have Hausdorff dimension $D_{\text{f}} = \min(d, \alpha)$ — a theorem of the stable-process literature (Blumenthal and Getoor, 1960), not a metaphor.

Figure 1: One system, four exponents. The mammalian cortex as the four literatures see it. Statistical physics measures its spike avalanches and finds power-law scaling whose size and duration exponents satisfy a crackling-noise relation (Beggs and Plenz, 2003, Fontenele et al., 2019); the avalanche size distribution itself is the heavy tail, power-law over the measured decades; the neurons' dendritic arbors carry a fractal dimension near 1.4 (Smith et al., 2023); and the human cortical field potential has a $1/f$-type spectrum with a knee at 3–16 Hz, corresponding to intrinsic timescales of 10–50 ms (Gao et al., 2020). Every number in the plate is a row of the audited datasets behind Parts IV–VII, with its source and grade; the four were measured on different preparations, windows, and species, and no experiment has measured all four at once. Whether the four numbers *must* agree — whether they are one exponent seen four ways — is the question Part VIII puts to the whole record.

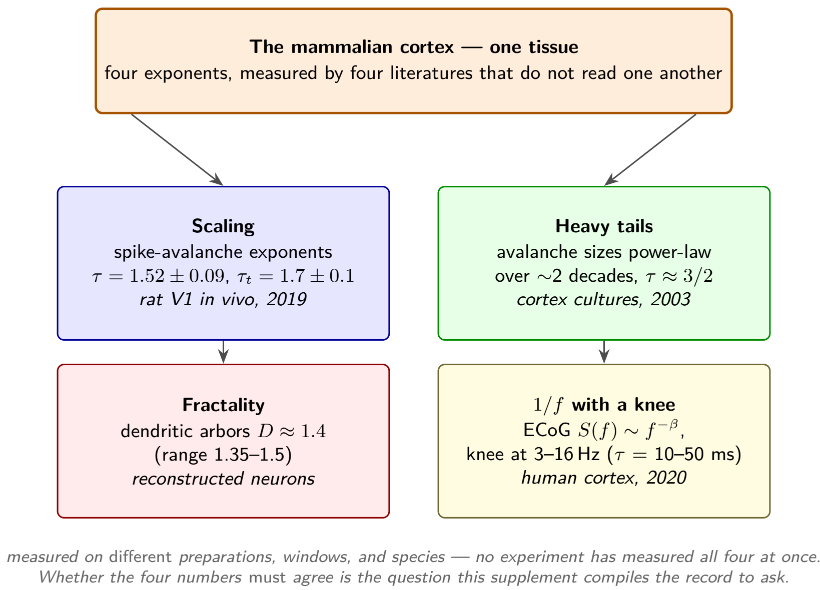

4. $1/f$ **band with two knees.** The superposition of the window's relaxation modes produces $S(f) \propto f^{-\beta}$ between an infrared knee f_{IR} set by the largest retained scale and an ultraviolet knee f_{UV} set by the smallest, with β fixed by α and the mode weighting.

So the four literatures of the four regularities are, on this account, four instrument panels wired to one dial. The account is falsifiable in a way no single-literature explanation is: if the same system yields a step exponent μ, a dimension D_{f}, and a spectral slope β that violate the dictionary, the one-generator claim fails for that system no matter how well any single exponent was fitted. Conversely, the account makes the four skeptical literatures — each of which has spent decades showing that its own regularity is less clean than advertised — allies rather than opponents: a compilation that overstates the record would sabotage the audit that is the point of this supplement.

Figure 1 fixes the situation the supplement starts from. One tissue carries all four signatures; four communities measured them; the measurements have never been brought to one table.

16 The register of the review, and the reader

Three registers coexist below, and the reader deserves to know which is in force where. One structural guarantee first, restated from Part I because it governs everything: the audits are built so that a reader who rejects the program keeps them whole — Parts IV–VII are measurements and their published critiques, and Part VIII's arithmetic uses only relations that are standard mathematics, decades older than this program. What the program adds — the claim that the window and the exponent have a *cause*, and that the knees have predicted places — is examined in Parts XI onward, with the record already on the table.

Parts IV–VII are audits. Each takes one regularity and does four things: the history of the idea, told by dates and papers; the measured record, compiled at scale into one table and one landscape figure; the skeptical case, given at full strength in the words of the literature that made it; and a closing statement of what survives. The compilation follows a fixed protocol, stated once here. Every row of every table carries its system, its measured value with the published uncertainty, the number of decades the fit spans where the source reports it, the source, and a grade: PRIMARY when the number was read from the primary source's own text during this compilation, COMPILED when it was taken from a named review or secondary compilation, UNVERIFIED when a standard literature value could not be checked against its primary text (almost always a paywall) — printed, flagged, and excluded from Part VIII's audit. No number and no citation in the tables was invented or recalled from memory; rows that could not be sourced were dropped by the compilation and the counts reported are the counts that survived. Where a category landed short of a round number, the short count is what is printed.

Part VIII is arithmetic. It assembles the multi-signature systems and computes. Its figure is generated from the published datasets by one script, error propagation included, and every candidate pair that could not be used is named on the figure itself.

Parts X onward are the program's — the CFT and AdS/CFT review, the framework recap, the derivation with its lock and failure theorems, the nine worked cases of Part XIII, and the significance and conclusions that close the supplement.

The intended reader is the same one S1-EP was written for: a scientist who uses one of these regularities and has always suspected the other three were relatives — the biophysicist who fits avalanche exponents, the ecologist burned by the Lévy debate, the neuroscientist who parameterizes aperiodic spectra. Nothing below assumes the program's formalism until Part X, and every claim that depends on it says so.

17 Closing remarks: the audit posture

One warning, restated at the threshold: the four literatures below have all been burned by enthusiasm, and this compilation found the skeptics right more often than the enthusiasts — the retracted albatross data, the one-decade fractals, the biological knee that no primary source reports. Those findings print at the same size as the confirmations. The pattern that survives the skeptics is the only pattern worth deriving — and, per POS-7, the only one worth risking a program on.

Part IV
Conformality and Scaling Laws: the Observational Record

From Kleiber's line to the renormalization group, the measured exponents at scale, and the century-long war over 3/4

This Part audits the oldest of the four records: the power law in *size*. It is the record with the deepest history — the first entry in Table 2 was measured in 1932 — the widest span (a metabolic fit crossing twenty claimed decades of body mass, from bacteria to whales), and the most disciplined internal war, because the two candidate exponents, 3/4 and 2/3, are close enough that a century of data has been needed to fail to separate them. It is also the record where the connection to fundamental physics is not an analogy: the critical exponents of the renormalization group are scaling exponents in exactly the same operational sense as Kleiber's, and the conformal bootstrap has now computed one of them to nine digits while the best fluid experiment checks two. Both halves — the biological line and the critical scoreboard — belong in one Part because the Qi-CON claim makes them one subject: exponents of homogeneous generators, differing only in how much of the generator the community measuring them can see.

Read against Part II, the stake is concrete: the geometry that fixed the constants of the Standard Model offers, through the boundary law, a derived origin for the exponent this record has fought over since 1932. Nothing in the compilation below assumes the offer is good. The record is audited on its own terms, and the confrontation is deferred to Parts XI–XII.

18 Historical development: from Kleiber's line to the renormalization group

18.1 The surface law and its failure

The idea that metabolism is set by geometry is older than the data. Rubner argued in 1883 that a homeotherm loses heat through its surface, so resting metabolic rate B should scale with body mass M as surface area does:

$$B \propto M^{2/3}, \tag{4}$$

the *surface law*. The physics intuition is a dimensional argument and nothing more: if heat production must balance heat loss, and loss goes through a surface $\propto L^2$ while mass fills a volume $\propto L^3$, the exponent is 2/3 by arithmetic. The argument is honest, falsifiable — and, on the data Kleiber assembled in 1932, apparently wrong. Fitting resting metabolism from rats to steers, Kleiber (1932) found $b \approx 0.74$ over about 2.6 decades of mass and proposed the round value 3/4 that carries his name. Brody's cattle curves and Hemmingsen's compilations pushed the range to unicells and to five decades, and by mid-century "Kleiber's law" $B \propto M^{3/4}$ was textbook biology — a quarter-power, not a third-power, and therefore a number that geometry alone could not supply.

The physics content of that discrepancy deserves to be stated the way a physicist would state it. An exponent of 2/3 says the limiting resource is a *surface*. An exponent of 3/4 says the limiting resource is something with an effective dimension of four — Blum's observation that $3/4 = 3/(3+1)$ — or, less numerologically, that the organism's supply system fills three-dimensional space so efficiently that it behaves as if it had an extra dimension. That is the intuition the modern network models make precise.

18.2 The network derivations

West et al. (1997) derived 3/4 from three assumptions: the supply network is a space-filling fractal branching tree; the terminal units (capillaries) are size-invariant; and evolution has minimized the energy dissipated in transport. Under these assumptions the number of terminal units — and with it the deliverable power — scales as $M^{3/4}$. The derivation's engine is the third assumption: for a pulsatile, area-preserving arterial tree the impedance minimization forces the branching ratios into the configuration whose terminal count scales with the 3/4 power. Banavar et al. (1999) reached the same exponent with far weaker hypotheses — any directed transport network that supplies a d-dimensional volume through local links delivers at most $B \propto M^{d/(d+1)}$, hence 3/4 in three dimensions — at the price of predicting an inequality rather than a value. The physics intuition for both: *a body is fed through a network, and a network that must reach every cell pays a tax of one dimension.* Whether nature pays exactly that tax is what the record must decide.

18.3 Scaling becomes exact: the renormalization group

While the biologists fitted lines, physics made scaling a derived concept. The Widom–Kadanoff scaling hypothesis organized the critical exponents of phase transitions into a homogeneous form; Wilson's renormalization group (Wilson, 1971) explained *why* observables near a critical point are homogeneous functions — the flow to a fixed point washes out every microscopic scale — and Onsager's exact solution of the two-dimensional Ising model (Onsager, 1944) had already supplied exponents that any such theory had to hit exactly ($\beta = 1/8$, $\nu = 1$). The conformal bootstrap completed the arc: by demanding only crossing symmetry and unitarity of the operator algebra, Kos et al. (2016) located the 3D Ising exponents in an island of allowed values, $\Delta_\sigma = 0.5181489(10)$, sharpened in 2024 to $\Delta_\sigma = 0.518148806(24)$ (Chang et al., 2024) — nine significant digits, from consistency conditions alone, with no Hamiltonian ever written down.

The relevance to this supplement is structural, not decorative. The RG is the one context where the questions the allometry war argues about — is the exponent universal? what fixes it? when do two systems share it? — have exact answers: exponents are properties of fixed points, not of materials; they are shared within a universality class and differ between classes; and their values are computable. The Qi-CON claim of GG-A7-Qi4 Part V is that the same logic, run through the projected boundary generator, covers the biological records too — with the window and the exponent supplied by the projection rather than by proximity to a critical point. Part XII takes up that claim; this Part's business is the record.

19 What is actually measured: allometric, urban, and critical exponents

Three operationally distinct exponent families appear in Table 2, and conflating them is the commonest abuse in the popular literature. It is worth five paragraphs to keep them straight.

Allometric exponents come from ordinary least squares (or phylogenetically corrected) regression of $\log Y$ on $\log M$ across species:

$$\log_{10} B \;=\; \log_{10} B_0 \;+\; b \log_{10} M \;+\; \varepsilon, \tag{5}$$

and everything about them is conditional on the fitting protocol: which species enter, whether data are binned, whether temperature is normalized (metabolism is Arrhenius-sensitive, so cross-taxon fits without a Boltzmann correction mix scaling with thermodynamics), and whether phylogeny is treated as covariance structure. The record shows exactly this sensitivity: the same decade of literature contains $b = 0.686 \pm 0.014$ for temperature-normalized mammalian basal rates (White and Seymour, 2003), 0.712 (CI 0.699–0.724) for the unbinned compilation, and 0.737 (CI 0.711–0.762) for the same data binned by size class (Savage et al., 2004) — the binning decision alone walks the exponent a third of the way from 2/3 to 3/4. Physics intuition: binning equalizes the leverage of the sparse large animals, so the choice of estimator is silently a choice about *which masses count*, and the confidence intervals of any single protocol understate the protocol variance the record displays.

Urban and Zipf exponents are the same regression run on cities instead of species (Bettencourt et al., 2007, Bettencourt, 2013). The finding that made the field is not any single value but the split: socioeconomic quantities (wages, patents, AIDS cases) scale *superlinearly*, $\beta \approx 1.12$–1.27, while material infrastructure (road surface, gasoline stations) scales *sublinearly*, $\beta \approx 0.77$–0.85, with accounting identities like total housing at $\beta \approx 1.00$ sitting exactly where bookkeeping demands. The theoretical reading (Bettencourt, 2013) is a network argument again — social interactions densify with city size while infrastructure amortizes — and the two bands in Figure 2 are drawn at the record's own values.

Critical and avalanche exponents are different animals: they are measured inside one system as a control parameter approaches a critical value, or on the event statistics of a driven system, and they come with the RG's exactness guarantees when the identification with a universality class is right. Table 3 collects the scoreboard: bootstrap and Monte Carlo values against the best experiments — the binary-liquid coexistence exponent $\beta = 0.328(4)$ against the bootstrap-derived 0.32642, the helium λ-point story told in §21, the liquid-crystal interface hitting the exact KPZ 1/3 to one percent (Takeuchi and Sano, 2010), and the two clean Barkhausen universality classes of Durin and Zapperi (2000). The neuronal avalanche block of Table 2 belongs to this family — $\tau = 1.50 \pm 0.008$ in cortex cultures (Beggs and Plenz, 2003), $\tau = 1.52 \pm 0.09$ with $\tau_t = 1.7 \pm 0.1$ in vivo (Fontenele et al., 2019) — and it is the family where exponent *relations* (the crackling-noise identity Part VIII tests) are theorems rather than hopes.

One more distinction matters for everything downstream. An exponent fitted over n decades constrains a homogeneous generator only over those n decades. Table 2 therefore carries the fitted range wherever the source reports one, and the *absence* of a reported range — the commonest single fact about the record — is itself data about the field's habits.

20 The record: 52 systems

Figure 2 plots every row of the scaling record against the three reference values the century has argued about, and Table 2 prints the rows with their uncertainties, ranges, sources, and grades. The compilation protocol is the one stated in §16; after the verification pass, 42 of the 52 rows are grade P (read from the primary source), 6 are C, and 4 are U? — still flagged and excluded from any arithmetic.

Three features of the landscape deserve the reader's eye before the critiques arrive.

First, **the metabolic block does not sit on either line.** The modern temperature-normalized fits cluster near 0.69–0.75 with confidence intervals that exclude neither canonical value across the block; the three-group active-metabolism fits of DeLong et al. (2010) (prokaryotes 1.96 ± 0.18, protists 1.06 ± 0.07, metazoans 0.79 ± 0.04) refuse a single exponent altogether; and the log–log *curvature* measured by Kolokotrones et al. (2010) — a local slope rising from 0.57 at small mass to 0.87 at large — is a direct measurement of inhomogeneity across the window. Anyone selling a single clean 3/4 across all life is selling something the record does not contain.

Second, **the negative exponents are the same physics.** Damuth's law — population density falling as $M^{-0.75}$ over about seven decades (Damuth, 1981) — multiplied against Kleiber gives the energy-equivalence rule (community energy use independent of body size), and mammalian heart rate at $M^{-0.251}$ against lifespan at $M^{0.2}$–0.25 gives the roughly invariant total heartbeat count. These quarter-power *ratios* are cleaner than the quarter powers themselves — a point the one-generator account predicts, since exponent ratios cancel the window-dependent corrections that move individual exponents.

Third, **the avalanche block is where scaling meets its theorems.** Its four rows carry the only exponents in the biological record whose values are cross-checked by an identity (Part VIII), and they sit at the mean-field values 3/2 and 2 to within their stated errors.

Table 2: The scaling record: 52 measured exponents. Every allometric, urban, ecological, neural, geophysical, and avalanche scaling exponent compiled for this supplement, grouped by domain exactly as Figure 2 plots them. Value carries the published uncertainty where the source states one; Dec. is the number of decades the fit spans where reported; G is the verification grade — P: read from the primary source during this compilation; C: from a named compilation; U?: standard literature value whose primary text could not be fetched, excluded from the Part VIII audit. Full citations are in the References; the machine-readable dataset with URLs and per-row notes is published beside this supplement.

System	Quantity	Value	Dec.	Year	Source	G
METABOLIC						
mammal basal metabolic rate	$B \sim M^b$	0.686 ±0.014 (as published)	∼5	2003	White & Seymour	P
mammal basal metabolic rate (unbinned)	$B \sim M^b$	0.712 95% CI 0.699-0.724	∼5.5	2004	Savage et al	P

continued on next page

Table 2, continued.

System	Quantity	Value	Dec.	Year	Source	G
mammal BMR, binned by size class	$B \sim M^b$	0.737 95% CI 0.711-0.762	~5.5	2004	Savage et al	P
mammal field metabolic rate	$FMR \sim M^b$	0.749 95% CI 0.695-0.802	–	2004	Savage et al	P
mammal BMR log-log curvature	local b rises 0.57 to 0.87	0.540 single-b fit; b2=0.0322±0.0053	~6	2010	Kolokotrones et al	P
homeotherm metabolism (classic)	$B \sim M^b$	0.74 range argued 2/3-3/4	~2.6	1932	Kleiber	P
prokaryote active metabolism	$B \sim M^b$	1.96 ±0.18 SE	–	2010	DeLong et al	P
protist active metabolism	$B \sim M^b$	1.06 ±0.07 SE	–	2010	DeLong et al	P
metazoan active metabolism	$B \sim M^b$	0.79 ±0.04 SE	–	2010	DeLong et al	P
eukaryote metabolism within groups	$B \sim M^b$	0.75	–	2019	Hatton et al	P
eukaryote metabolism across all eukaryotes	$B \sim M^b$	1.0	–	2019	Hatton et al	P
eukaryote max growth rate	rate $\sim M^{-b}$	-0.25	–	2019	Hatton et al	P
teleost fish resting metabolism	$B \sim M^b$	0.793 ±0.020 (95% CL)	–	1999	Clarke & Johnston	C
fish standard metabolism (intraspecific)	$B \sim M^b$	0.89 SE 0.021; CrI 0.81-0.99	–	2019	Jerde et al	P
insect metabolism (interspecific)	$B \sim M^b$	0.830 ±0.036	–	2005	Glazier	C
passerine bird BMR	$B \sim M^b$	0.711 ±0.109	–	2005	Glazier	C
unicellular organisms metabolism	$B \sim M^b$	0.66 ±0.092 (95% CL)	–	1981	Phillipson	C
plant biomass production (algae to trees)	$G \sim M^b$	0.75	–	2001	Niklas & Enquist	C
mammal heart rate	$f \sim M^b$	-0.251 95% CI -0.285 to -0.218	–	2004	Savage et al	P
biological times (twitch to lifespan)	$t \sim M^b$	0.250 ±0.011 SE	–	2004	Savage et al	P
mammal maximum lifespan	$t\_max \sim M^b$	0.2 0.15-0.3 (primary range)	–	2005	Speakman	P
ECOLOGY						
mammal population density vs mass	$D \sim M^b$	-0.75 SE 0.026	~7	1981	Damuth	P
plant max density vs mass (self-thinning)	$D \sim M^b$	-0.757 95% CI -0.773 to -0.741	–	2002	Belgrano et al	P
eukaryote abundance vs mass	$D \sim M^b$	-0.75 ~-1 across groups	–	2019	Hatton et al	P

continued on next page

Table 2, continued.

System	Quantity	Value	Dec.	Year	Source	G
population variance vs mean (Taylor's law)	Var $\sim$ mean^b	1.5 range 1-2	–	1961	Taylor	U?
fluctuation scaling across complex systems	$\sigma \sim$ <f>^{a}	0.75 range 0.5-1	–	2008	Eisler	P
species-area relationship	S $\sim$ A^z	0.27 mean of 794 SARs	–	2006	Drakare et al	U?
mammal home range vs mass	H $\sim$ M^b	1.0	–	2004	Jetz et al	P
predator vs prey community biomass	B_pred $\sim$ B_prey^k	0.74	–	2015	Hatton et al	P
NEURO						
white vs gray matter volume, mammal cortex	W $\sim$ G^b	1.23 ±0.01	~5-6	2000	Zhang & Sejnowski	P
cortical folding, mammals	A_t*T$^{0.5}$ $\sim$ A_e^a	1.305	–	2015	Mota & Herculano-Houzel	U?
cortical folding across human individuals	A_t*T$^{0.5}$ $\sim$ A_e^a	1.25	–	2019	Wang et al	P
human tumor metabolic activity vs volume	SUV $\sim$ V^b	1.27 range 1.25-1.3	–	2020	Perez-Garcia et al	P
mammal brain mass vs body mass	M_br $\sim$ M^b	0.75 CI 0.742-0.758	–	2019	Burger et al	P
URBAN						
city GDP vs population (China)	Y $\sim$ N$^\beta$	1.15 95% CI 1.06-1.23	–	2007	Bettencourt et al	P
city total wages vs population (USA)	Y $\sim$ N$^\beta$	1.12 95% CI 1.09-1.13	–	2007	Bettencourt et al	P
new patents vs city population (USA)	Y $\sim$ N$^\beta$	1.27 95% CI 1.25-1.29	–	2007	Bettencourt et al	P
new AIDS cases vs city population (USA)	Y $\sim$ N$^\beta$	1.23 95% CI 1.18-1.29	–	2007	Bettencourt et al	P
gasoline stations vs city population (USA)	Y $\sim$ N$^\beta$	0.77 95% CI 0.74-0.81	–	2007	Bettencourt et al	P
road surface vs city population (Germany)	Y $\sim$ N$^\beta$	0.83 95% CI 0.74-0.92	–	2007	Bettencourt et al	P
total housing vs city population (USA)	Y $\sim$ N$^\beta$	1.00 95% CI 0.99-1.01	–	2007	Bettencourt et al	P
gross metropolitan product (USA 2006)	Y $\sim$ N$^\beta$	1.126 ±0.023	–	2013	Bettencourt	P
road lane miles (USA 2006)	Y $\sim$ N$^\beta$	0.849 ±0.038	–	2013	Bettencourt	P
city size distribution (Zipf)	P_rank $\sim$ rank^{-a}	1.09 meta-analytic mean	–	2005	Nitsch	U?

continued on next page

Table 2, continued.

System	Quantity	Value	Dec.	Year	Source	G
word frequency (Zipf's law)	f $\sim$ rank^{-a}	1.0 canonical $\sim$1; own fits 0.51-3.68	–	2014	Piantadosi	P
GEO						
earthquake frequency-magnitude, S. California	G-R b-value	0.994 ±0.02	–	2023	arXiv:2307.03457	P
earthquake frequency-magnitude (classic; S. California)	G-R b-value	1.0 typical range 0.6-1.4	–	1944	Gutenberg & Richter	C
river basin: length vs area (Hack's law)	L $\sim$ A^h	0.6 0.6 (0.7 Arizona)	–	1957	Hack	P
AVALANCHE						
neuronal avalanche size (cultures/slices)	P(s) $\sim$ s$^{-\tau}$	1.50 ±0.008	–	2003	Beggs & Plenz	P
neuronal avalanche lifetime (cultures/slices)	P(T) $\sim$ T^{-a}	2.0 initial slope	–	2003	Beggs & Plenz	P
spike avalanche size, rat V1 in vivo	P(s) $\sim$ s$^{-\tau}$	1.52 ±0.09	–	2019	Fontenele et al	P
spike avalanche duration, rat V1 in vivo	P(T) $\sim$ T^{-t}	1.7 ±0.1	–	2019	Fontenele et al	P

Table 3: The critical-exponent scoreboard. The precision frontier of the scaling record: conformal-bootstrap values against the best measurements for the 3D Ising, O(2), 2D Ising, percolation, KPZ, avalanche, and holographic-bound universality classes. This table carries the two rows that anchor Part VIII's inset: the helium λ-point specific-heat exponent, where theory and experiment are both at four digits and disagree at 8σ, and the 2024 bootstrap determination of Δ_σ at nine digits. Grades and columns as in Table 2.

System	Quantity	Value	Dec.	Year	Source	G
3D ISING						
3D Ising CFT (conformal bootstrap)	Delta_sigma	0.5181489 0.0000010	–	2016	Kos-Poland-Simmons-Duffin-Vichi	P
3D Ising CFT (conformal bootstrap)	Delta_epsilon	1.412625 0.000010	–	2016	Kos-Poland-Simmons-Duffin-Vichi	P
3D Ising CFT (stress-tensor bootstrap)	Delta_sigma	0.518148806 0.000000024	–	2024	Chang et al arXiv:2411.15300	P
3D Ising CFT (stress-tensor bootstrap)	Delta_epsilon	1.41262528 0.00000029	–	2024	Chang et al arXiv:2411.15300	P
3D Ising CFT	ν (derived)	0.629971 0.000004	–	2016	derived from Kos et al Delta_epsil	C

continued on next page

Table 3, continued.

System	Quantity	Value	Dec.	Year	Source	G
3D Ising CFT	eta (derived)	0.0362978 0.0000020	–	2016	derived from Kos et al Delta_sigma	C
isobutyric acid + water (binary liquid)	β	0.328 0.004	–	1976	Greer	P
n-heptane + nitrobenzene (binary liquid)	β	0.367 0.006	–	2006	Fameli-Balzarini	P
fluid experiments (survey)	β (experimental consensus b	0.325-0.327	–	2006	cited in Fameli-Balzarini	C
aqueous electrolyte solution	γ; ν; eta	1.238; 0.629; 0.032 0.012; 0.003; 0.013	–	2009	Sengers-Shanks J Stat Phys 137 857	C
FeF2 uniaxial antiferromagnet	β	0.325 0.005	–	1994	Mattsson et al	C
3D XY / O(2)						
superfluid He-4 lambda point (zero-g shuttle)	α (specific heat)	-0.0127 0.0003	–	2003	Lipa et al	P
superfluid He-4 lambda point	A+/A- amplitude ratio	1.053 0.002	–	2003	Lipa et al	P
O(2) model (conformal bootstrap)	Delta_s (charge-0 scalar)	1.51136 0.00022	–	2020	Chester et al	P
O(2) model (Monte Carlo)	ν	0.67169 0.00007	–	2020	quoted in Chester et al	C
superfluid He-4 (from Lipa alpha via hyperscaling)	nu_exp	0.6709 0.0001	–	2020	quoted in Chester et al	C
He-4 vs O(2) theory	theory-experiment tension	8 σ	–	2020	Chester et al abstract	P
2D ISING						
2D Ising model (exact)	β	1/8 (exact) 0	–	1952	Yang	C
2D Ising model (exact)	ν; α	1 (exact); 0 (log) 0	–	1944	Onsager	C
lipid membrane / plasma membrane vesicles	β	0.124 0.03	–	2008	Honerkamp-Smith et al	P
lipid membrane / plasma membrane vesicles	ν	1.2 0.2	–	2008	Honerkamp-Smith et al	P
2D MODEL HC						
lipid membrane (dynamics)	z_eff (dynamic exponent)	2.8 0.2	–	2011	Honerkamp-Smith-Machta-Keller	P

continued on next page

Table 3, continued.

System	Quantity	Value	Dec.	Year	Source	G
2D PERCOLATION						
2D critical percolation (SLE proof)	β	5/36 (exact) 0	–	2001	Smirnov-Werner Math Res Lett 8	C
2D critical percolation (SLE proof)	ν	4/3 (exact) 0	–	2001	Smirnov-Werner Math Res Lett 8	C
KPZ						
KPZ equation 1+1d (exact)	β; α	1/3; 1/2 (exact) 0	–	1986	Kardar-Parisi-Zhang	C
liquid-crystal turbulence interface (DSM2)	β (growth)	0.336 0.011	–	2010	Takeuchi-Sano	P
liquid-crystal turbulence interface (DSM2)	α (roughness)	0.50 0.05	–	2010	Takeuchi-Sano	P
ABBM/FRONT DEPINNING						
Barkhausen noise class 1 (polycrystalline SR)	τ (avalanche size)	1.50 0.05	–	2000	Durin-Zapperi	P
FRONT DEPINNING SR						
Barkhausen noise class 2 (amorphous LR)	τ (avalanche size)	1.27 0.03	–	2000	Durin-Zapperi	P
SOC						
rice pile (elongated grains)	energy dissipation exponent	∼2	–	1996	Frette et al	C
SOC/BEAN STATE						
superconducting vortex avalanches (Nb tube)	avalanche size distribution	power law; τ 1.4-2.2	2	1995	Field-Witt-Nori-Ling	C
ADS/CFT						
KSS holographic bound	eta/s lower bound	1/(4pi) = 0.0796 0 (exact in limit)	–	2005	Kovtun-Son-Starinets	C
ADS/CFT BENCHMARK						
quark-gluon plasma (RHIC/LHC flow)	(eta/s)_QGP	∼0.18; range (1-2.5)/(4pi)	–	2015	Shen-Heinz arXiv:1507.01558	P
quark-gluon plasma (Bayesian global fit)	eta/s near Tc	0.085 +0.026/-0.025	–	2019	Bernhard-Moreland-Bass	C

21 Critiques and the exact scope: the 3/4 war, curvature, and power-law statistics

The scaling record has the most disciplined skeptical literature of the four, and this section gives it the floor.

Figure 2: The scaling landscape: 52 measured exponents across six domains. Every row of Table 2, grouped by domain, plotted against the three reference values the literature has argued over for a century: the geometric surface law 2/3, Kleiber's 3/4, and linearity 1, with the urban record's own sublinear and superlinear bands shaded at the values measured in Bettencourt et al. (2007), Bettencourt (2013). Negative exponents — Damuth's density law, mammalian heart rate — are rate and density laws plotted on the same axis because their quarter-power values are part of the same record. Filled markers carry a published uncertainty (drawn); open markers report none; (c) marks a value taken from a named compilation and (u?) a standard value whose primary source could not be fetched, excluded from Part VIII's arithmetic. Bracketed decade counts are the fitted ranges where the sources state them. The figure is generated from the published dataset by one script; nothing is drawn that is not in Table 2.

21.1 The 3/4-versus-2/3 war is not settled, and saying so is the honest summary

The modern phase of the war opened when White and Seymour (2003) re-fitted mammalian basal metabolism with body temperature normalized and digestive state controlled, and recovered Rubner: $b = 0.686 \pm 0.014$, statistically indistinguishable from 2/3 and five standard errors from 3/4. Savage et al. (2004) answered with the largest compilation then assembled and recovered Kleiber under binning. Glazier (2005) surveyed the whole literature and concluded that intraspecific and interspecific exponents differ systematically, that b varies with metabolic state (resting versus maximal), and that no single exponent describes metabolism — a conclusion Kolokotrones et al. (2010) made quantitative by showing the mammalian data are *curved* in log–log, so that any single b is an average over a window and moves when the window does. Physics intuition: curvature in log–log is precisely the statement that the effective generator is *not* homogeneous across the fitted range — the window contains a crossover, and the two canonical exponents may simply own different ends of it. That reading — 2/3 physics at small mass yielding to network-limited 3/4 physics at large — is explicit in the surface-area work of White and Seymour (2003) and consistent with the DeLong three-group split. On the compiled record, the defensible statement is: the mammalian exponent lies between 2/3 and 3/4, is not constant across the window, and neither round value survives as a universal constant of biology.

21.2 The statistics of power-law fitting arrived late and weakened the older record

Clauset et al. (2009) formalized what the physics folklore knew: a straight stretch on a log–log plot is weak evidence. Maximum likelihood estimation of the exponent, explicit estimation of the lower cutoff, and likelihood-ratio comparison against lognormal and stretched-exponential alternatives are the minimum standard, and when Stumpf and Porter (2012) applied that standard retrospectively, much of the claimed power-law canon thinned. The scaling record inherits this critique in a specific form: regressions of the form (5) are fits of a *mean relation*, not of a distribution tail, so they escape the worst of the Clauset–Shalizi–Newman pathology — but the urban and Zipf rows do not, and the Zipf row of Table 2 accordingly carries its own reanalysis literature in its note. The lesson this supplement takes: exponent values below are quoted with the estimator named wherever the source names it, and Part VIII's audit never rests on a single fitting protocol.

21.3 What the critical scoreboard contributes: the asymmetry

Table 3 quantifies something the allometry war cannot: what agreement looks like when it is real. Where the identification with a universality class is secure, theory and experiment agree to the experiment's full precision — the 2D Ising lipid-membrane exponents (Honerkamp-Smith et al., 2008; 2011), the KPZ liquid-crystal interface (Takeuchi and Sano, 2010), the binary-liquid β (Greer, 1976). And where they disagree, the disagreement is a crisis worth decades: the helium λ-point specific-heat exponent, measured in microgravity to $\alpha_{\text{exp}} = -0.0127(3)$ (Lipa et al., 2003), sits eight standard deviations from the O(2) bootstrap-and-Monte-Carlo value $-0.01507(21)$ (Chester et al., 2020) — the most precise unresolved discrepancy in the physics of criticality, carried into Part VIII's audit figure as its inset. The asymmetry between that scoreboard and the metabolic block — nine digits against a disputed first digit — is the cleanest available measure of how far the biological scaling record is from the exactness its popular tellings borrow.

22 Closing remarks: what a life scientist should take from this Part

Four sentences survive the audit. Metabolic scaling is real, quarter-power-*like*, and not a single universal exponent — the record shows protocol dependence, taxon dependence, and measured curvature, and the honest value for mammals lies between the two canonical fractions. Exponent *ratios* and *relations* are in better shape than exponents — energy equivalence, invariant heartbeat count, and the avalanche identities all hold at their error bars, which is exactly the pattern a homogeneous-generator account predicts when windows corrupt individual exponents but cancel in combinations. The critical scoreboard shows what settled looks like, and biology's scaling record is not settled. And the single highest value-per-page action available to the field is unchanged from what the skeptics have demanded for two decades: report the fitted range and the estimator alongside every exponent, because an exponent without its window is not yet a measurement of anything.

Part V
Lévy Flights and Heavy-Tailed Statistics

From stable laws to the search-strategy hypothesis, the measured record, and the retraction that taught the field its statistics

This Part audits the record of the power law in *step*: motion whose displacement distribution has no characteristic scale. It is the youngest of the four records as an empirical program — its founding observation was published in 1996 — and the only one whose founding observation was subsequently *retracted by reanalysis*, which gives it something none of the other three records has: a community-wide, published, adversarial lesson in how power laws should and should not be fitted. The record that survived that lesson is smaller than the record that preceded it, better measured, and genuinely cross-domain: sharks, T cells, tumor cells, bank notes, photons in hot vapor, and cold atoms in a dissipative lattice all appear in Table 4 with tail exponents between the ballistic and diffusive boundaries.

The top-down frame of Part II enters this record at exactly one place: the boundary law's fractional generator makes heavy tails a geometric consequence of the partial view rather than an optimized strategy, and it ties the tail exponent μ to the other three signatures through the dictionaries of Part VIII. The compilation below neither uses nor needs that claim; it is the material the claim will be tested against.

23 Historical development: Lévy, Mandelbrot, and the search-strategy hypothesis

23.1 The mathematics came first

The mathematics of this Part predates every observation in it by sixty years. Lévy asked which distributions are *stable* — closed under addition up to rescaling — and found the family parameterized by an index $0 < \alpha_s \leq 2$: the generalized central limit theorem says that sums of independent increments with infinite variance converge not to a Gaussian but to an α_s-stable law, the unique attractors besides the Gaussian itself (Gnedenko and Kolmogorov, 1954). The physics content is a single sentence: *if a random walk's steps have tails $P(\ell > L) \sim L^{-\alpha_s}$ with $\alpha_s < 2$, no amount of averaging makes it Gaussian* — the largest step in a sample remains comparable to the sum of all the others at every scale, which is visually the difference between diffusive jitter and flight-and-cluster motion. Mandelbrot imported the family into data analysis with cotton prices (Mandelbrot, 1963), and Shlesinger, Klafter and coworkers built the physics of *Lévy walks* — steps taken at finite velocity, so that long flights cost long times and moments stay finite — the version every biological application actually uses (Zaburdaev et al., 2015).

23.2 The foraging hypothesis

The empirical program began when Viswanathan et al. (1996) reported power-law flight durations in wandering albatrosses, and became a theory when Viswanathan et al. (1999) proved the optimality result the field still orbits: for a memoryless searcher seeking sparse, revisitable targets, the search efficiency is maximized by a step-length exponent

$$\mu_{\text{opt}} = 2, \qquad P(\ell) \sim \ell^{-\mu}, \quad 1 < \mu \leq 3, \tag{6}$$

the inverse-square walk — with $\mu \to 1$ ballistic motion wasting revisits and $\mu \geq 3$ collapsing to Brownian search by the central limit theorem. The physics intuition is bracketing: an inverse-square walk spends its time budget across all scales evenly (each decade of step length contributes equally), which is precisely the scale-democratic search a target field with no known scale demands. The Lévy foraging hypothesis — that natural selection has tuned real searchers to (6) — follows, and Figure 3 shows how much of the measured record clusters around $\mu = 2$.

24 What is actually measured: μ, and how the estimators disagree

Everything in this record is a fit to a tail, and the tail is where statistics is hardest. Four methodological facts govern the entire Part.

First, **the exponent conventions differ by one.** Movement ecology reports the *density* exponent μ in $P(\ell) \sim \ell^{-\mu}$; the stable index is $\alpha_s = \mu - 1$; and the finance literature reports the *survival* exponent, which equals α_s. The dictionary column of Table 4 does the conversion row by row, and Figure 3's axis is μ with the stable entries converted as each row states.

Second, **binning destroys tails.** The founding analyses fitted straight lines to log-binned histograms; Edwards et al. (2007) showed that protocol manufactures power laws from exponential data, and the field's methodological reformation — maximum likelihood for the exponent, explicit lower cutoff, likelihood-ratio model selection against exponential and composite alternatives (Clauset et al., 2009) — dates from that demonstration.

Third, **every biological tail is truncated.** An animal cannot take a step longer than its ocean, so the fitted object is a truncated power law and the honest quantity is the exponent *plus* the truncation scale. The bigeye tuna row of Table 4 shows what the correction does: the original binned fit gave $\mu = 2.4$; the MLE truncated refit gives 1.366 — both numbers are in the record, and the pair is the cleanest single measure of protocol sensitivity the field owns.

Fourth, **a composite of two Brownian walks mimics a Lévy walk** over two decades or so (Auger-Méthé et al., 2015): an animal switching between intensive (short-step) and extensive (long-step) Brownian modes produces an apparent power law between the two mode scales. Model selection can distinguish them in principle; over the window lengths most tracking data supply, it frequently cannot in practice. This is the record's standing ambiguity, and no honest compilation can remove it — only report which rows carry model comparison and which do not.

25 The record: 43 entries

Figure 3 plots the 30 quantitative exponents of the record inside the Lévy regime $1 < \mu \leq 3$, against the ballistic and diffusive boundaries and the optimum (6); Table 4 prints all 43 entries including the thirteen verdict rows — the reanalyses, retractions, and model-selection findings that are as much a part of the record as the exponents. Grades after the verification pass: 39 P, 4 C, 0 U? — the record's second generation is now verified end to end.

The reader should take three structural facts from the landscape.

First, **the marine-predator block is the record's core.** The 2008 tracking campaigns (Sims et al., 2008) measured over a million displacement steps across sharks, tunas, cod, turtles and penguins, found $\mu = 2.12 \pm 0.31$ pooled — astride the optimum — and, decisively for this supplement, measured *three* exponents on the same dive series (μ, the Hurst exponent, and the spectral slope), making it Part VIII's best multi-signature system. The 2010 follow-up across fourteen species found $1 < \mu \leq 3$ in 61 of 66 dataset sections (Humphries et al., 2010). Whatever the mechanism, open-ocean predators move on scale-free step distributions inside the Lévy window; that finding survived the field's statistical reformation.

Second, **the cellular block is the record's growth area, and it carries its own internal control.** Effector T cells hunting parasites in infected brain move with $\mu = 2.15$ (Harris et al., 2012); metastatic cancer cells in vivo move with $\mu = 2.36$, their non-metastatic sister lines with $\mu > 3$ — diffusive — across three matched cell-line pairs (Huda et al., 2018). A migration exponent that separates metastatic from non-metastatic lines is the record's most consequential single entry, and the matched-pair design makes it the hardest to attribute to environment alone. The reanalysis literature has reached the T-cell data (a correlated-random-walk refit; Table 4), not yet the cancer data.

Third, **the physics block is where μ is an engineering parameter.** A Lévy glass built from scatterer-size distributions produces designed superdiffusion (Barthélemy et al., 2008); resonant photons in hot rubidium vapor measure $\mu = 2.41 \pm 0.12$ from first principles of Doppler line shapes (Baudouin et al., 2014); cold atoms in a dissipative lattice tune the exponent with laser depth (Sagi et al., 2012). These rows anchor the record's low-ambiguity end: where the mechanism is known and controllable, the Lévy phenomenology is exact, reproducible, and boring — which is what the biological rows aspire to and have not reached.

Table 4: The Lévy record: 43 entries, exponents and verdicts. Measured step-length tail exponents μ (density convention, $P(\ell) \sim \ell^{-\mu}$; stable index $\alpha_s = \mu - 1$) together with the reanalysis verdicts that are part of the record — rows whose quantity column reads "model selection" or similar carry the skeptical literature's findings and are listed rather than plotted. Grades and columns as in Table 2.

System	Quantity	Value	Dec.	Year	Source	G
ECOLOGY-CLASSIC						
wandering albatross flight durations	μ	2.0	–	1996	Viswanathan et al	P

continued on next page

Table 4, continued.

System	Quantity	Value	Dec.	Year	Source	G
spider monkeys	μ	2.18	–	2004	Ramos-Fernandez et al	P
ECOLOGY						
albatross + deer + bumblebee reanalysis	model selection	no Levy	–	2007	Edwards et al	P
wandering albatross GPS (126 birds)	fraction Levy	0.31	–	2012	Humphries et al	P
marine predators pooled (24 individuals)	μ	2.12 sd 0.31; range 1.34-2.91	∼2-3	2008	Sims et al	P
basking shark	μ	2.3	∼2-3	2008	Sims et al	P
bigeye tuna	μ	2.4	∼2-3	2008	Sims et al	P
Atlantic cod	μ	1.9	∼2-3	2008	Sims et al	P
leatherback turtle	μ	1.7	∼2-3	2008	Sims et al	P
Magellanic penguin	μ	2.4	∼2-3	2008	Sims et al	P
bigeye tuna refit after critique	μ (truncated PL; MLE)	1.366	–	2012	Humphries	P
14 open-ocean predator species	μ range	$1<\mu\leq 3$ in 61/66 sections	–	2010	Humphries et al	P
mussels pattern formation (original)	μ	2.03 methods range 1.930-2.174	–	2011	de Jager et al	P
mussels reanalysis (single PL; MLE)	μ	1.397	–	2012	Jansen	P
mussels as Weierstrassian LW	μ	2.195	–	2014	Reynolds	P
displaced honeybees	μ	2.0	–	2007	Reynolds et al	P
Drosophila larvae CPG-generated turning	μ	1.96 ±0.39 SD (brain-blocked)	–	2019	Sims et al	P
ECOLOGY-META						
Levy foraging hypothesis critique	n/a	abandonment argued	–	2015	Pyke	P
CCRW vs LW distinguishability	n/a	CCRW often mimics LW	–	2015	Auger-Methe et al	P
CELLS						
CD8+ T cells in infected brain	μ (run lengths)	2.15	–	2012	Harris et al	P
brain T cells reanalysis	model selection	CRW not Levy	–	2023	F1000Research 12:87	P
metastatic melanoma B16-F10 in vivo	μ (persistence; TPL)	2.36 ±0.13	–	2018	Huda et al	P
metastatic lines PC-3M/MDA-MB-231/B16-F1	μ	$1<\mu<3$ source Table 1	–	2018	Huda et al	P
non-metastatic lines PC-3/MCF-7/B16-F0	μ	>3 (diffusive)	–	2018	Huda et al	P

continued on next page

Table 4, continued.

System	Quantity	Value	Dec.	Year	Source	G
swarming B. subtilis & S. marcescens	MSD a; tail g; stable b	a=1.6; g=2.5; b=1.27	–	2015	Ariel et al	P
HUMAN						
mobile phone users (100k; 16.3M jumps)	β of truncated PL	1.75 ±0.15	–	2008	Gonzalez	P
banknote dispersal USA	μ = 1+β	1.59 β=0.59±0.02	–	2006	Brockmann	P
banknote rest/waiting times	waiting exponent 1+a	1.60 a=0.60±0.03	–	2006	Brockmann et al	P
human GPS walks, 5 outdoor sites	truncated-Pareto tail index	0.66-1.02 by site pauses 0.45-1.68	–	2011	Rhee et al	P
Hadza hunter-gatherers	LW best-fit fraction	0.40	–	2014	Raichlen et al	P
rural human foragers	truncated PL flights	reported	–	2018	PLOS ONE 13:e099	P
FINANCIAL-CLASSIC						
S&P 500 returns central region	stable α	1.4	–	1995	Mantegna & Stanley	C
FINANCIAL						
index returns central region re-measure	α	1.6 (pos) / 1.7 (neg) ±0.1	–	1999	Gopikrishnan et al	P
index return tails (inverse cubic)	tail α	2.95 (pos) / 2.75 (neg) ±0.07 / ±0.13	–	1999	Gopikrishnan et al	P
PHYSICS-CLASSIC						
CdSe quantum dot blinking	m of P(t)$\sim$t^{-m}	1.53 ±0.02	–	2001	Shimizu et al via Frantsuzov revie	C
PHYSICS						
resonant photons in hot Rb vapor	step α	2.41 ±0.12	–	2013	Baudouin et al	P
Levy glass (engineered scatterer)	designed α	1.0	–	2008	Barthelemy	C
ultracold Rb, 1D dissipative lattice	Levy exponent (depth-tuned)	1-2 range	–	2012	Sagi et al	P
CdTe quantum dot blinking	m	1.6 ±0.1	–	2001	same group via Frantsuzov review	C
energetic ions upstream of termination shock	MSD exponent a	1.30 1.29-1.32	–	2009	Perri & Zimbardo	P
energetic particles at heliospheric shocks	μ (a=3-μ)	1<μ<2	–	2015	Perri et al	P

continued on next page

Table 4, continued.

System	Quantity	Value	Dec.	Year	Source	G
THEORY						
theory benchmark: sparse targets	optimal μ	2.0	–	1999	Viswanathan et al	P
META						
cross-domain compendium	review anchor	n/a	–	2015	Zaburdaev	P

26 Critiques and the exact scope: the albatross retraction as the field's own case study

No episode in any of the four records is more instructive than the rise and fall of the founding albatross result, and the audit gives it in full.

The 1996 flight-duration data carried an artifact: wet-dry logger records counted time sitting on the water as flight, and the longest "flights" — the tail that made the power law — were birds on the sea surface. When Edwards et al. (2007) corrected the artifact and refitted with likelihood methods, the albatross data preferred a gamma distribution; the same paper reanalyzed the deer and bumblebee datasets that had extended the original claim and rejected Lévy fits for those too. The founding observation of the field was, by its own founders' participation in the reanalysis, withdrawn.

What happened next is why this record deserves respect rather than dismissal. The field adopted the estimator reforms wholesale; the 2008–2012 marine campaigns were designed *around* the critique (GPS rather than wet-dry loggers, MLE rather than binning, model selection built in); and when the higher-resolution albatross GPS data arrived, the verdict was neither the original claim nor its negation: about a third of individual birds show truncated power-law movement, the rest do not (Humphries et al., 2012). Meanwhile the skeptical literature matured into its own program: Pyke (2015) argues the optimality result itself is fragile (destructive versus non-destructive targets, learning, memory); Auger-Méthé et al. (2015) formalized the composite-walk mimicry; and the mussel-bed case shows the full cycle in miniature — an original $\mu = 2.0$ (de Jager et al., 2011), a single-power-law refit at 1.397, and a Weierstrassian-walk rereading at 2.195, all three in Table 4, none of them final.

The scope that survives: *scale-free movement inside the Lévy window is established across marine predators, immune and metastatic cells, human mobility aggregates, and engineered photonic and atomic systems; the adaptive hypothesis — that the exponent is tuned to $\mu = 2$ by selection — remains open; and any single-system claim stands only as strongly as its estimator and its model comparison.* That is a weaker sentence than the field's popular tellings and a stronger one than its obituaries.

Figure 3: The Lévy landscape: measured tail exponents against the ballistic and diffusive boundaries and the optimum $\mu = 2$. The 30 quantitative exponents of Table 4, grouped by domain, on the density convention $P(\ell) \sim \ell^{-\mu}$ with stable-law and mean-square-displacement entries converted per each row's own dictionary. The shaded band is the Lévy regime $1 < \mu \leq 3$; the solid line is the sparse-target optimum $\mu = 2$ of Viswanathan et al. (1999). The thirteen entries that cannot sit on this axis — the reanalysis verdicts, the no-Lévy findings, the fraction-of-fits rows — are printed in the footnote strip of the figure itself, because the skeptical half of the record is part of the record. Markers and grade tags as in Figure 2.

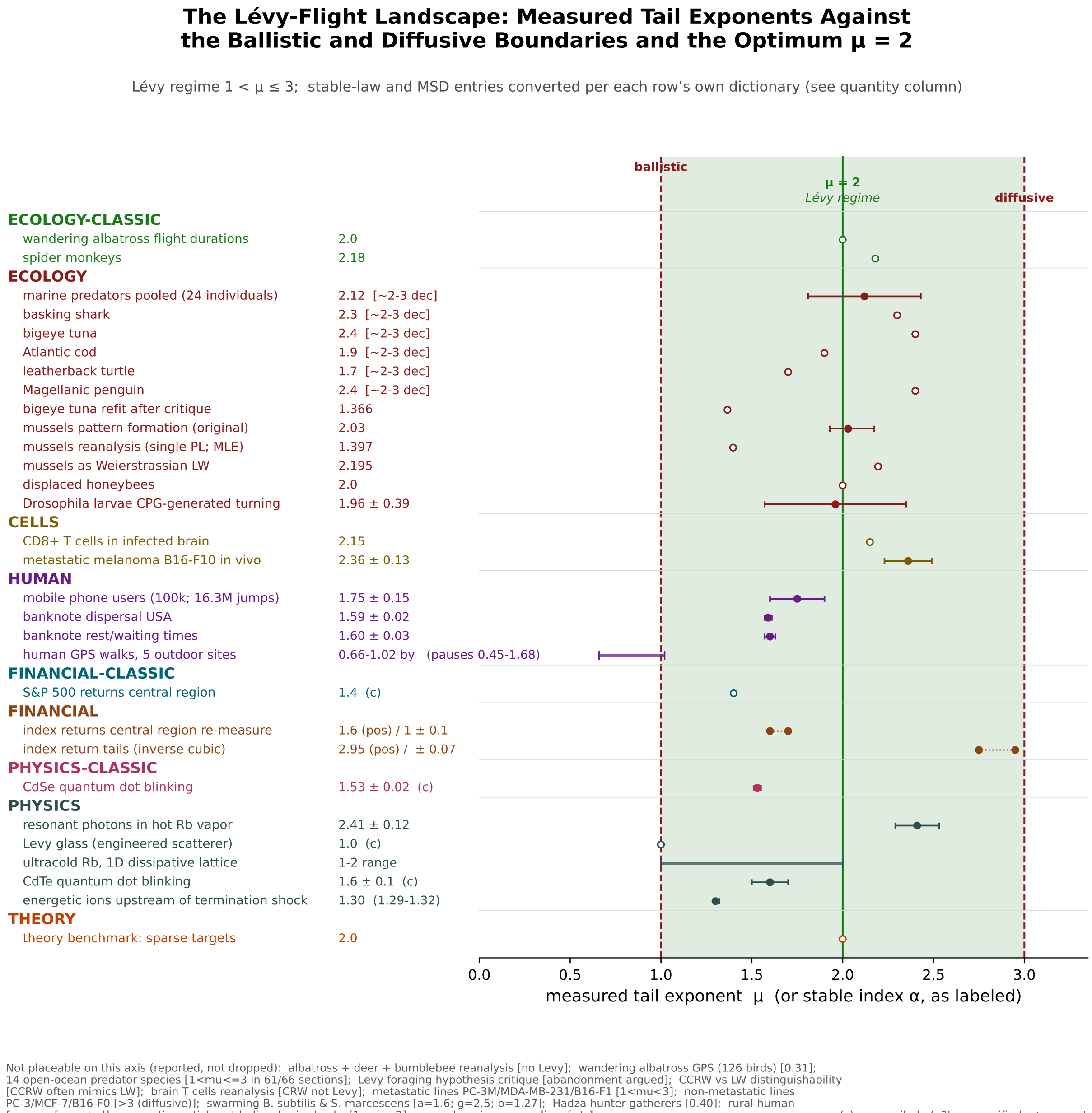

27 Closing remarks: what a life scientist should take from this Part

Three things. First, the reformation worked: post-2007 rows of Table 4 rest on likelihood fits with explicit cutoffs and model comparison — this record's second generation earned the trust its first squandered. Second, the exponent alone underdetermines the mechanism: $\mu \approx 2$ is consistent with tuned search, composite Brownian switching, or environment-imposed step structure, and only auxiliary measurements — waiting times, turn angles, a second signature — separate them: one more reason Part VIII's audit is the right instrument. Third, the cellular rows change what is at stake: a migration exponent that separates metastatic from non-metastatic lines means the question this record asks stopped being about albatrosses some time ago.

Part VI
Fractality

From Richardson's coastline to the exact dimensions of critical geometry, the measured record, and the one-decade problem

This Part audits the record of the power law in *space*: sets whose measured content scales with a non-integer exponent of the measuring scale. It is the record with the largest gap between its best and worst entries. At the top sit dimensions that are *theorems* — the exact values of two-dimensional critical geometry, proved through Schramm–Loewner evolution, which turn fractal dimension from a fitted number into a rigorous branch of conformal field theory and make this Part the natural bridge between the biological records and Part X's CFT review. At the bottom sits the published finding, from inside the field, that the median claimed "fractal" in the experimental literature spans barely more than one decade of scale — too little to distinguish a fractal from almost anything. The audit's job is to keep both truths in one table.

For the program of Part II, this record supplies the spatial face of the one exponent: the dimension dictionary that Part VIII tests, and that Part XII derives, reads the fractal dimension of a living structure as the same generator the tails and the spectra measure. The one-decade problem cuts against that claim as sharply as against any other, and the grades below are assigned with it in view.

28 Historical development: from Richardson's coastline to critical geometry

28.1 The coastline and the divider

Richardson measured the west coast of Britain with dividers of decreasing span ε and found the measured length growing without bound,

$$L(\varepsilon) \propto \varepsilon^{1-D}, \qquad D \approx 1.25, \tag{7}$$

an observation Mandelbrot (1967) turned into a question — *How long is the coast of Britain?* — and an answer: the question has no answer, and the exponent that replaces it is a dimension between the topological 1 and the embedding 2. The physics intuition that made the paper a founding document: a coastline is roughness *all the way down* the measured window, so the right invariant is not a length but the rate at which length diverges. Richardson's own data already showed the second lesson of the record — the exponent is not universal (Britain 1.25, Australia 1.13, South Africa 1.02, the smooth end) — and Mandelbrot's 1982 synthesis built the vocabulary (box, divider, mass, correlation dimensions) the whole record now uses.

28.2 Growth models and the laboratory

The 1980s made fractals physics rather than description. Diffusion-limited aggregation (Witten and Sander, 1981) showed that a trivially simple growth rule — random walkers sticking where they land — generates clusters of dimension $D \approx 1.71$ in the plane, reproduced in electrodeposition, viscous fingering, and dielectric breakdown ($D \approx 1.7$; Niemeyer et al., 1984); colloid aggregation split into two universality classes, diffusion-limited ($D \approx 1.86$) and reaction-limited ($D \approx 2.1$), each confirmed across chemically distinct systems (Lin et al., 1989). The lesson these entries carry in Table 5: where a growth mechanism is identified, the dimension is reproducible across systems to a few percent — the fractal record's analog of universality, and the standard the field entries mostly do not meet.

28.3 Dimension becomes exact

The record's top block is the twenty-first century's contribution. For two-dimensional critical systems, conformal invariance plus Schramm's one-parameter family of conformally invariant random curves (SLE_κ) yields *exact* dimensions: the self-avoiding walk at 4/3 (Lawler et al., 2001, Nienhuis, 1982), the planar Brownian frontier at 4/3 (proved, not conjectured; Lawler et al., 2001), the percolation hull at 7/4 and its external perimeter at 4/3, the percolation cluster mass dimension at 91/48. These values do for fractality what Onsager did for scaling: they supply the exact targets that make measured agreement meaningful. Where a laboratory system can be argued into one of these classes, its dimension is predicted to four digits before anyone measures — which is the standard of success the Qi-CON account must ultimately be held to as well.

29 What is actually measured: box, mass, correlation — and why they differ

The word "dimension" covers at least five estimators, and rows of Table 5 are comparable only within an estimator. The three that carry most of the record:

Box dimension. Cover the set with boxes of side ε; count $N(\varepsilon) \sim \varepsilon^{-D_0}$. It is the workhorse and the most abused: finite samples bound the accessible window from below by resolution and above by set size, and the fitted slope is exquisitely sensitive to where the fit starts and stops.

Mass dimension. For a connected object, mass within radius R of a point: $M(R) \sim R^{D_m}$. This is the growth-model estimator, and the one the exact SLE values refer to.

Correlation dimension. The pair-count integral $C(r) \sim r^{D_2}$ of dynamical-systems practice; always $D_2 \leq D_0$, with equality only for homogeneous fractals — so a measured gap between estimators is not error, it is multifractality, and the turbulence rows (information dimension $D_1 = 2.87$, interface dimension ≈ 2.4) are the record's standing example (Sreenivasan and Meneveau, 1986).

Two consequences for reading the record. First, an *anisotropic* or *self-affine* object — a fracture surface, a river's long profile — has direction-dependent scaling, and its "dimension" is a roughness exponent in disguise: the fracture rows are printed as the roughness ζ their literature reports

($\zeta \approx 0.78$ universal at large scales, ≈ 0.5 quasistatic at small; Bouchaud, 1997), with the crossover scale a material property. The two-regime structure — one exponent below a crossover, another above — recurs across the record and is exactly the windowed-homogeneity picture the Qi-CON account requires; the fracture literature found it by measurement a decade before anyone asked for it. Second, biological "dimensions" from clinical imaging (cortex, trabecular bone, retinal vessels) inherit every artifact of segmentation, and their spread across methods — the human cortex row spans 2.09–2.8 across studies — measures the methods more than the cortex.

30 The record: 45 dimensions

Figure 4 plots 43 of the 45 rows against the exact values and the embedding dimensions (the Avnir survey row is a statement about the record itself, held for §31, and the galaxy homogeneity scale is a length, not a dimension); Table 5 prints all 45. Grades after the verification pass: 34 P, 8 C, 3 U? — the pass reached even the older field literature through abstracts and faithful mirrors, and the three surviving U? rows (DLCA, trabecular bone, the soil interface) stay flagged.

Three observations organize the landscape.

First, **the exact block and the growth block agree, and that agreement is the record's bedrock.** Laboratory DLA sits on the theoretical 1.71; dielectric breakdown sits with it; the two colloid classes are textbook universality. Where mechanism is known, dimension behaves like a critical exponent — reproducible, class-dependent, predictable.

Second, **the biological block is genuinely fractal but narrowly windowed.** Vascular networks separate cleanly — tumor vasculature at 1.89 ± 0.04 against normal at 1.70 ± 0.03, a diagnostic-grade difference (Baish and Jain, 2000) — retinal vessels sit near 1.7, the CT-measured airway tree at 1.56, and dendritic arbors at 1.4; but the arbor study itself reports fractality over ~ 1.5 decades (4–141 μm) with single dendrites nearly line-like at 1.035 (Smith et al., 2023) — ensemble fractality built from non-fractal parts, over a window the width of Avnir's complaint. The block is real; its windows are short; both facts are in the table.

Third, **the astrophysical rows end the record's oldest controversy in a draw with a boundary.** Galaxy clustering is fractal-like with $D_2 \approx 2$ at small scales — the Sylos-Labini school was right there — and crosses to homogeneity, $D_2 \to 3$ within one percent, by $71\,h^{-1}$ Mpc on the WiggleZ sample (Scrimgeour et al., 2012) — the homogeneity school was right at large. A fractal regime with a measured upper knee: the record's largest-scale instance of the bounded window every other block shows.

Figure 4: The fractality landscape: measured dimensions against the exact values of two-dimensional critical geometry. The 43 plottable rows of Table 5, grouped by domain. Diamonds are exact values (SLE/CFT theorems and the KPZ roughness 1/2); gray verticals mark embedding dimensions $d = 1, 2, 3$; dashed purple lines mark the exact 4/3, 7/4, and 91/48. Ranges (method-dependent clinical values, the soil interface, Lisbon's growth) are drawn as bars without central markers, because the spread is the datum. The two rows not plottable on a dimension axis — the Avnir decade census and the $71\,h^{-1}$ Mpc galaxy homogeneity scale — are printed on the figure's footnote strip. Markers and grade tags as in Figure 2.

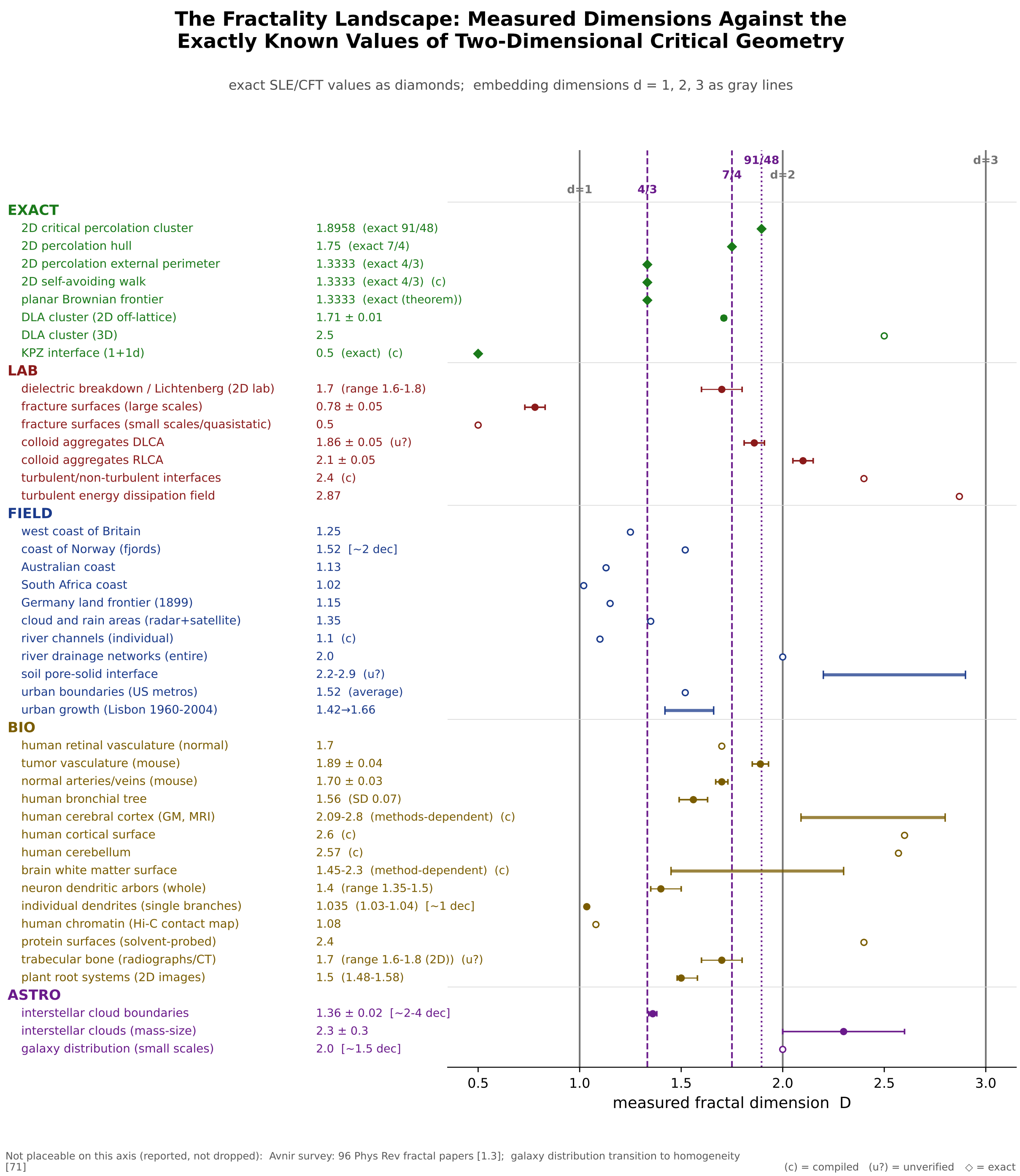

Table 5: The fractality record: 45 measured dimensions. Box, mass, correlation, divider, and surface dimensions across exact two-dimensional critical geometry, laboratory growth, field geomorphology, biology, and astrophysics. The exact SLE/CFT block anchors the table: those dimensions are theorems, and every measured row can be judged against the honesty of its Dec. column — the compilation's two-decade concern of §31 applies throughout. Grades and columns as in Table 2.

System	Quantity	Value	Dec.	Year	Source	G
EXACT						
2D critical percolation cluster	mass dimension	1.8958 exact 91/48	–	1987	den Nijs / Nienhuis exact	P
2D percolation hull	hull dimension	1.75 exact 7/4	–	1987	Saleur & Duplantier	P
2D percolation external perimeter	perimeter dimension	1.3333 exact 4/3	–	1999	Aizenman	P
2D self-avoiding walk	path dimension	1.3333 exact 4/3	–	1982	Nienhuis	C
planar Brownian frontier	frontier dimension	1.3333 exact (theorem)	–	2000	Lawler	P
DLA cluster (2D off-lattice)	mass dimension	1.71 ∼±0.01	–	1981	Witten & Sander	P
DLA cluster (3D)	mass dimension	2.5	–	1983	Meakin	P
KPZ interface (1+1d)	roughness α	0.5 exact	–	1986	Kardar	C
LAB						
dielectric breakdown / Lichtenberg (2D lab)	branch dimension	1.7 range 1.6-1.8	–	1984	Niemeyer	P
fracture surfaces (large scales)	roughness ζ	0.78 ±0.05	–	1997	Bouchaud	P
fracture surfaces (small scales/quasistatic)	roughness ζ	0.5	–	2001	Bouchaud and co-workers	P
colloid aggregates DLCA	mass dimension	1.86 ∼±0.05	–	1989	Lin et al	U?
colloid aggregates RLCA	mass dimension	2.1 ±0.05	–	1990	Lin et al	P
turbulent/non-turbulent interfaces	surface dimension	2.4	–	1986	Sreenivasan & Meneveau	C
turbulent energy dissipation field	information dimension D1	2.87	–	1988	Meneveau & Sreenivasan	P
FIELD						
west coast of Britain	divider dimension	1.25	–	1967	Mandelbrot	P
coast of Norway (fjords)	divider/box dimension	1.52	∼2	1988	Feder	P
Australian coast	divider dimension	1.13	–	1967	Mandelbrot	P
South Africa coast	divider dimension	1.02	–	1967	Mandelbrot	P

continued on next page

Table 5, continued.

System	Quantity	Value	Dec.	Year	Source	G
Germany land frontier (1899)	divider dimension	1.15	–	1967	Mandelbrot	P
cloud and rain areas (radar+satellite)	area-perimeter dimension	1.35	–	1982	Lovejoy	P
river channels (individual)	divider dimension	1.1	–	1988	Hjelmfelt via Tarboton ScD thesis	C
river drainage networks (entire)	network dimension	2.0	–	1988	Tarboton et al	P
soil pore-solid interface	surface dimension	2.2-2.9	–	2001	Dathe et al	U?
urban boundaries (US metros)	boundary dimension	1.52 average	–	1994	via Batty & Longley	P
urban growth (Lisbon 1960-2004)	urban form dimension	1.42→1.66	–	2004	via fractal-city compilation	P
BIO						
human retinal vasculature (normal)	box/mass dimension	1.7	–	2004	Masters	P
tumor vasculature (mouse)	vessel network dimension	1.89 ±0.04	–	2000	Baish & Jain	P
normal arteries/veins (mouse)	vessel network dimension	1.70 ±0.03	–	2000	Baish & Jain	P
human bronchial tree	airway tree dimension	1.56 SD 0.07	–	2018	Bodduluri et al	P
human cerebral cortex (GM, MRI)	box dimension	2.09-2.8 methods-dependent	–	2023	Grosu et al	C
human cortical surface	surface dimension	2.6	–	1988	Majumdar & Prasad via Grosu	C
human cerebellum	surface/volume dimension	2.57	–	2003	Liu et al via Grosu	C
brain white matter surface	surface dimension	1.45-2.3 method-dependent	–	1996	Cook / Free via Grosu	C
neuron dendritic arbors (whole)	box dimension	1.4 range 1.35-1.5	≤1.5	2023	Smith lab	P
individual dendrites (single branches)	dimension	1.035 1.03-1.04	∼1	2023	Smith lab	P
human chromatin (Hi-C contact map)	$P(s) \sim s^{-g}$	1.08	–	2009	Lieberman-Aiden et al	P
protein surfaces (solvent-probed)	surface dimension	2.4	<1	1985	Lewis & Rees	P
trabecular bone (radiographs/CT)	texture/box dimension	1.7 range 1.6-1.8 (2D)	–	1999	Majumdar et al and successors	U?

continued on next page

Table 5, continued.

System	Quantity	Value	Dec.	Year	Source	G
plant root systems (2D images)	box dimension	1.5 1.48-1.58	–	1989	Tatsumi	P
ASTRO						
interstellar cloud boundaries	perimeter dimension	1.36 ±0.02	∼2-4	1991	Falgarone	P
interstellar clouds (mass-size)	mass dimension	2.3 ±0.3	–	1996	Elmegreen & Falgarone	P
galaxy distribution transition to homogeneity	D2 reaches 3 within 1% at 71 h	71 ±8 h^{-1} Mpc	–	2012	Scrimgeour et al	P
galaxy distribution (small scales)	correlation D2	2.0	∼1.5	1998	Sylos Labini et al	P
META						
Avnir survey: 96 Phys Rev fractal papers	decades of scaling (mean)	1.3 range 0.5-2.0	–	1998	Avnir	P

31 Critiques and the exact scope: the one-decade problem

The fractal record's great critique came from inside, and it is quantitative. Avnir et al. (1998) surveyed 96 experimental papers in the Physical Review journals reporting fractal analyses and found the claimed scaling ranges averaged **1.3 decades**, with the bulk between 0.5 and 2.0 — windows over which, as they put it, a power law cannot be distinguished from many alternatives, so that most claimed empirical fractals are, on the published evidence, statements about curve fitting over an octave and a half. The critique was resisted and never refuted; twenty-five years later the dendritic-arbor study — among the best modern biological entries — reports fractality over 1.5 decades and says so plainly.

This supplement's response is structural rather than rhetorical. The Dec. column of Table 5 prints the fitted range wherever the source reports one; its *blankness* across most of the field and biological blocks is the Avnir finding, reproduced in this compilation's own experience; and Part VIII's audit uses no dimension whose pairing does not survive at the published uncertainties. The exact and growth blocks are immune to the critique — theorems have no windows, and the growth experiments span 2–3 decades with mechanism identified — which is precisely why they anchor the Part.

Beside the decade problem, two standing cautions. Estimator mismatch: comparing a box dimension to a mass dimension to a correlation dimension across studies manufactures spread — the cortical range 2.09–2.8 is substantially this. And self-affinity: quoting one dimension for an anisotropic set averages two exponents the better literature keeps separate.

32 Closing remarks: what a life scientist should take from this Part

The exact block means fractal dimension is not a metaphor: in two dimensions the values are theorems, and agreement with them is as sharp a test as physics owns. The growth block means dimensions travel in universality classes when mechanism is fixed — a measured dimension is a fingerprint, as the tumor-vasculature pair shows. The Avnir census means most claimed biological fractals are windowed statements; a dimension without window and estimator is decoration. And the record's repeated finding of *bounded* regimes — fracture's crossover, the galaxy homogeneity scale, the arbor's 1.5 decades — is not fractality failing but its actual empirical shape: scale invariance lives in windows — the form the Qi-CON account predicts and Part XII derives.

Part VII
$1/f$ Spectra and the Two Knees

From Johnson's vacuum tubes to the aperiodic cortex, the measured record, and the census of where the band actually ends

This Part audits the record of the power law in *time*. It is the oldest continuously open problem of the four — the founding measurement is Johnson's 1925 study of current fluctuations in vacuum tubes, and the phenomenon has been called the oldest unsolved problem in condensed-matter physics without much exaggeration — and it is the record where the Qi-CON account stakes its most distinctive claim. Everyone predicts the slope; slopes near $\beta = 1$ fall out of half a dozen mechanisms. What the boundary law predicts is a *band*: $S(f) \sim f^{-\beta}$ between an infrared knee f_{IR} set by the largest retained scale and an ultraviolet knee f_{UV} set by the smallest, both at derivable places. So this Part does something the $1/f$ literature itself almost never does: alongside the census of slopes (§35), it compiles a census of *knees* (§36) — every system in the compilation for which the literature reports where the band bends, or reports having looked and found no bend. The censuses are unequal in size, and the inequality is the finding.

Part II's frame sharpens the stake further: in the boundary law the two knees are not free parameters but the two ends of the projection window — the largest and smallest retained scales of the partial view — which is why the knee census, and not the slope census, is where the account is most exposed.

33 Historical development: from Johnson noise to the aperiodic cortex

33.1 Electronics owns the first fifty years

Johnson found the excess low-frequency noise in thermionic tubes in 1925 (Johnson, 1925); Schottky named a wrong mechanism for it within the year, and the field has been naming mechanisms since. The empirical shape settled early: voltage or current fluctuations with

$$S(f) \;\propto\; \frac{1}{f^{\beta}}, \qquad \beta \approx 0.8\text{–}1.4, \tag{8}$$

in metals, semiconductors, carbon resistors, and eventually every electronic device class anyone measured (Dutta and Horn, 1981, Voss and Clarke, 1976), with Hooge's empirical formula organizing the semiconductor magnitudes (Hooge, 1969) and the McWhorter and Dutta–Horn frameworks supplying the standard mechanism: a broad distribution of activated two-state switchers. That mechanism deserves its three lines of mathematics, because it is the null model every deeper account must beat. A single two-state fluctuator with relaxation time τ contributes a Lorentzian,

$$S_\tau(f) = \frac{4\,\tau}{1 + (2\pi f \tau)^2}, \tag{9}$$

flat below its knee $1/(2\pi\tau)$ and f^{-2} above. Superpose fluctuators with activation energies spread flat over a range — so that $p(\tau) \propto 1/\tau$ over $\tau_{\min} < \tau < \tau_{\max}$ — and the sum integrates to

$$S(f) \;\propto\; \frac{1}{f} \qquad \text{for} \qquad \frac{1}{2\pi\tau_{\max}} \;\ll\; f \;\ll\; \frac{1}{2\pi\tau_{\min}}, \tag{10}$$

exactly $1/f$, and — the point this Part keeps returning to — *bounded by two knees at the edges of the τ distribution.* The textbook mechanism itself says the band must end somewhere at both ends; the literature built on it almost never reports finding either end. Physics intuition: $1/f$ means every decade of timescale contributes equal power, so the spectrum is a census of the system's active timescales, and its knees are the census takers' first and last entries.

33.2 The phenomenon leaves the laboratory

Voss and Clarke found $1/f$ in the loudness and pitch fluctuations of music and speech (Voss and Clarke, 1975); Hurst had already found its integrated cousin in the Nile minima in 1951, the origin of the Hurst exponent (Hurst, 1951); heartbeat intervals (Kobayashi and Musha, 1982, Peng et al., 1993), human gait (Hausdorff et al., 1995), reaction-time series (Gilden et al., 1995), internet traffic (Leland et al., 1994), and accreting black holes (González-Martín and Vaughan, 2012) followed. Self-organized criticality (Bak et al., 1987) offered a unifying mechanism in 1987 — driven dissipative systems poised at a critical point generate scale-free avalanches and $1/f$-like spectra without tuning — and its career since (the original model's spectrum turned out to be $1/f^2$ in the relevant regime; real sandpiles mostly do not oscillate the way the model does; rice piles do, for elongated grains) is the field's standing caution about beautiful mechanisms. The modern neuroscience chapter is the record's most active: the cortical field potential is dominated by an aperiodic $1/f$-like component, now parameterized as a matter of standard practice (Donoghue et al., 2020), with a measured knee corresponding to intrinsic timescales of tens of milliseconds (Gao et al., 2020), systematic flattening with age, and a proposed reading of the slope as an excitation–inhibition balance — the one community that has begun treating the knee as data rather than nuisance.

34 What is actually measured: β, its estimators, and its dictionaries

The spectral exponent arrives through at least three estimator families, and the record mixes them.

Direct spectral fits (periodogram, Welch, multitaper) give β over a stated band — when the band is stated. The neuroscience literature's current practice separates the aperiodic component from oscillatory peaks and fits $L(f) = b - \log(k + f^\chi)$, whose knee parameter k maps to a timescale $\tau = 1/(2\pi f_k)$ (Donoghue et al., 2020); this is the methodological reason the knee census's best-populated column is neural.

Detrended fluctuation analysis gives a scaling exponent α_{DFA} of the integrated series; for stationary fractional Gaussian noise the dictionary is

$$\beta \;=\; 2\,\alpha_{\mathrm{DFA}} - 1 \qquad (\text{fGn},\, 0 < \beta < 1), \tag{11}$$

and for nonstationary fractional Brownian motion $\beta = 2\alpha_{\mathrm{DFA}} + 1$. The two branches meet at the $1/f$ point $\beta = 1$, $\alpha_{\mathrm{DFA}} = 1$ — which is one honest reason the biological literature keeps finding values near 1: it is the boundary of two estimator regimes as well as a possible attractor. Table 6 converts DFA and Hurst entries only where the row says so, and Part VIII tests the dictionary itself on the systems where both sides were measured independently.

Hurst rescaled-range estimates from the hydrology and traffic literatures relate as $\beta = 2H - 1$ for stationary increments; Hurst's ensemble mean $K \approx 0.72$ over 690 geophysical records and Ethernet's $H = 0.85$–0.95 enter the landscape through that dictionary.

One warning owned by the cognitive block: estimator bias against alternatives. Wagenmakers et al. (2004) showed that the reaction-time $1/f$ claims of Gilden et al. (1995) weaken severely under spectral re-estimation with proper accounting for the white-noise floor — the record's cleanest case of a celebrated $\beta \approx 1$ dropping to a task-dependent 0.3–0.65 under reanalysis, and both rows are printed.

35 The record: 44 spectral exponents

Figure 5 plots the 38 quantitative rows against the white ($\beta = 0$), pink ($\beta = 1$), and Brownian ($\beta = 2$) references with the $1/f$ band $0.5 \le \beta \le 1.5$ shaded; Table 6 prints all 44. Grades after the verification pass: 26 P, 16 C, 2 U?. At the compilation checkpoint this record was much the weakest of the four (7 P, 25 U?), because its founding literature (1925–1981) sits behind paywalls; the dedicated verification pass recovered nearly all of it through abstracts, author mirrors, and named secondaries — and turned up five corrections along the way, printed in the rows they correct.

Structure worth the reader's eye. The electronics block sits on $\beta = 1$ by construction — those rows are the definition of the phenomenon — with the Dutta–Horn survey's honest spread 0.8–1.4. The neural block does *not* sit on 1: broadband ECoG runs 2–2.5, with a documented steepening to ≈ 4 above 75 Hz (Miller et al., 2009), scalp EEG and MEG sit at 1.3 and 1.1, and BOLD at 0.8 — the modality dependence is systematic, not noise, and any account that predicts a single cortical β without specifying the measurement operator is already wrong. The physiological and cognitive blocks cluster on 0.8–1.1 with the Wagenmakers caveat standing. The climate block is split by the record itself into two regimes — $\beta \approx 0.4$–0.6 below the centennial scale, 1.3–1.6 above it (Huybers and Curry, 2006) — the one entry where a spectral *break* is the headline rather than a footnote. And the astrophysical rows carry their own pairs of slopes about measured break frequencies, long the standard practice of X-ray timing — the one older community that always reported its knees, because its knees scale with black-hole mass and were therefore interesting.

Figure 5: The $1/f$ landscape: measured spectral exponents across eleven domains. The 38 quantitative rows of Table 6, grouped by domain, on the convention $S(f) \sim 1/f^{\beta}$. The shaded band is $0.5 \leq \beta \leq 1.5$; dashed lines mark white noise ($\beta = 0$) and Brownian noise ($\beta = 2$). Split values joined by dots are the slopes below and above a break the source reports (astrophysical timing, the climate continuum, high-frequency ECoG). DFA and Hurst entries are converted by their stated dictionaries only. The six rows not plottable on a β axis are printed on the figure's footnote strip. Markers and grade tags as in Figure 2; note that this record carries the compilation's highest unverified fraction, and every (u?) row is excluded from Part VIII.

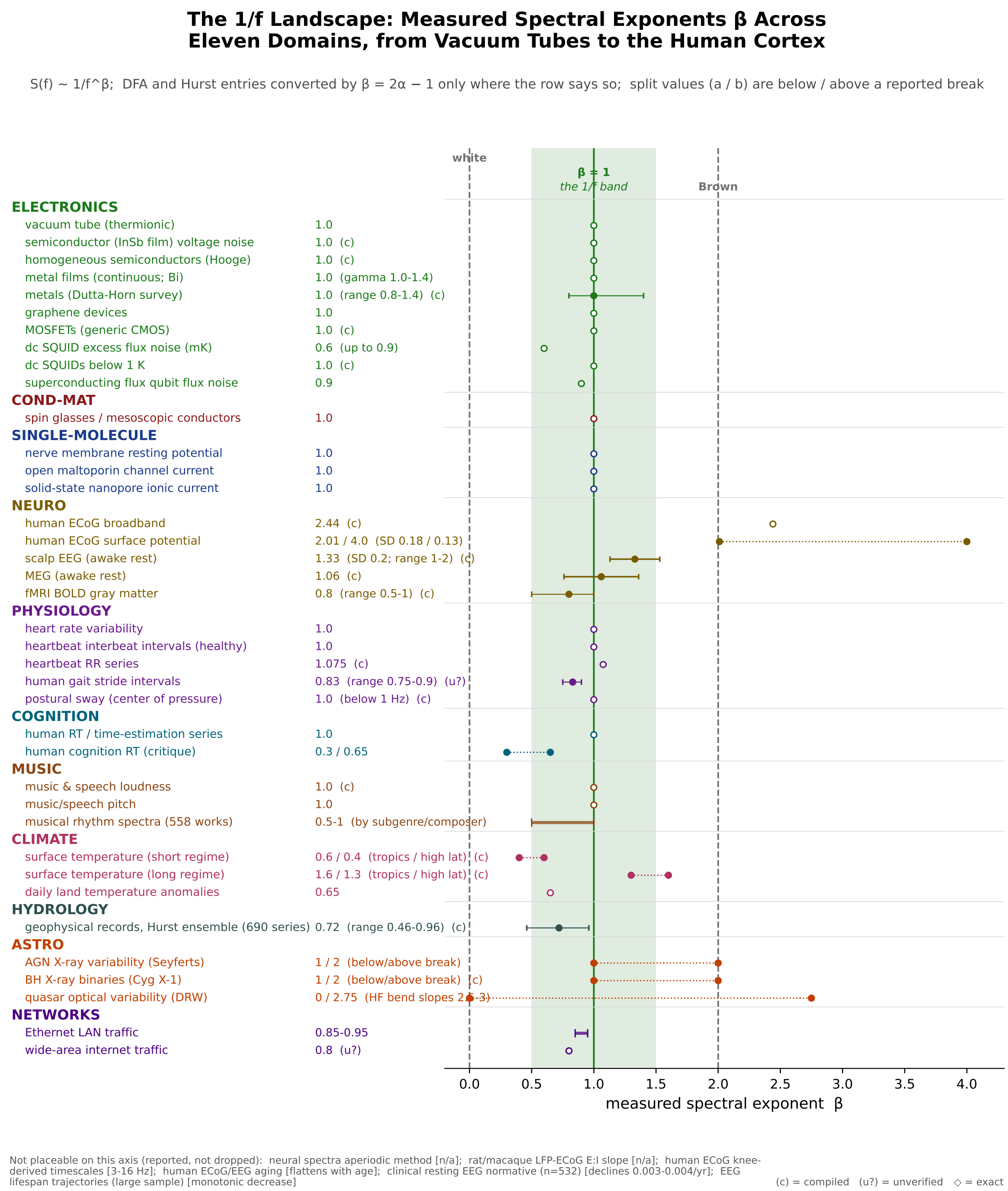

Table 6: The $1/f$ record: 44 measured spectral exponents. Spectral exponents β (in $S(f) \sim 1/f^{\beta}$) from electronics, condensed matter, single molecules, neuroscience, physiology, cognition, music, climate, hydrology, astrophysics, and network traffic. Dec. here reports the measured frequency band where the source states one. DFA and Hurst entries are converted only where the row's quantity column says so. Grades and columns as in Table 2.

System	Quantity	Value	Dec.	Year	Source	G
ELECTRONICS						
vacuum tube (thermionic)	β	1.0	excess below ∼few hund..	1925	Johnson	P
semiconductor (InSb film) voltage noise	β	1.0	$1{\times}10^{-6.3}$ to 1 Hz	1974	Caloyannides	C
homogeneous semiconductors (Hooge)	β	1.0 alpha_H = $2{\times}10^{-3}$ (1969); device ra..	–	1969	Hooge	C
metal films (continuous; Bi)	β	1.0 γ 1.0-1.4	–	1976	Voss & Clarke	P
metals (Dutta-Horn survey)	β	1.0 range 0.8-1.4	–	1981	Dutta & Horn	C
graphene devices	γ	1.0	f < 100 kHz	2013	Balandin	P
MOSFETs (generic CMOS)	β	1.0	–	2013	Balandin review	C
dc SQUID excess flux noise (mK)	α	0.6 up to 0.9	10 Hz-100 kHz	2011	Drung et al	P
dc SQUIDs below 1 K	β	1.0	–	1987	Wellstood	C
superconducting flux qubit flux noise	α	0.9	0.01-100 Hz and 0.2-20..	2011	Yan et al	P
COND-MAT						
spin glasses / mesoscopic conductors	β	1.0	–	1988	Weissman	P
SINGLE-MOLECULE						
nerve membrane resting potential	β	1.0	–	1968	Verveen & Derksen	P
open maltoporin channel current	β	1.0	–	2000	Bezrukov & Winterhalter	P
solid-state nanopore ionic current	β	1.0	f < ∼100 Hz	2008	Smeets et al	P
NEURO						
human ECoG broadband	β	2.44	1-100 Hz	2010	He et al	C
human ECoG surface potential	β	2.01 / 4.0 SD 0.18 / 0.13	15-80 and 80-500 Hz	2009	Miller et al	P
scalp EEG (awake rest)	β	1.33 SD 0.2; range 1-2	0.1-10 Hz	2010	Dehghani et al	C
MEG (awake rest)	β	1.06 SD 0.3 (noise-corrected)	0.1-10 Hz	2010	Dehghani et al	C
fMRI BOLD gray matter	β	0.8 range 0.5-1	f < 0.1 Hz	2011	He	C

continued on next page

Table 6, continued.

System	Quantity	Value	Dec.	Year	Source	G
neural spectra aperiodic method	χ (method)	n/a	1-50 Hz typical	2020	Donoghue et al	P
rat/macaque LFP-ECoG E:I slope	β	n/a	30-50 Hz window	2017	Gao	P
human ECoG knee-derived timescales	f_knee	3-16 Hz	aperiodic fit	2020	Gao et al	P
human ECoG/EEG aging	β	flattens with age	–	2015	Voytek et al	P
clinical resting EEG normative (n=532)	aperiodic exponent	declines 0.003-0.004/yr	1-45 Hz	2025	Frontiers Aging Neurosci 17:154004	P
EEG lifespan trajectories (large sample)	aperiodic exponent	monotonic decrease	–	2025	bioRxiv preprint	P
PHYSIOLOGY						
heart rate variability	β	1.0	1×10^{-4} to 1×10^{-2} Hz	1982	Kobayashi & Musha	P
heartbeat interbeat intervals (healthy)	β	1.0	several decades	1993	Peng et al	P
heartbeat RR series	β	1.075	several decades	nr	Scholarpedia 1/f compilation	C
human gait stride intervals	alpha_DFA	0.83 range 0.75-0.9	–	1995	Hausdorff et al	U?
postural sway (center of pressure)	β	1.0 below 1 Hz	split at ∼1 Hz	nr	via Scholarpedia compilation	C
COGNITION						
human RT / time-estimation series	β	1.0	∼1e-3 to 0.1 cyc/trial	1995	Gilden	P
human cognition RT (critique)	β	0.3 / 0.65 RT / temporal estimation	–	2004	Wagenmakers	P
MUSIC						
music & speech loudness	β	1.0	∼3 decades	1975	Voss & Clarke	C
music/speech pitch	β	1.0	–	1978	Voss & Clarke	P
musical rhythm spectra (558 works)	β	0.5-1 by subgenre/composer	–	2012	Levitin	P
CLIMATE						
surface temperature (short regime)	β	0.6 / 0.4 tropics / high lat	decadal-centennial	2006	Huybers & Curry	C
surface temperature (long regime)	β	1.6 / 1.3 tropics / high lat	centennial-Milankovitch	2006	Huybers & Curry	C
daily land temperature anomalies	alpha_DFA	0.65	1 day-decades	1998	Koscielny-Bunde et al	P

continued on next page

Table 6, continued.

System	Quantity	Value	Dec.	Year	Source	G
HYDROLOGY						
geophysical records, Hurst ensemble (690 series)	Hurst H	0.72 range 0.46-0.96	1-800 yr	1951	Hurst	C
ASTRO						
AGN X-ray variability (Seyferts)	β	1 / 2 below/above break	break at 0.01-few days	2012	Gonzalez-Martin & Vaughan	P
BH X-ray binaries (Cyg X-1)	β	1 / 2 below/above break	break at fractions of ..	2012	same A&A compilation	C
quasar optical variability (DRW)	β	0 / 2.75 HF bend slopes 2.5-3	bend at 1×10^2-1×10^3 days	2024	Arevalo et al	P
NETWORKS						
Ethernet LAN traffic	Hurst H	0.85-0.95 0.75 low load to 0.95 busy	10 ms-100 s+	1994	Leland et al	P
wide-area internet traffic	Hurst H	0.8	–	1995	Paxson & Floyd	U?

36 The knee census

The claim that distinguishes the Qi-CON account from the slope literature is the bounded band of (10): both knees exist and sit at derivable places. So the compilation asked the record a question the record is rarely asked: *for which systems does the literature actually report where the* $1/f$ *band ends?* Figure 6 is the complete answer across the whole 245-row compilation — eight systems, on a frequency axis spanning nineteen decades.

The census splits with almost embarrassing cleanness.

Neural systems always show the knee. Human ECoG bends at 3–16 Hz, mapping to intrinsic timescales of 10–50 ms that follow the cortical hierarchy (Gao et al., 2020); macaque single-unit autocorrelations give 50–350 ms across seven areas, ordered sensory-to-prefrontal (Murray et al., 2014). Where the nervous system is measured, the infrared knee is not only present but *informative* — it is a map of the processing hierarchy.

Solid-state $1/f$ **has never shown one.** The classic semiconductor measurement tracked $1/f$ down to $10^{-6.3}$ Hz — a three-month record — without flattening (Caloyannides, 1974), and the modern flux-qubit measurement extends unbroken $1/f^{\sim1}$ flux noise across *fourteen decades*, 10^{-5} Hz to ~ 1 GHz, with no infrared knee and a superohmic crossover at the high end (Quintana et al., 2017). Whatever bounds the electronic band, no experiment has reached it from inside.

Climate bends the other way. The temperature continuum *steepens* at the centennial scale (0.4–$0.6 \to 1.3$–1.6; Huybers and Curry, 2006), and sea-surface temperatures cross over near one year (Bunde et al., 2004) — knees, but of the opposite sense to the flattening the two-knee picture

Figure 6: The knee census: every system in the compilation for which the literature reports where the $1/f$ band bends — or reports having looked and found no bend. Eight systems on a common $\log_{10} f$ axis spanning nineteen decades. Down-triangles are flattening (infrared-type) knees with their measured ranges; up-triangles are steepening crossovers; thin bands are the measured frequency ranges; open end-caps mark bands searched without finding any knee. Neural systems always show the knee, and it is informative (it maps the processing hierarchy); solid-state $1/f$ shows none over up to fourteen decades; climate bends the opposite way at the centennial scale. The sparsity of this figure against the density of Figure 5 is the finding: the literature fits slopes and rarely asks where they end, so the two-knee claim is largely untested. The often-quoted 0.005 Hz heart-rate knee is absent because no primary source for it could be found.

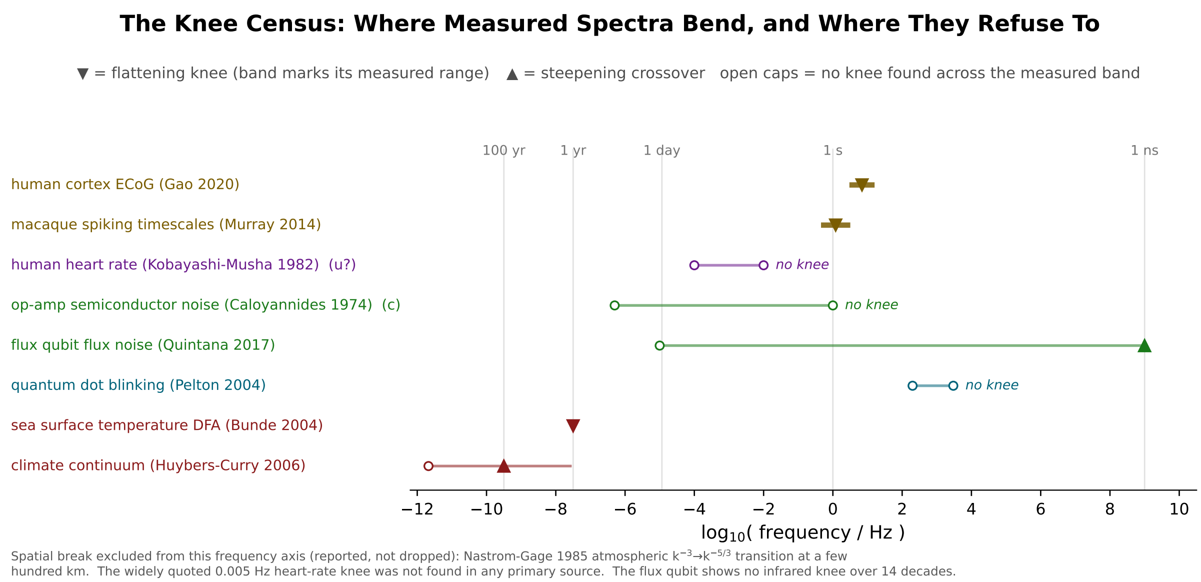

names f_{IR}.

And one negative result of the census deserves its own sentence, because this compilation went looking for the number and failed to find it: **the widely quoted ∼0.005 Hz heart-rate knee could not be traced to any primary source** — the classic data show unbroken $1/f$ down to 10^{-4} Hz (Kobayashi and Musha, 1982) — and until a primary measurement surfaces, this supplement treats the cardiac infrared knee as unmeasured.

The asymmetry between Figure 5 and Figure 6 — thirty-eight slopes, eight knees — is this Part's principal finding, and it cuts in a specific direction: *the two-knee prediction is largely untested rather than confirmed.* For the derivation Parts that is good news soberly stated — a prediction the record has not yet had the chance to falsify — and for the experimental reader it marks the highest value-per-measurement target this supplement can point to: extend any biological $1/f$ measurement two decades toward DC, and either find the knee the account requires or falsify it for that system.

37 Critiques and the exact scope: many mechanisms, and the nonstationarity trap

The $1/f$ record's skeptical literature makes three standing points, each of which this audit adopts as a constraint.

Ubiquity of the shape is not community of cause. The Lorentzian-superposition route (10), SOC, intermittency, stochastic feedback, and simple nonstationarity all produce $1/f$-like stretches, and Weissman (1988)'s review — still the subject's most rigorous — catalogs how measured $1/f$ in condensed matter arises from materially different kinetics in different systems. A one-generator account does not deny this; it predicts, additionally, relations between β and the other three exponents that mechanism-agnostic mimics have no reason to satisfy. That is why Part VIII, not the slope census, carries the discriminating weight.

Nonstationarity mimics $1/f$. A stationary process observed through a drifting baseline, or a process with slow parameter wander, produces low-frequency power that fits $\beta \approx 1$ over the window. The DFA literature exists largely to defeat this, and the cognitive-block reanalysis (Wagenmakers et al., 2004) shows how much of a celebrated β can evaporate when the accounting is done properly.

SOC's cautionary career. The proposal that launched a thousand power laws (Bak et al., 1987) claimed $1/f$ from its own dynamics; the model's actual spectrum in the relevant regime is closer to $1/f^2$, and the experimental sandpile literature delivered SOC statistics only in special geometries (elongated rice grains). The mechanism survives as an important idea with a corrected scope — and as the field's permanent reminder that a mechanism producing power laws is not yet a mechanism producing *these* power laws, with *these* knees, in *these* bands.

38 Closing remarks: what a life scientist should take from this Part

Four sentences. The slope is real and easy: across eleven domains, β near 1 is as common as the literature says, and measuring one more slope adds almost nothing. The knee is real and rare: only neuroscience and X-ray astronomy treat the band's ends as data, and where they do, the knee carries system-specific information the slope never carried. The verification pass brought this record from the worst profile of the four to 26-of-44 primary-verified, and its five corrections — among them the task-dependent cognitive slopes and the Hurst-ensemble attribution — are the pass's argument for itself. And the experimental frontier of the whole supplement, if the one-generator account is right, is two decades of patience: the band's ends, not its middle, are where the theory lives.

Part VIII
The Cross-Consistency Audit: One Exponent or Four?

The relations any one-generator account must satisfy, every system where they can be tested, and what the arithmetic shows

Parts IV–VII audited four records separately, the way their four literatures keep them. This Part does the one thing no single literature can do: it puts the records into arithmetic with one another. If the four signatures flow from one homogeneous generator — the Qi-CON claim, or any claim of that shape — then on any single system the four measured exponents are not four free numbers. They are one number wearing four disguises, and the disguises are related by dictionaries that are theorems of standard mathematics. The audit is therefore parameter-free: no fit, no tuning, one identity line. What it needs is the rare commodity Parts IV–VII were compiled to find — systems where two or more of the exponents were measured *independently on the same data*.

This is also where the posture of Part II is put to work. A program that derives its exponents owes the record an arithmetic it can fail; the audit below is built as that instrument, in the discipline of POS-7.

39 The relations the framework predicts

Five dictionaries carry the audit, and each is stated here with its provenance and its exact scope, because a relation applied outside its scope manufactures either false confirmation or false refutation.

(R1) Tail and stable index. A step distribution $P(\ell) \sim \ell^{-\mu}$ in the Lévy window $1 < \mu < 3$ has stable index $\alpha_s = \mu - 1$; the generalized central limit theorem then fixes the coarse propagator to the α_s-stable law. Scope: independent (or weakly dependent) increments; truncation pushes the effective α_s toward 2 at the largest scales.

(R2) Path dimension. An α_s-stable process in embedding dimension d has sample paths of Hausdorff dimension

$$D_f \;=\; \min(d,\ \alpha_s) \tag{12}$$

(Blumenthal and Getoor, 1960). Scope: the flight geometry itself, not the landscape the flights are drawn on; for Lévy *walks* (finite velocity) the relation acquires known corrections at the ballistic end.

(R3) The spectral dictionaries. Stationary fractional Gaussian noise with Hurst H has $\beta = 2H - 1$; its nonstationary integral (fBm) has $\beta = 2H + 1$; equivalently $\beta = 2\alpha_{\mathrm{DFA}} - 1$ on the fGn branch (11). Scope: Gaussian long-memory processes; heavy tails bias DFA estimators in documented ways.

(R4) The fractal point-process relation. A point process whose counting statistics are fractal — Fano factor growing as T^{γ_F} — has a power-law spectral exponent equal to the same γ_F; count-based and spectrum-based estimates of one exponent must agree. Scope: the estimators saturate differently (the Fano factor cannot exceed its dead-time ceiling), a bias the auditory-nerve literature dissected (Lowen and Teich, 1996).

(R5) The crackling relation. Avalanche size and duration exponents τ, τ_t and the size–duration scaling $\langle s\rangle(T) \sim T^{1/(\sigma\nu z)}$ satisfy

$$\frac{\tau_t - 1}{\tau - 1} = \frac{1}{\sigma\nu z}, \tag{13}$$

an identity of the scaling hypothesis (Sethna et al., 2001), exact at criticality for any system in a crackling class. Scope: requires the scaling regime; away from criticality all three quantities drift.

The Qi-CON account adds one clause that the dictionaries alone do not carry: the *same* α appears in all of them for a given system and window, because all four signatures read one generator (Arisaka, 2026, A7-Qi4). The dictionaries are the audit's instrument; that clause is what the audit tests.

40 The audit set: what the record actually contains

The compilation scanned roughly thirty candidate literatures — every block of Parts IV–VII — for systems reporting two or more dictionary-linked exponents measured on the same data. Table 7 is the complete finding: seventeen entries, of which exactly **four** are true same-data pairs with quantitative errors on both sides: the marine-predator dive series (step exponent, Hurst exponent, and spectral slope on identical records; Sims et al., 2008); the cat retinal and geniculate spike trains (Fano and spectral exponents on the same cells; Teich et al., 1997); quantum-dot blinking (switching-time tails and power spectrum on the same dots; Pelton et al., 2004); and the avalanche systems, where size and duration exponents on the same recordings feed the crackling identity (Beggs and Plenz, 2003, Durin and Zapperi, 2000, Fontenele et al., 2019). The remainder are near-misses of specific, recorded kinds: exponents measured on the same *system* but different data, relations tested by the source itself in a form this audit can quote but not re-derive, or pairs with one side unverified.

Two absences are as informative as the presences. No study was found that tests the path-dimension relation (12) on measured animal trajectories — the movement-ecology and trajectory-fractal literatures run parallel without intersecting, decades after both were founded. And outside the avalanche communities, no biological study was found that measures a second signature *in order to* check the first — every multi-exponent entry in Table 7 measured its exponents for separate reasons. The dictionaries that would bind the four records together are almost never used where they could be. That is the audit's first finding, and it required no plot.

Table 7: The audit set: every system in the compilation where two or more dictionary-linked exponents were measured on the same data. Seventeen entries from roughly thirty candidate literatures scanned — the rarity is itself a finding (§40). Values quotes the measured exponents; Relation states the dictionary prediction each pair tests. G as in Table 2. The machine-readable rows carry the agreement statements and per-row caveats in full.

System	Measured values	Relation tested	Source	G
Rat V1 spiking avalanches (urethane + freely moving)	tau=1.52+/-0.09; tau_t=1.7+/-0.1 at spiking variability CV*∼1.4	(tau_t-1)/(tau-1)=1/(sigma nu z) crackling relation	Fontenele et al	P
Rodent cortex in vivo across days (homeostatic plasticity)	tau and alpha fit per animal; DCC=|beta_observed-beta_predicted| near zero in controls; exact exponents in s..	beta=(alpha-1)/(tau-1) (crackling)	Ma et al	P
Organotypic cortex culture LFP avalanches	tau=1.50+/-0.008 (electrode count), 1.49+/-0.005 (LFP amplitude); sigma=1.04+/-0.19 (single-electrode initia..	critical branching process predicts tau=3/2 and sigma=1	Beggs & Plenz	P
Barkhausen noise, polycrystalline SiFe ribbons	tau=1.50+/-0.05; alpha=2.0+/-0.2; cutoff scaling 1/sigma_k=0.57+/-0.10	(alpha-1)/(tau-1)=1/(sigma nu z); depinning theory with long-range dipolar for..	Durin & Zapperi	P
Barkhausen noise, amorphous ferromagnets	tau=1.27+/-0.03; alpha=1.5+/-0.1; cutoff scaling 1/sigma_k=0.79+/-0.10	same crackling relation; short-range elastic class	Durin & Zapperi	P
Crackling noise cross-system framework	framework relations among size, duration, shape exponents	exponent relations from RG/scaling	Sethna	C
Cat retinal ganglion cells and their LGN targets, spike trains	Fano-factor exponent: RGC 0.76+/-0.22, LGN 0.64+/-0.23; PSD exponent: RGC 1.18+/-0.51, LGN 0.93+/-0.55	fractal point process predicts count exponent ∼ spectral exponent	Teich et al	P
Auditory-nerve spike trains	periodogram and Allan variance reveal fractal exponents >1 where Fano factor saturates at 1 (estimator ceili..	count-based and spectral exponents should agree for fractal point process	Lowen & Teich	C
Human heartbeat increments	increment histogram Levy-stable; scale-invariant anticorrelations up to 10^4 beats (no numeric exponents in ..	independent tail index and correlation exponent on same series	Peng et al	P

continued on next page

Table 7, continued.

System	Measured values	Relation tested	Source	G
Human heartbeat 24-h series	DFA alpha $\sim$ 1 healthy (Peng 1995 Chaos); 1/f spectrum over $\sim 10^{-4}$ to 10^{-2} Hz (Kobayashi & Musha 1982)	beta = 2*alpha - 1 (fGn dictionary)	Peng et al	C
Marine predators, dive/movement time series (5 species, n=24-31)	mu=2.12+/-0.31 (range 1.34-2.91); RMS-fluctuation alpha=1.08+/-0.17; spectral beta$\sim$0.8 (low-f regime)	Levy dictionary mu->alpha_stable=mu-1; fBm/fGn dictionary beta=2H-1	Sims et al	P
Spider monkey foraging trajectories	step-length mu=2.18 reported; waiting-time exponent also power-law	Levy walk optimal mu=2	Ramos-Fernandez et al	P
Human genome chromatin (Hi-C, GM06990)	P(s) $\sim$ s$^{-1.08}$ over 0.5-7 Mb; fractal (crumpled) globule: space-filling, unknotted, s^{-1} predicted	fractal globule predicts P(s)$\sim$s^{-1} vs equilibrium globule s^{-3}/2	Lieberman-Aiden et al	C
Lab turbulence: spectrum + pair dispersion	E(k)$\sim$k^{-5}/3 (K41, verified since Grant et al 1962 tidal channel); pair dispersion <r^2>$\sim$g eps t^3 with g=0.5..	Richardson t^3 follows dimensionally from -5/3 locality	Ott & Mann	C
Colloidal quantum dot blinking (CdSe, single dots + solution)	PSD exponent nu: 0.70+/-0.02 (glass), 0.75+/-0.03 (chloroform), per-dot 0.74+/-0.09; S(f)$\sim$f$^{(\nu-2)}$ i.e. beta..	Psi(T_on/off)$\sim$T$^{-(1+\nu)}$ implies S(f)$\sim$f$^{(\nu-2)}$: tail index and spectral slope l..	Pelton	P
Climate: atmosphere vs ocean surface temperature	F&B 2003: alpha$\sim$0.5 inner continents, alpha$\sim$1 (1/f) SST/oceans, monthly data; Comment (Bunde et al): contine..	beta=2*alpha-1	Fraedrich & Blender	P
Climate continuum, instrumental + proxy temperature	1.1-100 yr: beta=0.37+/-0.05 (high lat), 0.56+/-0.08 (tropics); 100-15000 yr: beta=1.64+/-0.04 (high lat), 1..	beta=2H-1 links to DFA climate values (alpha 0.65-1 gives beta 0.3-1)	Huybers & Curry	P

41 The audit

Figure 7 runs the arithmetic. For every usable pair, one exponent (or an exact theory value, where the relation's prediction side is a theorem) generates a prediction through its dictionary; the partner exponent, measured independently, supplies the ordinate; errors propagate through the relation with no other processing. Seventeen points, one identity line, no parameters. Grade discipline carries through: any pair with an unverified input is drawn open and argued from nowhere.

What the plot shows, quadrant by quadrant. The **exact-theory pairs** sit on the line at high precision: the liquid-crystal KPZ exponents on 1/3 and 1/2 (Takeuchi and Sano, 2010), the lipid-membrane pair on the 2D Ising 1/8 and 1 (Honerkamp-Smith et al., 2008; 2011), the binary liquid on the bootstrap β (Greer, 1976), cortical τ on the branching 3/2 with σ on 1 (Beggs and Plenz, 2003) and the Barkhausen ratio on the mean-field 2 (Durin and Zapperi, 2000). Where identification with a class is secure, the dictionary is not approximately right — it is right. The **cross-estimator pairs** scatter around the line at their (large) error bars: both Teich pairs sit above it (spectral exponents systematically exceeding Fano exponents, an estimator bias their own literature documented), the Hi-C contact exponent sits at 1.08 against the fractal-globule 1, and the climate pairs straddle it within errors that include a published dispute. The **tension pairs** are two: the marine-predator spectral slope ($\beta \approx 0.8$) against $2H - 1 = 1.16 \pm 0.34$ from the same series — consistent at one sigma only because the error is wide, and undiscussed by the source — and the quantum-dot pair, where the spectrum-side exponent is locked to the switching tails internally but sits well off the value the threshold-fitting literature reports for the same phenomenon, a discrepancy Pelton et al. (2004) themselves advanced as evidence the threshold method is biased. And the **inset** carries the audit's precision ceiling: the helium λ-point specific-heat exponent against the O(2) prediction — both sides at four digits, 8σ apart (Chester et al., 2020, Lipa et al., 2003) — the standing demonstration that when both sides of such a comparison reach real precision, agreement is not guaranteed even for the best-understood universality class in physics.

42 What the audit shows, and what it cannot show

Stated at the strength the evidence supports, in both directions.

What it shows. First, the dictionaries hold exactly where they should hold exactly: every pair with a secure universality class sits on the line at full published precision, across four decades of experiments and five different classes. The audit's instrument is sound. Second, on the biological and geophysical pairs the relations hold *loosely*: no usable pair refutes its dictionary at three sigma, most sit within one, and the scatter is dominated by estimator bias of kinds the source literatures have themselves documented. Third, the one-generator clause — same α, four signatures — is *consistent with* every usable pair, which is a weaker statement than confirmation and is the correct one: seventeen points, four of them same-data, cannot carry more.

What it cannot show. The audit cannot distinguish the Qi-CON account from any other one-generator account — the dictionaries are shared property, and only the derived *location* of the window and knees (Part XII) separates the candidates. It cannot yet test the path-dimension relation at all, for want of a single study measuring both sides. And it cannot exclude the null hypothesis that the loose agreements are what independently generated exponents in bounded ranges would do by coincidence — with seventeen points the audit constrains, it does not conclude.

Figure 7: The cross-consistency audit: exponents predicted by the dictionary relations against exponents measured directly. One point per usable pair from Table 7: the abscissa is the value predicted from the partner measurement through relations (R1)–(R5) (or the exact theory value where the prediction side is a theorem); the ordinate is the independent measurement; errors are propagated through the relations with no other processing; the line is the identity, and there are no free parameters anywhere in the figure. Open markers carry an unverified input. The five candidate pairs that could not be used are named on the figure itself. Inset: the helium λ-point specific-heat exponent against the O(2) bootstrap value — the comparison the rest of the plot aspires to, and an 8σ disagreement. The figure is generated from the published datasets by one script.

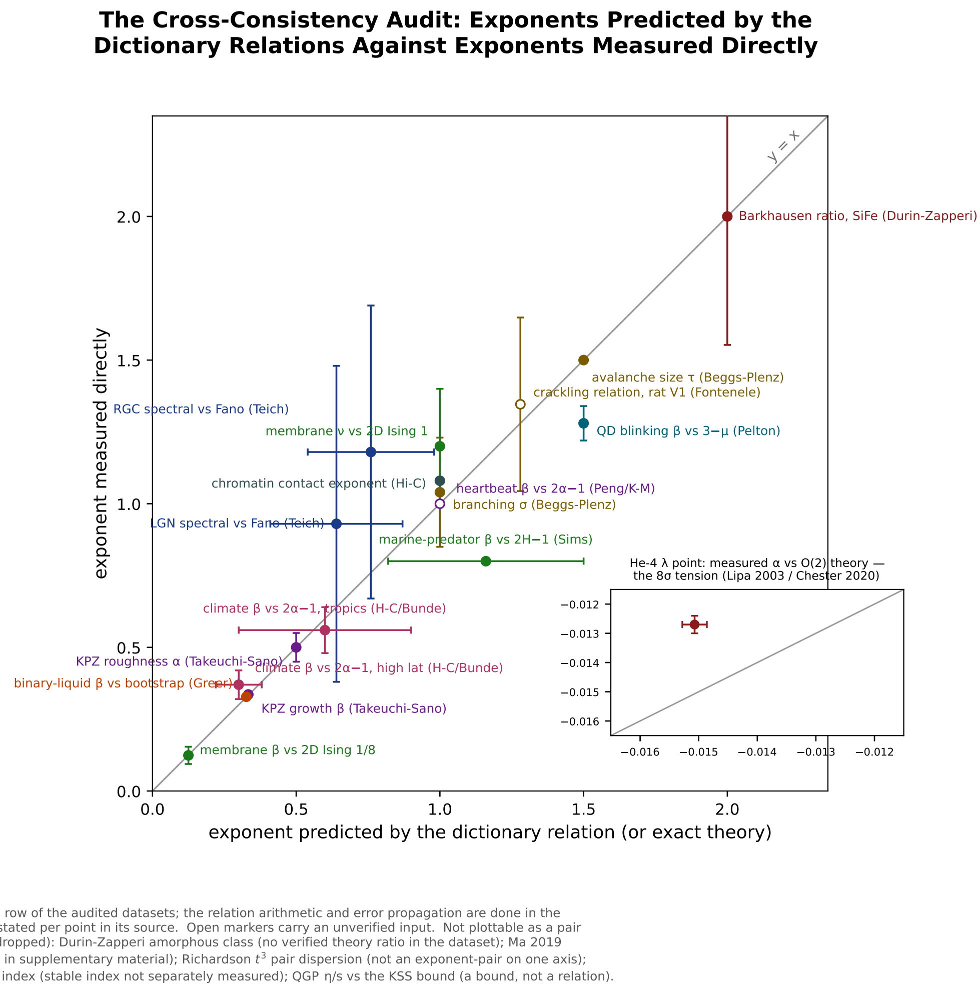

43 What would count as an answer

The audit converts the one-exponent question from rhetoric into a measurement program, and the program is short enough to state completely. (1) *Measure pairs on purpose.* Any tracking study that fits μ can compute the trajectory's box dimension from the same data and test (12) at zero marginal cost; no one has. (2) *Close the marine-predator tension:* re-estimate β and H on the same dive series with modern estimators and stated windows — the data exist. (3) *Find one biological* *infrared knee:* extend any physiological $1/f$ measurement two decades toward DC; the account requires a knee at the attractor scale, and the census of §36 shows the measurement has simply not been attempted outside cortex. (4) *Run the crackling identity prospectively* in one more system with pre-registered exponents. Four measurements, each feasible with existing instruments; any one of them can put a point far off the line in Figure 7, and the account has no mechanism for absorbing such a point.

44 The audit as a falsification instrument

One reading of this Part matters enough to be stated as its own section. The audit was built to POS-7's specification: it is not a case for the one-generator claim but an *instrument aimed at it*, and the instrument's kill conditions are concrete. Any system in which two signatures are measured independently and land off their dictionary by more than the propagated errors — outside the lawful failure modes of Part XII, which must announce themselves in the sub-record — puts a point far off the identity line where every reader can see it. Seventeen pairs have had the opportunity; the falsifier program of §80 numbers six measurements, all feasible now, that would create the eighteenth — four of them first stated in §43's language. A framework that survives this Part has not been proven; it has been *permitted to proceed to derivation* — and the same instrument stays armed against Parts XI–XII's account for as long as anyone cares to measure.

45 Closing remarks: the pattern is the evidence

What Parts IV–VII assembled separately, this Part put into arithmetic, and the result is a finding with a shape rather than a verdict. The four records are individually softer than their popular tellings — windowed, protocol-dependent, and policed by skeptical literatures this supplement has quoted at full strength. Yet the relations *between* the records, tested wherever the record permits a test at all, fail nowhere and hold exactly wherever the identifications are exact. Four literatures, each too soft alone to establish its own universality, keep landing on numbers that satisfy one another's arithmetic. That pattern — loose in every record, tight across them — is precisely what a single windowed generator would produce, and it is not what four unrelated mechanisms owe one another. It is interesting, and it is not proof. The Parts that follow take up the two questions the audit leaves: whether any existing framework already accounts for the pattern (Part IX), and whether the one exponent the four records keep pointing to is the one the boundary law computes (Parts XI–XII).

Part IX
Current Theoretical Approaches: Their Reach and Their Limits

Six frameworks given their best case — what each derives, what each assumes, and the three questions all of them leave open

The audit of Part VIII left a pattern on the table: four records, each soft alone, whose exponents satisfy one another's arithmetic wherever they can be put into arithmetic at all. Before this paper's own account of that pattern is examined (Parts X–XII), the existing accounts deserve their day — at full strength, in their own terms, judged by their own best results. None of them is a straw man. Each is exact somewhere, and the places where each is exact are recorded in the audits of Parts IV–VII with the same grades as everything else. The question this Part asks of each framework is the question the record forced in Part I: where does the exponent come from, where does the window come from, and what ties the four signatures to one another? The finding, stated in advance: every framework below answers pieces of the first question inside its own domain, none answers the second except as an afterthought, and none attempts the third — because each was built, honestly and productively, for one signature at a time.

46 The mechanistic $1/f$ theories: exact where they live

The oldest rival is also the most successful, and it is important to say so plainly. For $1/f$ noise in electronic materials, the superposed-relaxation framework — McWhorter's tunneling model and the Dutta–Horn thermal-activation generalization — is quantitative, falsifiable, and confirmed in its domain.

McWhorter (1957) located the germanium surface noise in charge exchange with oxide traps: each trap is a two-state relaxer with a Lorentzian spectrum, tunneling makes the relaxation time exponential in the barrier depth, and a uniform distribution of depths delivers the log-uniform distribution of timescales, $P(\tau) \propto 1/\tau$, that superposes to $1/f$ across the trap band. Everything is explicit: the band's edges are the shallowest and deepest traps, so the model *predicts its own knees*, and where the oxide can be characterized independently the prediction can be checked. Dutta and Horn (1981) generalized the mechanism to thermally activated processes with a broad distribution of activation energies and extracted a sharp test: if the mechanism is right, the frequency exponent $\beta(T)$ and the temperature dependence of the noise power are locked to one another through one relation. That relation has been verified in metal films — the framework's own falsifier, stated and passed (Weissman, 1988).

This is what a complete account of one record in one domain looks like, and the $1/f$ sections of this supplement lean on it (§33). Its limits are equally plain. The timescale distribution is an *input*: the theory converts a distribution of barriers into a spectrum, and the barrier distribution itself is measured, not derived. The account is per-material — germanium's traps say nothing about heartbeat intervals, and no one claims they do. And the framework is constitutionally single-signature: nothing in a trap band implies heavy-tailed steps or fractal support in the same system. Exact where it lives, silent on universality — the phrase this Part will keep reusing, and the mechanistic theories earn its first half more thoroughly than any rival below.

47 Self-organized criticality: the proposal, the corrections, the verdict

Bak et al. (1987) proposed the boldest answer the field has produced: slowly driven systems with threshold dynamics organize *themselves* to a critical point, with no tuning parameter, and the resulting avalanches deliver power laws and $1/f$ spectra for free. The proposal's force is real — it names a mechanism by which scale-invariance could be generic rather than exceptional, which is exactly the explanatory shape the ubiquity of the four records demands, and the modern review literature still credits it as the canonical route to criticality without fine tuning (Muñoz, 2018).

The corrections came from inside the program and deserve to be printed at the same size. The flagship claim — that the sandpile explains $1/f$ noise — failed its own model: the sandpile's spectrum was measured at $1/f^2$, not $1/f$ (Jensen et al., 1989), and the $1/f$ record of Part VII was never SOC's to claim. What survived is the crackling-noise program (Sethna et al., 2001): in driven disordered systems where thresholds and separation of timescales demonstrably exist — Barkhausen magnets (Durin and Zapperi, 2000), martensites, earthquakes — avalanche exponents are real, universal within classes, and locked to one another by scaling relations this supplement's audit uses as dictionary R5 (§39).

The verdict, in this Part's three questions. Exponent origins: SOC *relocates* the origin — the exponents come from the underlying universality class, exactly as at an ordinary critical point, so the origin question is answered only where the class is independently identified. Windows: the truncations are finite-size and finite-drive effects, treated as corrections rather than predictions; nothing in the framework says where a biological record's band should end. Cross-signature: none — an avalanche account of the cortex has nothing to say about the fractality of the same tissue's arbors, and does not claim to. And the framework's precondition — threshold dynamics under slow drive — is itself a hypothesis about each new system, earned for magnets and fault systems, asserted for most of the living record.

48 The neural criticality hypothesis: the evidence and the critiques

The strongest living-system form of the criticality idea is the neural criticality hypothesis: the cortex operates near a critical point of a second-order phase transition, and its avalanche statistics are the signature. The founding measurement (Beggs and Plenz, 2003) found avalanche size and duration power laws in cortical cultures with exponents at the mean-field directed-percolation values, and the program's best modern statement (Chialvo, 2010) argues the case at review length: a brain poised near criticality would inherit maximal dynamic range, maximal information capacity, and a flexible repertoire of spatiotemporal patterns — functional arguments for *why* evolution would hold a cortex there.

The critiques are quantitative and this supplement has already audited them. Power-law avalanche statistics can arise without criticality (Touboul and Destexhe, 2017) — stochastic surrogates with no phase transition reproduce the size and duration exponents, so the power laws alone underdetermine the hypothesis. The crackling identity that would discipline the claim is satisfied selectively across preparations (Fontenele et al., 2019) — the audit of Part VIII carries those rows with their grades. And the colloquium-level assessment of the whole living-criticality program is measured: some evidence remarkable, some limited, incomplete, or not fully convincing (Muñoz, 2018).

Against this Part's three questions: the hypothesis *postulates* proximity to a critical point rather than deriving an exponent — the exponents come from whichever universality class is assumed, and the class itself is contested row by row in the record. It has no window theory: the 10–50 ms knee in the cortical field spectrum (§36) is data, not prediction. And it is single-signature by construction: the avalanche account and the $1/f$ account of the same tissue are separate literatures that the cross-consistency audit of Part VIII had to join by hand.

49 Lévy foraging optimality: the theorem and its scope

The Lévy flight foraging hypothesis (Viswanathan et al., 1999) is the one rival with a genuine optimality theorem: for sparse, randomly distributed, revisitable targets, a searcher with power-law steps at $\mu = 2$ outperforms both ballistic and Brownian strategies, so natural selection should tune step statistics toward the Lévy window. The theorem is real mathematics, its assumptions are explicit, and the post-reform record — after the founding albatross data were retracted and refit (Edwards et al., 2007) — still contains marine predators whose verified step exponents sit where the theorem points (Humphries et al., 2010, Sims et al., 2008). Part V audits that record at full size, retraction first.

The scope limits are equally explicit, and the reformed literature itself states them (Auger-Méthé et al., 2015, Pyke, 2015). Optimality is a selection argument, not a mechanism: it predicts what statistics would be advantageous, not how a shark's locomotor system produces them, and it is silent wherever no foraging exists — bank notes, photons in hot atomic vapor, and cold atoms in dissipative lattices all sit in the same Lévy window of Table 4 with no fitness function anywhere in sight. The composite-correlated-random-walk critique (mimicry, audited in §26) bounds what any single trajectory can prove. And the framework is again single-signature: nothing in the foraging theorem speaks to the forager's $1/f$ physiology or its fractal vasculature. Where the boundary-law account and the optimality account overlap, they are not even rivals — Part XV argues the optimality theorem is best read as the *reason selection retains* statistics that the geometry supplies.

50 Scale-free networks and highly optimized tolerance: exponents from rules and from design

Two frameworks derive power laws from explicit generative structure, and both are exact about where their exponents come from — which makes them the cleanest contrast to the geometric account of Part XI.

Preferential attachment (Barabási and Albert, 1999) grows a network by attaching new nodes preferentially to well-connected ones and obtains a scale-free degree distribution — the model's measured exponent is $\gamma = 2.9 \pm 0.1$, against 2.3 for actor collaboration and 2.1 for the web in the founding paper itself. The exponent's origin is fully transparent: it comes from the growth rule, and modifying the rule moves it. That transparency is the limit. A tunable exponent is the opposite of a locked one — the framework accommodates any measured value by adjusting attachment kernels, which is why the follow-up literature found "scale-free" claims proliferating beyond what the statistics support (Clauset et al., 2009, Stumpf and Porter, 2012), and why degree exponents appear nowhere in the lock relations of Part XII: the framework predicts no relation between a network's degree tail and the same system's temporal spectrum, and none is claimed. The small-world result (Watts and Strogatz, 1998) is adjacent and orthogonal: short paths with high clustering, a topology statement with no power law and no bearing on the four signatures audited here.

Highly optimized tolerance (Carlson and Doyle, 1999) is the sharpest anti-criticality proposal in the field: power laws as the signature of *design* — systems optimized for yield against uncertain hazards allocate resources so that losses are heavy-tailed, with exponents set by the dimensionality of the resource constraint. In its model problems the account is exact, and its polemical point is well taken: heavy tails alone do not diagnose criticality, since constrained optimization produces them too — the same lesson Touboul and Destexhe (2017) taught the neural program from the stochastic side. Its limits: HOT requires an optimizer and a specified constraint structure, so each application is a bespoke design problem; its exponents are per-problem, not cross-signature; and it offers no account of windows beyond the resource cutoffs the modeler writes in. As with the foraging theorem, the deepest reading may be compatibilist: HOT describes what optimization does *with* heavy-tailed possibilities, not where the heavy tails of an un-designed record — Doppler photons, quantum dots — come from.

51 Renormalization-group explanations: proximity earned and proximity asserted

Behind every criticality-based rival stands the renormalization group itself (Wilson, 1971), and it is the standard the rest of this paper is measured against: at a critical point, exponents are computable properties of a fixed point, locked into classes, related by identities — the precision frontier of Table 3, where bootstrap values and helium measurements meet at four digits. Where proximity to a critical point is *earned* — a control parameter identified, a distance to criticality measured, corrections to scaling tracked — the RG account is not a rival to anything; it is simply the physics, and Part IV's critical scoreboard treats it as such.

The question is what the RG explains in the living record, where proximity is asserted rather than measured: no control parameter is identified for a foraging shark, no reduced temperature for a cortex, and the program of measuring a biological system's distance to its putative critical point is in its infancy (Muñoz, 2018). Absent that measurement, "the system is near a critical point" functions as a label for the observed scaling rather than an explanation of it — the exponent comes from a class chosen after the fact, the window from finite-size arguments fitted after the fact, and the tuning story — who holds the system at criticality, against what drift — is delegated to SOC or to selection, inheriting the limits of §47 above. The RG is not wrong anywhere in this record; it is *unanchored* in most of it.

52 The scoreboard

Table 8 states the comparison in this Part's three questions, one row per framework, with the boundary-law account of Parts XI–XII printed in the last row under the same columns — including the column where it is weakest, stated at the same size as everyone else's weaknesses.

Table 8: The rivals scoreboard: six frameworks against three questions. Each framework in its strongest domain, judged on the three questions of Part I: where the exponent comes from, whether the window (and its knees) is predicted, and whether any relation ties the four signatures together. "Input" means the quantity is supplied by measurement or modeling choice rather than derived inside the framework. The last row is this paper's account, held to the same columns: its exponent origin is derived conditional on the coupling weight γ (the L4 spectral condition of Part XII), its window and knees are theorems of the projection, and its cross-signature dictionaries are the audit of Part VIII — while its own weakest column, the numerical exponent of a named organism, is open and stated so in §81.

Framework	Exponent origin	Window / knees	Cross-signature law
Mechanistic $1/f$ (McWhorter, Dutta–Horn)	measured barrier distribution (input)	yes — trap-band edges, in its domain	none claimed
SOC / crackling	underlying universality class	finite-size corrections, not predictions	avalanche relations only (R5)
Neural criticality	postulated class (contested per row)	none — the measured knee is data	none between records
Lévy foraging optimality	selection toward $\mu = 2$ (theorem, foragers only)	none	none
Scale-free networks	growth rule (tunable)	none	none
HOT	constraint dimension, per design problem	resource cutoffs (modeled)	none
This paper (Parts XI–XII)	derived, conditional on γ (L4)	theorems: two knees at derivable places	five dictionaries, audited in Part VIII

53 The open problems, exactly

What the strongest existing frameworks jointly leave open is therefore a short and exact list, and it is the work order for the two Parts that follow the CFT review:

1. **An exponent origin that is neither tuned, chosen, nor grown.** Not a universality class assumed, not an attachment kernel adjusted, not a barrier distribution measured — a derivation in which the exponent is fixed by structure that was fixed for other reasons. Part XII attempts exactly this, and grades every step.

2. **A window theory.** Why every real record is bounded, and where the two knees sit — as predictions carrying error bars, not as corrections apologized for. Part XII derives both knees; §36 is the record they must face.

3. **A cross-signature law.** Relations among the step exponent, the dimension, the Hurst exponent, and the spectral slope that are forced, not assembled — with the audit of Part VIII as the standing test.

4. **A failure taxonomy.** A statement of how the signatures must degrade when the account's own conditions fail — so that imperfect data can confirm or kill the account rather than merely blur it. The failure theorem of Part XII is this paper's answer.

54 Closing remarks: a field of exact partial answers

Nothing in this Part is a demolition, and it would be dishonest to write one: the mechanistic theories are confirmed physics, the crackling program is real universality, the optimality theorem is real mathematics, HOT's warning about heavy tails is one this supplement's own audit enforces, and the RG is the standard everything here aspires to. The gap is structural, not a matter of effort or data. Each framework was built for one signature, and each derives its exponent from structure — a class, a rule, a design, a distribution — that must be re-supplied for every new system. What none of them contains is a reason the same exponent should surface four ways in one organism, inside a bounded window, with stated places for the bounds. That is the specific vacancy the boundary-law account applies for, and the next three Parts examine whether it earns the position — against the nearest exact theory first (Part X), then in the derivation itself (Parts XI–XII), with the audit of Part VIII standing as judge throughout.

Part X
CFT and AdS/CFT: What Can Be Borrowed, and What Cannot

Conformal field theory and the holographic dictionary — the exact theory of scale invariance, and a table drawn in the open before anyone has to ask

Parts IV–VII audited four records of *approximate*, windowed scale invariance in nature, and Part IX examined the frameworks built to explain them. This Part reviews the two bodies of theory in which scale invariance is *exact* and its consequences are theorems: conformal field theory, which turned critical exponents into operator dimensions and then computed one of them to nine digits from consistency alone, and the AdS/CFT correspondence, which showed that a conformal boundary theory can encode a gravitational bulk with one extra dimension whose radial coordinate is the scale itself. Both are reviewed for what this program can legitimately take from them — a calculus, a bookkeeping, and a set of exact calibration targets — and §58 states in a table, in the open, what GG-6 does not claim to be. A reader from high-energy theory will arrive at this supplement with exactly one question — *is this AdS/CFT with the serial numbers filed off?* — and this Part exists so that the answer is on the page before the question is asked. The answer is no, in six specific, checkable ways; and the borrowing that remains is the ordinary, honorable kind that transport theory does from thermodynamics.

55 Conformal field theory in brief: from scale invariance to nine digits

55.1 Scale invariance, conformal invariance, and the gap between them

A theory is *scale invariant* when its physics is unchanged under $x \mapsto \lambda x$ with the fields rescaled by their dimensions; it is *conformally invariant* when the same holds for every angle-preserving map — dilations, but also the special conformal transformations that dilate by a different factor at every point. The conformal group of d-dimensional flat space is finite-dimensional for $d > 2$, isomorphic to $\mathrm{SO}(d+1,1)$ in the Euclidean case, with $\frac{1}{2}(d+1)(d+2)$ generators: translations, rotations, one dilation, and d special conformal generators. Scale invariance does not automatically imply conformal invariance, but in unitary theories it almost always delivers it — a theorem in two dimensions (Polchinski, 1988), and in four dimensions a statement with strong evidence and no known counterexample. The working assumption of the critical-phenomena literature since the 1970s (Polyakov, 1970) is that the fixed points of the renormalization group — the objects whose exponents Part IV's scoreboard measures — are conformal, not merely scale invariant, and everything in this section flows from that upgrade.

Why the upgrade pays: conformal invariance is finitely more symmetry than scale invariance, and that finite increment is exactly enough to fix the low-point correlation functions completely. For primary operators O_i of dimension Δ_i,

$$\langle O_1(x_1)\, O_2(x_2)\rangle = \frac{\delta_{\Delta_1\Delta_2}}{|x_1 - x_2|^{2\Delta_1}}, \tag{14}$$

$$\langle O_1 O_2 O_3\rangle = \frac{C_{123}}{x_{12}^{\Delta_1+\Delta_2-\Delta_3}\, x_{23}^{\Delta_2+\Delta_3-\Delta_1}\, x_{13}^{\Delta_1+\Delta_3-\Delta_2}}, \tag{15}$$

with $x_{ij} = |x_i - x_j|$: two-point functions are pure power laws with no free function at all, and three-point functions are fixed up to one constant C_{123} per operator triple. The physics intuition: a symmetry that acts differently at every point leaves no room for a correlation function to carry any shape other than the one the dimensions dictate. Every power law in Parts IV–VII is, in this language, the two-point function (14) of *something*; the question a one-generator account must answer is what plays the role of the dimension, and over what window the form can hold.

55.2 The operator algebra and the bootstrap

The content of a CFT is its spectrum of primary dimensions $\{\Delta_i\}$ and its three-point constants $\{C_{ijk}\}$, because the operator product expansion closes the algebra: the product of two nearby operators is a convergent sum over the spectrum,

$$O_i(x)\, O_j(0) = \sum_k C_{ijk}\, |x|^{\Delta_k - \Delta_i - \Delta_j}\, \big[\, O_k(0) + \text{descendants}\, \big]. \tag{16}$$

Demanding that the four-point function computed by pairing operators one way equals the same function computed by pairing them the other way — *crossing symmetry* — plus unitarity (no negative-norm states) yields the conformal bootstrap: an infinite set of consistency conditions on $(\{\Delta_i\}, \{C_{ijk}\})$ with no Lagrangian anywhere. What began as a numerical program to carve out allowed regions (Rattazzi et al., 2008) became, within a decade, the most precise tool in critical phenomena: the 3D Ising dimensions were cornered in an island (Kos et al., 2016) and driven to $\Delta_\sigma = 0.518148806(24)$ (Chang et al., 2024), and the O(2) computation sharpened the helium discrepancy that sits in Part VIII's inset (Chester et al., 2020). The modern review is Poland et al. (2019). For this supplement the bootstrap plays one role, already exercised in Part IV: it supplies exponents that are *exact for reasons of consistency alone*, the hardest possible calibration targets for any measured record.

55.3 Two dimensions: where the geometry of Part VI becomes algebra

In two dimensions the conformal algebra becomes infinite-dimensional (the Virasoro algebra, with central charge c), and entire families of critical theories were solved exactly (Belavin et al., 1984): the minimal models carry closed-form dimensions, and through them the 2D Ising exponents ($\beta = 1/8$, $\nu = 1$) that Onsager had obtained by brute force. The bridge to Part VI's exact block is Schramm–Loewner evolution: the conformally invariant random curves SLE_κ (Schramm, 2000) realize the interfaces of 2D critical models, and their almost-sure fractal dimensions,

$$D_{\mathrm{f}}(\mathrm{SLE}_\kappa) = 1 + \frac{\kappa}{8} \qquad (\kappa \leq 8), \tag{17}$$

generate the values Part VI's record is anchored on: $\kappa = 8/3$ gives the self-avoiding walk's 4/3, $\kappa = 6$ gives percolation's 7/4 hull, and the duality $\kappa \leftrightarrow 16/\kappa$ maps hulls to external perimeters. When Part VI said the top block of the fractality record consists of theorems, this is the machinery the theorems come from — fractal dimension as an exact output of conformal symmetry.

56 AdS/CFT in brief: the dictionary, and the radial coordinate as scale

The correspondence (Maldacena, 1998) asserts the exact equivalence of two theories that do not look alike: type IIB string theory on the product spacetime $\mathrm{AdS}_5 \times S^5$, and $\mathcal{N} = 4$ supersymmetric Yang–Mills theory — a conformal field theory — living on the four-dimensional boundary of the anti-de Sitter factor. The working dictionary (Gubser et al., 1998, Witten, 1998) states that the generating functional of boundary correlators equals the bulk partition function with boundary conditions:

$$\Big\langle \exp\Big(\textstyle\int_\partial \phi_0\, O \Big) \Big\rangle_{\mathrm{CFT}} = Z_{\mathrm{bulk}}[\phi \to \phi_0], \tag{18}$$

each boundary operator O of dimension Δ pairing with a bulk field ϕ whose mass is fixed by

$$\Delta(\Delta - d) = m^2 L^2 \tag{19}$$

in AdS_{d+1} of radius L. Three features made the correspondence the dominant tool of two decades. First, it is a strong–weak duality: when the boundary theory is strongly coupled, the bulk is weakly curved classical gravity, so intractable gauge theory becomes tractable geometry. Second, *the radial coordinate is the renormalization scale*: moving into the bulk is coarse-graining the boundary theory, and Wilsonian RG flow becomes radial evolution — the single deepest structural idea the correspondence contributed. Third, it computes: its flagship transport output, the shear-viscosity bound $\eta/s \geq \hbar/4\pi k_B$ (Kovtun et al., 2005), sits in Part IV's scoreboard with the quark–gluon plasma measured within a factor of a few of saturating it.

The mechanics that matter for §57: boundary correlators are computed from bulk-to-boundary propagators, which in Euclidean AdS_{d+1} with radial coordinate ζ take the form

$$K_\Delta(\zeta; \vec{x}, \vec{x}') \;\propto\; \left(\frac{\zeta}{\zeta^2 + |\vec{x} - \vec{x}'|^2} \right)^{\Delta}, \tag{20}$$

homogeneous in $(\zeta, |\vec{x} - \vec{x}'|)$ jointly — no scale survives except the ratio — so that integrating out the radial direction hands the boundary pure power-law kernels. The reader who has come from Part III will recognize this expression: it is, functional form for functional form, the kernel of the Qi-CON projection in GG-A7-Qi4 Part V, and §57 is about what that coincidence does and does not mean.

57 What GG-6 shares with the holographic picture

Three structural elements are genuinely common, and it would be affectation to pretend otherwise.

A scale-carrying radial direction. The GG-6 bulk of Arisaka (2026, A2-GG6) is six-dimensional, and its radial coordinate is identified constitutionally as $r = \ln(E_{\mathrm{GUT}}/\mu)$ — the logarithm of the running scale. AdS/CFT arrived at the same identification from the other end: the radial direction *emerges* as the geometrization of the boundary theory's RG flow. Both frameworks store the renormalization structure of the boundary in one extra geometric dimension, and both therefore make scale a place rather than a parameter.

A homogeneous bulk-to-boundary kernel. The Qi-CON derivation (rerun in Part XII) projects boundary dynamics through a kernel of exactly the form (20); its homogeneity is what makes the projected generator fractional and the four signatures follow. This is not an independent invention and the program has never presented it as one: GG-A7-Qi4 Part V cites Maldacena (1998) at precisely that equation. The kernel form is forced by symmetry — any bulk with a scale-translation isometry hands its boundary a kernel depending only on ℓ/ζ — so sharing it is sharing a symmetry, not copying a theory.

Dimension bookkeeping. In both structures, boundary correlators are pure powers with exponents set by dimensions (2Δ in CFT; $2\Delta - \sigma$, repackaged as $d_{\mathcal{S}} + \alpha$, in the Qi-CON projection), and composite exponents follow by the same additive arithmetic. The audit relations of Part VIII are, from this vantage, the open-systems shadow of the CFT statement that all exponents descend from a spectrum of dimensions.

58 What GG-6 does not claim

Table 9 is this Part's reason for existing, and it is drawn as a table precisely so it cannot be misread as hedging. Each row is checkable against the companion papers.

Three of the rows deserve a sentence beyond the table. The *duality-versus-projection* distinction is the load-bearing one: AdS/CFT's power and its burden of proof both come from claiming two theories are secretly one, while GG-6 claims only that a bulk determines its boundary image — a strictly weaker and structurally different statement, with correspondingly weaker entitlements. The *no-inherited-computations* row is the honesty clause: a framework that borrowed the kernel but then quietly helped itself to holographic results would be doing exactly what this Part exists to disclaim; the KSS bound appears in Part IV's scoreboard as *AdS/CFT's* achievement, cited to its authors, full stop. And the *observer* row is where the two pictures are most deeply different in spirit: AdS/CFT's boundary is where the hologram is read; GDOS's boundary is where the physics happens, because the program's founding move (GG-A7-Qi4, Arisaka, 2026, A5-GDOS) is that every real description is a partial view from inside.

Table 9: What GG-6 shares with AdS/CFT, and what it does not claim — the differences, in the open. Six rows a high-energy reader will want checked, each stated so that it can be verified against the companion papers directly. The summary sentence of the whole table: GG-6 borrows the holographic *calculus* — a radial scale coordinate, homogeneous kernels, dimension bookkeeping — while claiming none of the holographic *dualities*; the borrowing is of the kind transport theory does from thermodynamics, and the program's results stand or fall with its own boundary law, not with any correspondence conjecture.

Question	AdS/CFT	GG-6
What is the claim?	A conjectured exact *duality*: two complete theories, equivalent	A constructed *projection*: one bulk, one boundary image of it — no equivalence claimed
What is the bulk?	Emergent $\mathrm{AdS}_5 \times S^5$ (or cousins) arising from a near-horizon limit of string theory	A postulated 6D geometry fixed by the constitutional axioms; no strings, no branes, no near-horizon limit
Supersymmetry and matter content	$\mathcal{N} = 4$ super Yang–Mills at large N in the canonical case	None anywhere in the program; the gauge content is the Standard Model's, fixed by the OGN-5 ledger
Status of the radial coordinate	Emergent; radial position *is* boundary RG scale, derived from the duality	Constitutional; $r = \ln(E_{\mathrm{GUT}}/\mu)$ is an axiom-level identification, not a derived equivalence
Where does the observer live?	On the conformal boundary at infinity, as a mathematical device	On the physical 4D boundary — the observer's world is the boundary, and the projection is the physics of partial views (OGGEP)
What computations are inherited?	Strong-coupling observables from weak-curvature gravity (e.g. η/s)	None of those; GG-6 takes only the scaling calculus and computes its own boundary law — it cannot, and does not claim to, do holographic strong-coupling calculations

59 What is legitimately borrowed

Having said what is not claimed, the positive list — four items, each already at work earlier in this supplement.

The scaling calculus. Homogeneous kernels, the scale-separating substitution, window-saturated integrals: the computational technology of §56 is symmetry mathematics, owned by no theory, and Part XII uses it exactly as holography does — integrate out the scale direction, read the surviving power law.

The dimension bookkeeping. The discipline of assigning every observable a scaling weight and letting composite exponents follow by arithmetic is CFT's great pedagogical export. Part VIII's audit is that discipline applied to field data.

The radial-RG intuition. Reading motion in the scale direction as coarse-graining — and therefore reading the *finiteness* of the accessible radial range as the origin of the observational window — is the holographic idea that does the most work in Part XII: the two knees of the $1/f$ band are, in this language, the two ends of the retained radial interval.

The exact targets. The bootstrap dimensions and the SLE dimensions are consistency-forced numbers, and Parts IV and IV have already used them as the calibration standard the measured records are judged against. A program that predicts windowed scale invariance owes its readers exactly this kind of target for its own exponents, and Part XII's grade table says how far it currently gets.

60 What operational conformality keeps, and what it surrenders

The comparison of §58 ran program against program. This section runs *concept* against *concept*, because the phrase "operational conformality" (GG-A7-Qi4 Part V; Part XII) borrows a word from the exact theory and owes the reader a precise account of how much of the exact theory's power comes with it. The answer is: the kinematics, not the algebra — and each half of that sentence is worth itemizing, because the surrendered half is exactly what a skeptical CFT reader will probe.

What is kept. Inside a Qi-CON window the projected generator is homogeneous, so the window inherits the *kinematic* consequences of scale covariance: two-point functions of pure power form (14) with exponents set by weights; dynamic scaling $t \sim \ell^{\alpha}$ replacing the CFT's $t \sim \ell^{z}$ with $z = \alpha$; and dimensional bookkeeping for composite observables, which is all Part VIII's arithmetic ever used. These survive because they follow from homogeneity alone — they are the part of conformal technology that never needed the full group.

What is surrendered. Four things, in ascending order of pain. *Special conformal covariance*: a finite window on a selected branch has boundaries and an attractor, and the angle-dependent dilations that complete the conformal group do not survive them; the program claims scale covariance and no more — which is why §55 was careful about the scale-versus-conformal gap (Polchinski, 1988). *The operator algebra*: there is no established analog of the OPE (16) for Qi-CON windows — no convergent expansion closing a set of boundary observables on itself — and without an algebra there is no crossing equation. *The bootstrap*: no algebra, no bootstrap; the program cannot at present corner its exponents by consistency alone the way Kos et al. (2016) cornered the Ising model's, and the grade table of §81 lists the numerical exponent as open partly for exactly this reason. *Unitarity bounds and a central charge*: the exact theory's structural invariants — dimension bounds, c, monotonicity of RG flow — have no derived Qi-CON counterparts, and this supplement does not pretend otherwise.

The honest summary sentence, in the register of Part III: operational conformality is to CFT what a windowed thermodynamic description is to statistical mechanics — the same covariance, radically less structure, bought at the price finite systems always pay. Whether some fragment of the algebraic structure survives projection — a window OPE, a monotone under window widening — is a genuinely open mathematical question, listed in §81 as such rather than promised.

61 Closing remarks: a neighbor, not a parent

The relationship between GG-6 and the conformal–holographic complex is the ordinary relationship between a new framework and the mature mathematics nearest to it: shared symmetry structures, shared computational technology, disjoint physical claims. CFT contributes exactness — the proof that scale invariance, taken seriously, fixes correlators and computes dimensions to nine digits. AdS/CFT contributes one structural idea — scale as geometry, RG as radial motion — which the GG-6 bulk implements by construction rather than by duality. What neither contributes, and what this supplement must therefore supply on its own, is the open-systems content: real records are windowed, real observers are partial, and the four signatures live between knees that no exact CFT possesses. That is the program's own burden, and the next two Parts take it up.

Part XI
The Framework at Depth: GDOS, GRIP, Qi-4, and the Selector

The boundary law derived sector by sector, the budget and its balance identity, the engine, the selector's three gauges, and where in the pillar stack Qi-CON geometrically originates

Before the derivation, the machinery — at working depth. The constructions in full live in Arisaka (2026, A5-GDOS), Arisaka (2026, A6-GRIP), and Arisaka (2026, A7-Qi4), and the extended plain-language review in S1-EP; what this Part supplies is everything Part XII will actually touch, with the one derivation per ingredient that shows *why* the ingredient has the form it has, and with the life-science reading attached at each step rather than appended at the end.

The one idea to hold before any detail: in this framework, *no observer stands outside*. Every description of every system is written by something finite, embedded, and partial, and the framework's founding move is to make the law of that partial view the fundamental object. The four signatures this supplement has audited are, on the program's account, what partial views of a scale-carrying bulk generically look like.

62 GDOS: the law of the partial view, sector by sector

Take anything — a molecule, a mouse, a market — and ask what an observer can actually have of it: never the whole state, always a handful of tracked quantities with everything else untracked. Arisaka (2026, A5-GDOS) makes that predicament the axiom (OGGEP, the open-system projection) and derives its law: the reduced description carries memory exactly (the Nakajima–Zwanzig form), becomes a semigroup when the environment forgets fast, and at the mesoscopic level becomes a continuity equation for a density $\rho(z,t)$ over the tracked coordinates,

$$\partial_t \rho + \nabla_a J^a = 0. \tag{21}$$

The current's four-sector form is not a menu; it is what survives of an arbitrary mesoscopic current once probability conservation and the existence of a scalar budget are imposed. Write the general linear-response current as $J^a = \rho\, v^a[\rho] - D^{ab}\partial_b \rho$, with v^a the systematic drift field and D^{ab} the positive-semidefinite mobility the projection induces. Decompose the drift against the budget F_{GFF} of §63: the component along the budget's gradient, the component that circulates without changing the budget, and the component along directions the budget cannot see at all. With $\Phi \equiv \delta F_{\mathsf{GFF}}/\delta\rho$, that is

$$v^a = -\,D^{ab}\partial_b \Phi \;+\; u^a_{\mathrm{c}} \;+\; u^a_{\mathrm{g}}, \qquad \nabla_a\big(\rho\, u^a_{\mathrm{c}}\big) = 0, \qquad u^a_{\mathrm{g}}\,\partial_a \Phi = 0, \tag{22}$$

so the current is

$$J^a = \underbrace{-\rho\, D^{ab}\partial_b \Phi}_{\text{gradient}} + \underbrace{\rho\, u_{\mathrm{c}}^a}_{\text{curl}} + \underbrace{-\, D^{ab}\partial_b \rho}_{\text{noise}} + \underbrace{\rho\, u_{\mathrm{g}}^a}_{\text{gauge}}\,. \tag{23}$$

The split is exhaustive by construction — any drift is gradient plus circulating plus budget-neutral — and each sector has a distinct job, a distinct life-science face, and a distinct role in the derivation ahead.

The gradient sector is downhill motion in the budget: relaxation, binding, folding, the burning of a substrate. In a cell it is the chemistry that runs because it is downhill in the generalized sense; in the derivation it supplies the confining tendency that keeps a selected branch near its attractor. It is the only sector that *spends* the budget.

The curl sector circulates on the budget's level sets: futile cycles, oscillations, the closed loops of a driven steady state. Detailed balance is exactly the statement $u_{\mathrm{c}} = 0$; living systems are the standing counterexample, and the curl sector is why a cell can turn over its entire economy while its budget reading barely moves. Under strong periodic driving it is also failure mode (F4)'s first face: spectral peaks riding on the band.

The noise sector is the projection's own fluctuation term — what the untracked coordinates do to the tracked ones. Its kernel is inherited from the bulk through OGGEP, and this inheritance is the whole story of Part XII: when the hidden coordinate carries scale, the noise sector's kernel is homogeneous, and the fractional generator $-D_\alpha(-\Delta_g)^{\alpha/2}$ is its leading form. The Qi-CON window is the regime where this sector, together with the gradient sector it balances against, leads the dynamics.

The gauge sector moves along maintained internal conventions — relabelings, reference frames, the freedom DGI formalizes. It does no work on the budget by construction ($u_{\mathrm{g}}\,\partial\Phi = 0$), and its role in this supplement is protective: §76 shows the measured exponents are invariant under everything this sector can do, which is why two calibrated instruments on one branch must agree.

Two facts about this law matter downstream. First, it is derived from the projection of the six-dimensional bulk (Arisaka, 2026, A2-GG6), so its kernels inherit the bulk's radial structure — where the exponent α will come from. Second, its window is physical: the projection retains a finite range of scales, bounded by what the instrument resolves and what the attractor confines — every "operational window" in this supplement is that retained range.

63 The budget and the balance identity

Arisaka (2026, A6-GRIP) organizes the boundary law from the geometric side: the four sectors descend from one scalar budget,

$$F_{\mathsf{GFF}}[\rho] = F_{\mathrm{GEP}}[\rho] + F_{\mathrm{CEP}}[\rho] = \int \rho\, U_{\mathrm{eff}}\,\mathrm{d}z \;+\; \Theta_{\mathrm{eff}} \int \rho \ln \frac{\rho}{\rho_{\mathrm{ref}}}\,\mathrm{d}z, \tag{24}$$

an energetic–geometric term plus an effective information temperature times a relative entropy. The budget is not decoration; it obeys a balance identity that assigns each sector its thermodynamic role. Differentiating (24) along the flow (21) and integrating by parts,

$$\frac{\mathrm{d}F_{\mathsf{GFF}}}{\mathrm{d}t} = \int \Phi\,\partial_t\rho\,\mathrm{d}z = -\int \Phi\,\nabla_a J^a\,\mathrm{d}z = \int (\partial_a\Phi)\,J^a\,\mathrm{d}z, \tag{25}$$

and inserting the four sectors: the curl term drops because $\int(\partial_a\Phi)\,\rho u_{\mathrm{c}}^a\,\mathrm{d}z = -\int \Phi\,\nabla_a(\rho u_{\mathrm{c}}^a)\,\mathrm{d}z = 0$; the gauge term drops by $u_{\mathrm{g}}\,\partial\Phi = 0$; and with Θ_{eff} uniform on the branch the gradient and noise sectors combine into a single negative-definite form,

$$\frac{\mathrm{d}F_{\mathsf{GFF}}}{\mathrm{d}t} = -\int \rho\,(\partial_a\Phi)\,D^{ab}(\partial_b\Phi)\,\mathrm{d}z \;\;\le\;\; 0. \tag{26}$$

Undriven, the budget is a Lyapunov function and the system relaxes; driven through open ports, the same identity becomes the bookkeeping of a steady state — import against the gradient, circulate through the curl, export the difference — and the *rate* in (26) is the housekeeping dissipation the open-systems literature measures. Where the fractional term lives: (26) survives when D^{ab} is promoted to the nonlocal mobility of Part XII's generator, because the fractional Laplacian is negative-semidefinite on the same domain — the Qi-CON window changes the *geometry* of relaxation, not its direction.

64 GRIP: the engine, and the attractor timescale as a derived object

GRIP, the recursive runtime engine of Arisaka (2026, A6-GRIP), drives selected structures through cycles of intake, processing, and export against the budget. For this supplement GRIP plays one role, but it is load-bearing: it is why selected branches *persist* long enough to have statistics at all. A branch that completes its cycles maintains an attractor; an attractor has a relaxation spectrum $\{\lambda_n\}$ — the eigenvalues of the linearized generator around the maintained state — and the slowest of them defines

$$\tau_{\mathrm{att}} = \frac{1}{\lambda_{\min}}, \tag{27}$$

the longest time over which the branch remembers a perturbation and the largest scale the branch's own dynamics can correlate. This number is not an input: given a branch and its budget it is a spectral property, in principle computable, in practice measured — and it is where Part XII pins the infrared knee, $f_{\mathrm{IR}} \sim 1/(2\pi\tau_{\mathrm{att}})$. The companion fact at the other end: the projection retains no process faster than the finest tracked time τ_{micro}, and between those two edges lives every timescale the observer's record can contain — the *bounded census* whose spectral shadow is the two-knee band. Persistence, in this framework, is not a background assumption; it is the physical reason the window exists.

65 Qi-EP: the selector and its three gauges

Arisaka (2026, A7-Qi4) builds the information side: the Qi-4 pillars, of which two act here. Qi-QUA denominates the boundary currents in one common unit through the Arisaka equation,

$$\frac{J_E}{\mathsf{Q_B}} = J_e = J_B = J_{Qi}, \tag{28}$$

which is why sector-resolved spectra share slopes across a common window: in the locked regime the four currents' spectra coincide up to the conversion factor, and realistic overhead leaves the *slopes* common even where amplitudes drift.

Qi-EP is the *selector*, and S1-EP is its extended treatment: one projected boundary functional whose stationary points fix which branch, which flux pattern, and which internal policy a persisting system actually holds. Its structure is a single functional read in three gauges, and the three gauges are the three extremal principles the open-systems literature spent a century proposing separately: the *path gauge*, which selects trajectories and returns the least-time and geodesic principles of transport; the *throughput gauge*, which selects stationary flux patterns and returns the entropy-production extremal principles — maximum entropy production where the drive is fixed and channels compete, minimum entropy production in the linear-regime confinement, with the domain of each derived rather than asserted; and the *inference gauge*, which selects internal models and returns the free-energy principle of the predictive-processing literature at its declared boundary. Every natural open system asks some combination of the selector's three questions — which path, which flux, which policy — and a cell asks all three at once: it chemotaxes along a path, maintains metabolic flux, and updates internal state against sensory mismatch. Nothing biological enters the derivation of any gauge; the theorems bind the class of open systems admitting a packet description, and organisms are members of the class by its checkable clauses, not by analogy.

The point that matters operationally for this supplement: every exponent in Parts IV–VII is a property of *a selected branch in a window*. Two records disagreeing about "the" exponent may be sampling different branches — a possibility the failure theorem makes precise (mode F3) and the mimicry debate has already met.

66 GSSB and the branch structure: where Qi-CON geometrically originates

The pillar stack now closes, and it is worth standing back to see where in it the Qi-CON claim actually lives, because the location is the answer to the question a skeptical reader should ask: *why would a geometric theory of particle physics have anything to say about a foraging shark?*

The chain has five links, each supplied by a different piece of the framework, none invented for this supplement. **(1)** The constitution makes the observer's partial view fundamental (AX-3, OGGEP) — openness is not an approximation but the axiom. **(2)** The bulk stores scale as a coordinate ($r = \ln(E_{\mathrm{GUT}}/\mu)$; Arisaka, 2026, A2-GG6) — so *partial* necessarily means partial *in scale*: every projection hides some of the radial direction. **(3)** GDOS turns the projection into the boundary law

(21)–(23), whose noise sector inherits the hidden radial structure as a kernel. **(4)** GSSB breaks the boundary dynamics into branches, Qi-EP selects the one the record samples, and GRIP keeps it there long enough to measure, which bounds the window. **(5)** On that selected, persisting, windowed branch, the inherited kernel is homogeneous — Part XII's computation — and homogeneity with one exponent *is* the four-signature quartet. Qi-CON is therefore not a hypothesis appended to the pillar stack; it is the stack's shadow on any record: the geometric origin of the exponent is link (2), the mechanism of inheritance is link (3), and the reason real records are windowed rather than infinite is links (4)–(5).

Branch structure carries one more consequence the audit relied on: exponents are *per branch*. GSSB fixes a universality class within a branch and permits different classes on different branches, so a measured α is constant along a selected branch, invariant under every gauge motion (§76), and free to differ across a switch — which is exactly what makes failure mode (F3) detectable, and what forbids averaging exponents across records that may not share a branch.

67 Closing remarks: three ingredients, one posture

A boundary law that makes openness constitutional; an engine and a budget that make persistence physical; a selector that says which branch is on the instrument. None of the three was built for this supplement — each does its original job in its own paper — and the derivation uses them exactly as imported. The posture is S1-EP's: every step below is derived, conditional with the condition named, or open and said to be open.

Part XII

The Derivation: Four Signatures from One Generator

The bulk-to-boundary kernel rerun at full depth, the four signatures with every step shown, and the two theorems that make the account falsifiable

This Part does what Part III promised: it reruns the Qi-CON derivation of GG-A7-Qi4 Part V at full depth, with every integral evaluated, every constant named, and physics intuition attached at the point of use — and then it adds the two theorems that Part VII, at seventeen pages, did not have room to state. The *lock theorem* of §78 is the formal content of Part VIII's audit: one exponent, four measurements, closed relations with no free parameters. The *failure theorem* of §79 is its complement, and the part of the account this supplement is proudest of: four named conditions under which the signatures *must* degrade, each with a computable observable consequence — several of which the measured record has already exhibited without knowing it was confirming anything. Throughout, notation follows GG-A7-Qi4: the boundary state patch has dimension $d_{\mathcal{S}}$, the generator exponent is α, and every step ends with a grade.

68 The imports, with their grades

Three objects are taken from the companions, and nothing else is assumed.

Import 1 — the boundary law with a radial past. From Arisaka (2026, A5-GDOS): the projected mesoscopic law (21) for the density $\rho(z,t)$ on a boundary patch U of dimension $d_{\mathcal{S}}$, whose kernels are images of six-dimensional bulk modes through the OGGEP projection, the bulk radial coordinate carrying scale as $r = \ln(E_{\mathrm{GUT}}/\mu)$ (Arisaka, 2026, A2-GG6). *Grade: derived upstream; imported whole.*

Import 2 — the selected branch. From Qi-EP (S1-EP; Arisaka, 2026, A7-Qi4): the observer's record samples one GSSB-selected branch γ_*, persisting on an attractor whose slowest relaxation time is τ_{att} and whose finest retained process time is τ_{micro}. *Grade: derived at the level S1-EP establishes; the branch's existence is conditional on the system actually persisting.*

Import 3 — the dominant mode data. For the selected branch, one dominant projected bulk mode with scaling weight Δ and an effective radial measure exponent σ (defined at Eq. (31) below). *Grade: the existence of a dominant mode is derived from the projection; the numerical values (Δ, σ) for a given physical system are at present inputs, not outputs — this is the account's largest open item, stated here before any reader has to hunt for it, and again in the grade table of §81.*

69 The reader's on-ramp: fractional operators, stable laws, and spectral representations

Three pieces of standard mathematics carry everything below; each gets a paragraph so that no step later has to break stride.

The fractional Laplacian. For $0 < \alpha \le 2$, the operator $(-\Delta)^{\alpha/2}$ is defined in Fourier space by multiplication, $\widehat{(-\Delta)^{\alpha/2}} f(k) = |k|^\alpha \widehat{f}(k)$, and in position space by the principal-value jump integral

$$(-\Delta)^{\alpha/2} f(z) = C_{d_{\mathcal{S}},\alpha}\ \mathrm{PV}\!\int \frac{f(z) - f(z')}{|z - z'|^{d_{\mathcal{S}}+\alpha}}\, \mathrm{d}z', \tag{29}$$

a nonlocal operator whose kernel is a pure power. Intuition: where the ordinary Laplacian moves probability to touching neighbors, the fractional Laplacian moves it everywhere at once, with a rate that falls as a power of distance — it is the generator of a jump process whose long jumps are never negligible. At $\alpha = 2$ it degenerates to the ordinary Laplacian and the jumps die (Metzler and Klafter, 2000).

Stable laws. The generalized central limit theorem (Gnedenko and Kolmogorov, 1954, Lévy, 1937) says sums of heavy-tailed increments converge to the α-stable family, with characteristic function $\exp(-D_\alpha t|k|^\alpha)$ in the symmetric case — the unique fixed points of aggregation besides the Gaussian. Whatever microscopic detail a window forgets, aggregation inside the window flows to this family; that is why one exponent can serve four literatures.

Spectral representations and Weyl's law. Any reversible relaxational generator has a mode expansion; correlation functions become weighted sums of decaying exponentials $e^{-\lambda|\tau|}$; and the density of modes of a Laplacian on a $d_{\mathcal{S}}$-dimensional patch obeys Weyl's asymptotic law $N(\lambda) \sim \lambda^{d_{\mathcal{S}}/2}$ (Weyl, 1912). The $1/f$ derivation in §74 is nothing but this bookkeeping applied to the fractional operator.

A two-mode toy, to fix intuition. Superpose just two Lorentzians, $C(\tau) = A_1 e^{-\lambda_1|\tau|} + A_2 e^{-\lambda_2|\tau|}$ with $\lambda_1/\lambda_2 = 10^3$: across the inter-scale range the log–log spectrum's local slope sweeps continuously from 0 through -1 to -2, and over any single decade it can pass for a power law. Two scales already fake a band; that is why nothing below rests on the *appearance* of $1/f$ — the derivation's content is a mode *density* with a derived exponent (46) and two knees at derivable places, and the failure theorem's mode (F3) is this toy's heavy-tailed cousin.

70 From the 6D bulk to the homogeneous boundary kernel: where α comes from

The derivation begins in the bulk. A dominant projected mode of weight Δ reaches the boundary through the bulk-to-boundary propagator whose form the scale isometry forces (§57; Maldacena, 1998),

$$K_\Delta(\zeta; z, z') = \left(\frac{\zeta}{\zeta^2 + \ell^2}\right)^{\Delta}, \qquad \ell = d_g(z, z'), \tag{30}$$

with $\zeta = e^{-r/L}$ the positive scale coordinate (large ζ coarse, small ζ fine). A jump *rate* is an amplitude squared: the mode reaches each endpoint of the jump through one factor of the propagator, so the OGGEP projection, integrating over the hidden scale range with an effective radial weight

$$\omega(\zeta) = \zeta^{\sigma-1} w(\zeta), \qquad w(\zeta) \approx w_0 \text{ slowly varying,} \tag{31}$$

induces the boundary jump kernel

$$W_\Delta(z, z') = \int_{\zeta_{\min}}^{\zeta_{\max}} \omega(\zeta) \left[K_\Delta(\zeta; z, z')\right]^2 \mathrm{d}\zeta \approx w_0 \int_{\zeta_{\min}}^{\zeta_{\max}} \frac{\zeta^{\sigma+2\Delta-1}}{(\zeta^2+\ell^2)^{2\Delta}} \, \mathrm{d}\zeta. \tag{32}$$

Substituting $\zeta = \ell u$ separates the scales: each factor of ζ contributes one power of ℓ, the denominator contributes $\ell^{-4\Delta}$, and the measure one more, so

$$W_\Delta(z, z') \approx w_0 \, \ell^{\sigma-2\Delta} \int_{\zeta_{\min}/\ell}^{\zeta_{\max}/\ell} \frac{u^{\sigma+2\Delta-1}}{(1+u^2)^{2\Delta}} \, \mathrm{d}u. \tag{33}$$

Inside the operational window $\zeta_{\min} \ll \ell \ll \zeta_{\max}$ the limits recede to 0 and ∞ and the integral saturates to a pure number, which this supplement evaluates rather than names: with $\int_0^\infty u^{a-1}(1+u^2)^{-b}\,\mathrm{d}u = \frac{1}{2}B(\frac{a}{2}, b-\frac{a}{2})$,

$$C_{\Delta,\sigma} = \int_0^\infty \frac{u^{\sigma+2\Delta-1}}{(1+u^2)^{2\Delta}} \, \mathrm{d}u = \frac{1}{2} B\left(\Delta + \frac{\sigma}{2},\ \Delta - \frac{\sigma}{2}\right), \tag{34}$$

finite precisely when $2\Delta > \sigma > -2\Delta$ — the convergence condition and the admissibility bounds below are the same fact seen twice. (Appendix A (§107) carries the full algebra, including the finite-window corrections that §79 turns into failure mode F1. A note of record: an earlier draft of GG-A7-Qi4 wrote this step, in that paper's Part V schematic, with a single propagator factor, for which the substitution yields $\ell^{\sigma-\Delta}$ rather than the printed $\ell^{\sigma-2\Delta}$; the discrepancy was found while this appendix was being extended, and the published version carries the exchange form. Both papers now print the same derivation, and the identification (36) that every downstream result uses is unchanged by the repair.) Therefore

$$W_\Delta(z, z') \ \propto\ \ell^{-(2\Delta-\sigma)}, \tag{35}$$

a power-law kernel with no intrinsic scale: the hidden radial integral has been traded for boundary homogeneity. Identifying the homogeneity degree with that of a fractional jump kernel,

$$2\Delta - \sigma = d_{\mathcal{S}} + \alpha, \qquad 0 < \alpha \le 2, \tag{36}$$

gives $W_\Delta(z, z') \propto d_g(z, z')^{-(d_{\mathcal{S}}+\alpha)}$ — exactly the kernel of (29) — so the leading nonlocal generator on the branch is

$$\mathcal{J}_\alpha = -\, D_\alpha \, (-\Delta_g)^{\alpha/2}. \tag{37}$$

The admissibility window is forced, not chosen: $\alpha = 2$ is the Gaussian boundary where the kernel becomes a heat semigroup; $\alpha > 2$ would make the kernel more singular than the principal value can absorb (the operator stops being dissipative — the standard Riesz-potential bound); $\alpha \le 0$ makes it non-integrable at large separation. In bulk terms: $(d_{\mathcal{S}}+\sigma)/2 < \Delta \le (d_{\mathcal{S}}+\sigma+2)/2$ — comfortably inside the convergence window $|\sigma| < 2\Delta$ of (34).

Physics intuition, because this is the step everything rides on: the observer cannot see the scale coordinate, only its integral. Integrating out a direction whose isometry is dilation leaves the boundary with the only kernel dilation permits — a power law — and the exponent the boundary inherits is the bulk mode's weight, twice, minus what the projection's measure keeps. The exponent α is not fitted to any dataset; it is the shadow of (Δ, σ). [Grade: **derived**, conditional on the window separation $\zeta_{\min} \ll \ell \ll \zeta_{\max}$ — which is the same window every empirical Part of this supplement kept finding.]

71 First signature: operational conformality

On the selected branch the full projected equation carries drift, local diffusion, the nonlocal term, and sources; the Qi-CON window is the regime where the homogeneous term leads:

$$\partial_t \rho = -\, D_\alpha (-\Delta_g)^{\alpha/2} \rho \ + \ \text{sub-leading}. \tag{38}$$

Under $z \mapsto \lambda z$, a direct Fourier computation gives $\mathcal{S}_\lambda^{-1}(-\Delta_g)^{\alpha/2}\mathcal{S}_\lambda = \lambda^\alpha(-\Delta_g)^{\alpha/2}$, so (38) is invariant under

$$z \mapsto \lambda z, \qquad t \mapsto \lambda^\alpha t \tag{39}$$

— no preferred length or time inside the window, with dynamic exponent $z_{\text{dyn}} = \alpha$. The point-source solution makes the covariance concrete: Fourier transforming (38) and inverting,

$$p_\alpha(t,z) = t^{-d_{\mathcal{S}}/\alpha}\, \Phi_\alpha\!\left(\frac{z}{t^{1/\alpha}}\right), \qquad p_\alpha(\lambda^\alpha t, \lambda z) = \lambda^{-d_{\mathcal{S}}} p_\alpha(t,z), \tag{40}$$

and any scale-covariant observable O of effective weight Δ_O obeys, in the window,

$$\langle O(\lambda z, \lambda^\alpha t)\, O(0,0)\rangle = \lambda^{-2\Delta_O} \langle O(z,t)\, O(0,0)\rangle, \qquad \langle O(z) O(0)\rangle \propto |z|^{-2\Delta_O}, \tag{41}$$

which is GG-A7-Qi4's operational conformality theorem (T-Qi4-11.4) with the proof displayed. The word "operational" is doing exact work: the claim is homogeneity over a finite window on a selected branch — the empirical shape Parts IV–VII found everywhere — not a global CFT, and Part X has already drawn the line between the two. In the record, this signature owns the critical scoreboard of Table 3 — where homogeneity is exact and the account must reduce to the standard theory — and it is what the estimator literature probes whenever a collapse of curves under $(z,t) \to (\lambda z, \lambda^\alpha t)$ is attempted. [Grade: **derived**.]

72 Second signature: Lévy statistics

Project onto one coarse coordinate X_t. In the drift-free leading regime its density obeys the one-dimensional form of (38), so its characteristic function is

$$\phi_{X_t}(k) = \mathbb{E}\big[e^{\mathrm{i}kX_t}\big] = \exp\big[-D_\alpha t|k|^\alpha\big] \tag{42}$$

— the defining form of the symmetric α-stable law (Gnedenko and Kolmogorov, 1954). Three consequences, each doing empirical work in Part V's record:

1. **Self-similarity:** $X_t \overset{d}{=} t^{1/\alpha} X_1$ — the same exponent that scaled the semigroup.

2. **Heavy tails:** for $0 < \alpha < 2$,

$$p(x,t) \;\sim\; \frac{D_\alpha\, t\,\Gamma(1+\alpha)\sin(\pi\alpha/2)}{\pi\,|x|^{1+\alpha}} \qquad (|x| \to \infty), \tag{43}$$

   so the step-length *density* exponent is $\mu = 1 + \alpha$ and the survival exponent is $\alpha_{\mathrm{s}} = \alpha$ — the dictionary (R1) of Part VIII, here as an output.

3. **Truncation is physical, not a nuisance:** the same attractor cutoff L_{att} that will bound the spectral band tempers the tail at the largest scales, so the account predicts *truncated* stable statistics over the window — the object the post-reformation movement literature actually fits — and never an infinite-scale law.

Intuition: inside a window with no scale, the walk cannot afford a mean step — a mean step would be a scale. Heavy tails are not exotic here; they are what scale-freedom forces on increments. In the record, this signature owns every row of Table 4, and its estimator dictionary is the one the reformation built: truncated maximum likelihood with stated windows, whose bias directions are exactly the tempering interpolation of Appendix B (§108). [Grade: **derived**.]

73 Third signature: fractal support

Self-similarity fixes the geometry of the trajectory. A time interval δt produces excursions $\delta x \sim (\delta t)^{1/\alpha}$; resolving the path at scale ε therefore costs $\delta t \sim \varepsilon^\alpha$ per segment, and an observation of duration T supplies $N_T(\varepsilon) \sim T\varepsilon^{-\alpha}$ segments — capped by the $\varepsilon^{-d_{\mathcal{S}}}$ boxes the ambient patch owns. Hence

$$N(\varepsilon) \sim \varepsilon^{-D_{\mathrm{f}}}, \qquad D_{\mathrm{f}} = \min(d_{\mathcal{S}}, \alpha), \qquad \ell_{\mathrm{micro}} < \varepsilon < L_{\mathrm{att}}, \tag{44}$$

the box-counting form of the exact stable-path theorem (Blumenthal and Getoor, 1960), and dictionary (R2) of Part VIII as an output. If GSSB confines the branch to an attractor support $A \subset U$, then $D_A \le D_{\mathrm{f}}$ — selection can only lower the dimension. Two empirical echoes: the trajectory dimension is capped by $\alpha < 2$ no matter how roomy the ambient space, which is why Part VI's biological block lives so far below its embedding dimensions; and the window in (44) is the same window again — the account predicts fractality over $\log_{10}(L_{\mathrm{att}}/\ell_{\mathrm{micro}})$ decades and no more, which is Avnir's finding read as a theorem rather than a scandal. In the record, this signature owns the trajectory-like rows of Table 5 — the flight geometry itself, in the scope dictionary R2 declares — while the grown structures (arbors, vasculature, aggregates) test it only through the process that drew them. [Grade: **derived**.]

74 Fourth signature: the $1/f$ band and both knees

Let $X(t)$ be a centered observable on the branch, with mode expansion of its autocorrelation over the generator's relaxation spectrum:

$$C_X(\tau) = \int_{\lambda_{\mathrm{IR}}}^{\lambda_{\mathrm{UV}}} A_X(\lambda)\, e^{-\lambda|\tau|}\, \rho(\lambda)\, \mathrm{d}\lambda. \tag{45}$$

The mode density is not free: Weyl's law for the Laplacian on a $d_{\mathcal{S}}$-patch, $N(\lambda) \sim \lambda^{d_{\mathcal{S}}/2}$, lifts through the functional calculus (the fractional operator shares eigenspaces, with eigenvalues $\lambda_n^{\alpha/2}$) to

$$\rho_\alpha(\lambda) \sim \lambda^{d_{\mathcal{S}}/\alpha - 1}, \tag{46}$$

so with an observable weight $A_X(\lambda) \sim \lambda^{\gamma - d_{\mathcal{S}}/\alpha}$ the soft-mode product is a power, $A_X \rho_\alpha \approx A_0 \lambda^{\gamma-1}$, $0 \le \gamma < 1$. The spectrum follows from one Lorentzian integral:

$$S_X(\omega) = 2\int_{\lambda_{\mathrm{IR}}}^{\lambda_{\mathrm{UV}}} \frac{\lambda\, A_X(\lambda)\rho(\lambda)}{\lambda^2+\omega^2}\, \mathrm{d}\lambda = 2A_0\, \omega^{\gamma-1} \int_{\lambda_{\mathrm{IR}}/\omega}^{\lambda_{\mathrm{UV}}/\omega} \frac{u^\gamma}{1+u^2}\, \mathrm{d}u, \tag{47}$$

and the three regimes separate exactly as in Part VII's null model (10) — but now with the density *derived* rather than postulated:

$$S_X(f) \approx \begin{cases} S_0, & f < f_{\mathrm{IR}}, \\ A\, f^{-\beta}, \quad \beta = 1-\gamma, & f_{\mathrm{IR}} < f < f_{\mathrm{UV}}, \\ B\, f^{-2}, & f > f_{\mathrm{UV}}, \end{cases} \tag{48}$$

using $\int_0^\infty u^\gamma (1+u^2)^{-1} \mathrm{d}u = \frac{\pi}{2}\sec(\pi\gamma/2)$ in the middle band. The knees are the window's own edges in frequency dress:

$$f_{\mathrm{IR}} = \frac{\lambda_{\mathrm{IR}}}{2\pi} \sim \frac{1}{2\pi\, \tau_{\mathrm{att}}}, \qquad f_{\mathrm{UV}} = \frac{\lambda_{\mathrm{UV}}}{2\pi} \sim \frac{1}{2\pi\, \tau_{\mathrm{micro}}}, \tag{49}$$

the infrared knee at the attractor's slowest relaxation (GRIP's persistence scale, §64), the ultraviolet knee at the finest retained process time. This is GG-A7-Qi4's two-knee theorem (T-Qi4-11.7) with the mode-density pedigree displayed. Intuition: a $1/f$ band is a census of active timescales, and a *selected, persisting, projected* system has a bounded census — bounded above by what it resolves and below by what it survives. That the census's edges are almost never measured is Part VII's principal empirical finding; that they must exist is this section's principal theoretical one. In the record, this signature owns Table 6 and the knee census both — and of the four it is the one whose *distinctive* content is not the slope (every mechanism predicts a slope) but the two knees at derivable places. [Grade: the band and knees are **derived**; the slope's numerical value is **conditional** on the observable's coupling weight γ — uniform soft-mode coupling gives $\gamma \approx 0$, $\beta \approx 1$ — and the knee *locations* for a named physical system require that system's $\tau_{\mathrm{att}}, \tau_{\mathrm{micro}}$, which the program does not compute from first principles. Both conditions are in the grade table.]

75 The spectral dictionaries, derived rather than borrowed

Part VIII used two dictionaries this Part has not yet touched: the fGn/fBm relation $\beta = 2H \mp 1$ (R3) and the fractal point-process relation (R4). Both follow from the spectral representation already in hand, and deriving them here closes the loop between the audit's instruments and the generator.

The Hurst dictionary. Let $Y(t) = \int_0^t X(s)\,\mathrm{d}s$ be the integrated record of a windowed observable with spectrum $S_X(f) \propto f^{-\beta}$, $0 \le \beta < 1$ (the stationary, fGn branch). The variance of the increment over lag τ is the standard spectral integral

$$\begin{aligned}\langle [Y(t+\tau) - Y(t)]^2 \rangle &= \int_0^\infty S_X(f)\,\frac{\sin^2(\pi f\tau)}{(\pi f)^2}\,\mathrm{d}f \;\propto\; \int_0^\infty f^{-\beta-2}\sin^2(\pi f\tau)\,\mathrm{d}f \\ &= \tau^{\beta+1}\int_0^\infty u^{-\beta-2}\sin^2(\pi u)\,\mathrm{d}u, \end{aligned} \tag{50}$$

with $u = f\tau$; the dimensionless integral converges at both ends precisely for $0 \le \beta < 1$, i.e. on the stationary branch inside the band. Writing the increment scaling as τ^{2H} identifies

$$2H = \beta + 1 \qquad \Longleftrightarrow \qquad \beta = 2H - 1, \tag{51}$$

the fGn dictionary; differentiating rather than integrating shifts the spectrum by f^2 and gives the fBm branch $\beta = 2H + 1$. So (R3) is not an independent assumption of the audit: it is the two-knee spectrum (48) read through an integrator, and it holds exactly on the band and fails exactly at the knees — which is why Part VIII's climate pairs, fitted across a reported break, carry the widest honest error bars.

The point-process dictionary. For a counting record $N(T)$ driven by rate fluctuations with the band spectrum (48), the count variance over windows T inside the band inherits the increment scaling (50): the rate contribution to $\operatorname{Var} N(T)$ grows as $T^{1+\beta}$, so the Fano factor

$$F(T) \;=\; \frac{\operatorname{Var} N(T)}{\langle N(T)\rangle} \;=\; 1 + \left(\frac{T}{T_F}\right)^{\beta}, \qquad 0 < \beta < 1, \tag{52}$$

carries the *same* band exponent as the spectrum (Appendix C (§109) displays the integral), so count-based and spectrum-based estimates of the one exponent must agree on the band — relation (R4) — while the estimators saturate differently at the knees, which is the bias the auditory-nerve literature dissected (Lowen and Teich, 1996) and the reason the Teich pairs sit off the identity line at exactly the offset their own methods paper predicts. (An earlier draft of this section wrote the Fano exponent as $1 - \beta$; the displayed integral gives β, and Appendix C (§109) is the check.)

The Allan dictionary. The same spectral integral read through the two-sample (Allan) variance extends the dictionary where the Hurst integral fails: for $S_X(f) \propto f^{-\beta}$ on the band, $\sigma_A^2(\tau) \propto \tau^{\beta-1}$ for $0 \leq \beta < 3$, $\beta \neq 1$ (logarithmic at $\beta = 1$), so the Allan slope tracks the band through and beyond the nonstationary boundary $\beta = 1$ that stops (50) — which is why the clock literature, which lives at that boundary, adopted it. On the band all three instruments — spectrum, Fano, Allan — are one exponent in three dresses; at the knees they part company in computable ways, and an experimenter who measures all three brackets the band edges without ever fitting a knee directly.

[Grade: **derived** on the band, for both dictionaries; the knee-adjacent corrections are computable case by case and are where the audit's cross-estimator scatter is predicted to live.]

76 Why the exponents are runtime invariants

One more property the audit quietly relied on deserves its derivation: that a measured exponent is a property of the *branch*, not of the observer's coordinates or instruments. Three runtime layers enforce this (GG-A7-Qi4 Part V, §43, restated here with the mechanism visible). DGI acts on the effective generator by similarity — gauge conjugation $\mathcal{L} \mapsto G\mathcal{L}G^{-1}$ — and similarity preserves spectra: α, the mode density (46), β, and both knee rates are spectral data, hence gauge invariants. GSSB fixes the universality class: exponents are constant *within* a selected branch and free to differ *between* branches, which is why failure mode (F3) — branch switching — is detectable at all: a switch changes spectral data that no gauge transformation can change. And Qi-QUA's locking (28) extends the invariance across the four current sectors, making the shared slope of (L4) a cross-observable statement rather than a per-instrument accident. The operational content for an experimenter is one sentence: *if two calibrated instruments on one branch and window return different exponents, the discrepancy is physics — estimator bias, sector mixture, or branch switching — never convention.* [Grade: **derived**, at the level the runtime theorems are established upstream.]

77 Why any open system is predicted to follow Qi-CON

Everything so far concerned one branch of one system. The reach of the claim — the reason a supplement about sharks, neurons, and resistors can carry one derivation — is a structural observation stated in GG-A7-Qi4 and expanded here, because it is the hinge on which the whole cross-domain program turns. Any open system with

1. **scale separation** — a nontrivial gap between its microscopic process time and its macroscopic persistence time;
2. **a selected, persisting branch** — an attractor Qi-EP has fixed and GRIP maintains;
3. **repeated throughput** — energy, matter, or information cycled through open ports, so the branch is driven rather than dead; and
4. **a partial view** — observer access only to a projected coarse state, with the scale coordinate hidden

is a candidate for an operational Qi-CON window, because those four conditions are exactly the hypotheses the derivation above consumed — nothing else was used. And the four conditions are generic, not special. Scale separation is the default state of matter organized into levels: molecules are faster than cells, cells than organisms, organisms than populations. Selection and persistence are the price of admission to any record — a system that does not persist is not measured, so every dataset in this supplement's tables is drawn from the persisting class by construction. Throughput is the definition of being alive, and of being a driven device. And the partial view is not an experimental shortcoming but the constitution's axiom: no finite observer ever holds the full state. A reader should notice what this argument does and does not license. It does *not* predict that every dataset shows clean power laws over many decades — finite size, forcing, poor scale separation, instrument bandwidth, and branch switching all shorten or bury the window, and the failure theorem below prices each. It predicts something sharper and more falsifiable: *wherever* a selected open system exhibits a clear intermediate scale regime, that regime's statistics must be the Qi-CON quartet — one exponent, four signatures, two knees — and not some fifth thing. The prediction is conditional in form and universal in scope, which is what makes the audit of Part VIII a single test of many systems at once.

Table 10 states the expectation by domain, in the same posture as GG-A7-Qi4's own domain tables: placements, not predictions — the value of the table is that it says in advance where the account expects *two* knees rather than one, and which coarse observable should carry them.

Table 10: Where the window should sit, by domain. The four structural conditions read across five domains: the typical coarse observable an experimenter actually records, the physical scales expected to set the two knees, and the expected Qi-CON readout. The entries are organizational placements in GG-A7-Qi4's sense — they orient measurement, and none is offered as evidence; the audited evidence lives in Parts IV–VIII. What the table adds to the record is the advance commitment of *where the knees belong*: an infrared knee at the homeostatic, behavioral, or institutional relaxation time, an ultraviolet knee at the reaction, synaptic, or event time — so a measured knee far from its column, or a verified two-decade search below the attractor scale finding no knee at all, is evidence against the account (falsifier F-S2-3 of §80).

Domain	Coarse observable	Expected knees (IR / UV)	Expected readout
Transport, devices	channel current, arrival times	device turnover / scattering time	power-law transit statistics, band-limited current noise
Molecular machines	dwell times, cycle currents	whole-cycle return / chemical substep	heavy-tailed dwells, broad intermediate band
Cells, networks	fluxes, burst sizes, concentrations	homeostatic relaxation / reaction microtime	fractal switching, correlated fluctuations across scales
Brains	field potentials, avalanches	behavioral cycle / synaptic time	two-knee $1/f$, heavy-tailed events, scale-free dynamics
Ecologies, societies	populations, traffic, transactions	institutional or seasonal / individual event	truncated heavy tails, knee-bounded spectra

[Grade: **derived**, as a scope statement: the conditions are the derivation's own hypotheses, and the genericity arguments are structural. What is *not* claimed at this strength: that any particular system's window is wide enough to measure — that is an empirical question the record answers system by system.]

78 The lock theorem: one α, four measurements

Everything above can now be compressed into the statement Part VIII audited. It deserves theorem form, because its content is not any single signature — every signature has rival explanations — but the *arithmetic between* them, which rivals assembled from four separate mechanisms do not owe anyone.

Theorem 78.1 (The lock theorem, T-S2-1)**.** *Let a Qi-EP-selected branch possess a Qi-CON window with exponent $0 < \alpha < 2$ on a boundary patch of dimension $d_{\mathcal{S}}$, with window edges $(\tau_{\text{micro}}, \tau_{\text{att}})$. Then, over that window, the following are simultaneously forced, all by the one exponent:*

(L1) ***Dynamic scaling:*** *correlators are homogeneous under $z \mapsto \lambda z$, $t \mapsto \lambda^{\alpha} t$; equal-time correlators of a weight-Δ_O observable fall as $|z|^{-2\Delta_O}$; the dynamic exponent is $z_{\text{dyn}} = \alpha$.*

(L2) ***Step statistics:*** *coarse increments are (truncated) symmetric α-stable; the survival exponent is $\alpha_{\mathrm{s}} = \alpha$ and the step-length density exponent is $\mu = 1 + \alpha$.*

(L3) ***Path geometry:*** *trajectory ranges have box dimension $D_{\mathrm{f}} = \min(d_{\mathcal{S}}, \alpha)$, and any GSSB-confined support obeys $D_A \le D_{\mathrm{f}}$.*

(L4) ***Spectral band:*** *every observable with soft-mode overlap carries $S(f) \propto f^{-\beta}$ between the* common *knees $f_{\mathrm{IR}} \sim 1/(2\pi\tau_{\mathrm{att}})$ and $f_{\mathrm{UV}} \sim 1/(2\pi\tau_{\mathrm{micro}})$, with $\beta = 1-\gamma$ fixed by the observable's coupling weight, and with sector-resolved currents sharing one slope across the window by Qi-QUA locking.*

Consequently the closed relations

$$\mu - 1 \;=\; \alpha_{\mathrm{s}} \;=\; \alpha \;=\; z_{\mathrm{dyn}}, \qquad D_{\mathrm{f}} = \min(d_{\mathcal{S}},\, \mu - 1), \tag{53}$$

hold with no adjustable constant, and any two of μ, α_{s}, D_{f}, and z_{dyn}, independently measured on one system and window (the dimension usable when $d_{\mathcal{S}} \ge 2$), determine the rest.

Proof. (L1) is §71; (L2) is §72; (L3) is §73; (L4) is §74. Each was derived from the single leading generator (37), whose one exponent α appears in all four; (53) collects the identifications. The window edges in (L4) are those of the projection itself, hence common to all observables on the branch. ■

Two clauses of honesty, stated at theorem strength because they bound the claim. First, **the hard lock is (L1)–(L3)**: three exponents, one α, zero conditions beyond the window. The spectral slope in (L4) locks *conditionally* — it needs the coupling weight γ, and only the knees and the slope-sharing across currents are unconditional. A reader should therefore weight Part VIII's audit accordingly, and it was built accordingly: its hardest points test (L2) against (L3) and the crackling identity, and its spectral pairs carry the widest error bars. Second, **the lock is per branch and per window**: nothing in T-S2-1 licenses comparing a μ measured in one window with a β measured in another, and §79 makes the penalty for doing so computable.

Four corollaries put the theorem where each record's community can use it. **(Movement ecology.)** Any tracking study that fits a step exponent μ owns, at zero marginal cost, a predicted path dimension $D_{\mathrm{f}} = \min(d, \mu - 1)$ and a predicted survival exponent $\mu - 1$ on the same data — so every published μ is half of an untested lock point. **(Fractal geometry.)** A measured dimension of a *trajectory-like* structure predicts the step statistics of the process that drew it; a dimension without a window statement is, by F1 below, not yet a measurement of anything. **(Spectra.)** A band slope β alone constrains nothing in the lock — the hard content is the *knees*, which must sit at $1/(2\pi\tau_{\mathrm{att}})$ and $1/(2\pi\tau_{\mathrm{micro}})$ for independently estimable τ's, and the slope must be shared across simultaneously recorded currents. **(Avalanches.)** The crackling relation the audit uses as R5 is the lock's projection onto threshold-driven branches, which is why a prospective crackling test (F-S2-4) is a test of this theorem and not only of its own literature.

The theorem settles what would falsify the account, in the sentence Part VIII used: *a system yielding a step exponent, a dimension, and a dynamic exponent that violate* (53) *at published* *uncertainties, inside one verified window, refutes the one-generator claim for that system regardless of how well any single exponent was fitted.* The measurement program of §43 is the cheapest route to such a point.

79 The failure theorem: where the four signatures must degrade

A derivation that only predicts successes is decoration. The same construction that produces the signatures fixes where they break, and the four failure modes below are not caveats appended for safety — each is a computable consequence of the projection, with an observable fingerprint, and the measured record of Parts IV–VII already contains three of the four.

Theorem 79.1 (The failure theorem, T-S2-2)**.** *Under the hypotheses of T-S2-1, the four signatures degrade in the following named ways, and only in these ways, as the hypotheses are relaxed:*

(F1) ***Window collapse.*** *If the scale separation $\log_{10}(\zeta_{\max}/\zeta_{\min})$ falls toward one decade, the saturation step in (33) fails: the integral retains its limits, the kernel is no longer a pure power, and every fitted exponent acquires a dependence on the fitting range of relative order $1/\ln(\zeta_{\max}/\zeta_{\min})$. Fingerprint: exponents that drift when the fit window moves.*

(F2) ***Truncation and tempering.*** *The attractor cutoff L_{att} tempers the stable tail: beyond $\ell_c \sim L_{\text{att}}$ the density falls exponentially, and maximum-likelihood fits over ranges approaching ℓ_c return effective exponents biased toward the Gaussian ($\mu \to 3$ from below). Fingerprint: the fitted μ rises as the largest scales enter the fit.*

(F3) ***Branch switching.*** *If GSSB switches the selected branch on a timescale inside the observation, the record is a mixture of generators (α_1, D_1) and (α_2, D_2). A mixture of two* Gaussian *branches ($\alpha_i = 2$) with well-separated rates already produces an apparent power law across the inter-scale range; a mixture of stable branches produces an apparent single α that is a window-weighted compromise. Fingerprint: model selection prefers composite models, and single-exponent fits disagree across sub-records.*

(F4) ***Sector domination.*** *Outside the window — or inside it, under strong forcing — the drift, curl, or source sectors of the full boundary equation dominate the fractional term, and homogeneity fails sector by sector: deterministic drift inserts ballistic segments, periodic forcing inserts spectral peaks, and sources break stationarity. Fingerprint: signatures that appear only after the periodic and trend components are separated out.*

Proof. (F1): with finite limits, (33) is $\ell^{\sigma-2\Delta}$ times an incomplete-Beta expression whose ℓ-dependence enters through both limits; expanding around the saturated value (Appendix A (§107), where the drift law is derived and evaluated) gives corrections of relative size $(\ell/\zeta_{\max})^{2\Delta-\sigma} = (\ell/\zeta_{\max})^{d_S+\alpha}$ and $(\zeta_{\min}/\ell)^{2\Delta+\sigma}$, which are $O(1)$ once the window is a single decade. (F2): tempering the kernel at L_{att} restores all moments; the generalized CLT then drives aggregates toward the Gaussian fixed point, and the likelihood estimator interpolates. (F3): the two-branch mixture's increment distribution is the rate-weighted sum; between the two mode scales neither Gaussian dominates and the log–log slope is locally near-linear — the composite-walk construction of the movement-ecology literature, here as a corollary of GSSB. (F4): immediate from the sector decomposition of the full equation (21): homogeneity was a property of the fractional sector alone. ■

Each mode now gets its number, because a failure theory without magnitudes is still decoration. **(F1, quantitatively.)** For the representative case $d_{\mathcal{S}} + \alpha = 3$, $\sigma = 0$, the drift law of Appendix A (§107) gives a local fitted slope that spans roughly ± 0.3 — ten percent of the exponent — across the central half-decade of a 1.3-decade window, falling to $\pm 1\%$ at two decades and below $\pm 0.1\%$ at three: the one-decade "fractals" of the Avnir census are not sloppy measurements of a true exponent, they are windows in which no stable exponent exists to measure. **(F2, quantitatively.)** Tempering at ℓ_c restores a finite variance at rate $\alpha D_\alpha \ell_c^{2-\alpha}$ (Appendix B (§108)), so beyond the crossover time $t_c \sim \ell_c^\alpha / D_\alpha$ aggregation is Gaussian and a maximum-likelihood μ fitted across ℓ_c interpolates upward — the bigeye tuna refit's binned 2.4 against truncated-MLE 1.37 is this interpolation caught mid-stride. **(F3, quantitatively.)** Two Gaussian branches with diffusivities separated by a factor 10^3 produce an apparent inter-scale slope near the Lévy range across $\sim$1.5 decades — the two-mode toy of §69 in the step domain — indistinguishable from a genuine α by any single-record fit, and distinguishable at once by sub-record disagreement, which is the content of falsifier F-S2-5. **(F4, quantitatively.)** A periodic drive inserts a spectral line whose height relative to the band is set by the drive's share of the variance; at typical cortical rhythm weights the line dominates its neighborhood of the band, which is why the aperiodic-component literature separates before fitting (Donoghue et al., 2020), and why a slope fitted through an unremoved line is biased by an amount that literature tabulates.

The record has already met three of these, and the audit Parts said so in their own language. **(F1) is the Avnir census** — exponents fitted over 1.3 decades drifting with the window is exactly the incomplete-saturation regime, and Part VI's conclusion that scale invariance lives in windows is F1 read from the data side. **(F2) is the bigeye tuna refit**: binned $\mu = 2.4$ falling to truncated-MLE 1.37 is the tempering interpolation in action. **(F3) is the composite-walk mimicry** that Part V treated as the record's standing ambiguity: Auger-Méthé et al. (2015)'s construction is the two-Gaussian-branch mixture, and the account adds a prediction: where mimicry is the truth, sub-record fits must disagree, because a genuine Qi-CON branch has one α and a mixture does not. **(F4) is neuroscience's standard practice** — separating aperiodic from periodic components before fitting (Donoghue et al., 2020), because cortical records are the forced, sector-mixed case. The one mode without a clean exhibit is (F1) at controlled window width; a tunable-window system — the Lévy glass, the cold-atom lattice — could supply it, and §80 numbers it as F-S2-6.

80 The falsification program: F-S2-1 through F-S2-6

POS-7 requires that every central claim name, in advance, the measurement that would kill it, and the cohort states such falsifiers as numbered commitments. Here are this supplement's six — each feasible with existing instruments, each aimed at a specific theorem above, and each stated with its kill condition so that no reader has to infer what would count.

F-S2-1 A lock violation in one verified window. Measure any two of $\{\mu, \alpha_s, D_f, z_{dyn}\}$ independently on one system, one branch, one stated window. *Kill condition:* the pair violates (53) beyond its propagated uncertainties, with the sub-record checks of T-S2-2 excluding the lawful modes F1–F4. This is the general-purpose falsifier; the audit of Part VIII is its standing instrument, and any seventeenth pair qualifies.

F-S2-2 The marine-predator re-estimate. The dive series behind the record's best triple (§83) permit β and H to be re-estimated with modern methods and stated windows on the same data that gave μ. *Kill condition:* the refreshed (β, H) pair misses the R3 dictionary, or the implied α misses the step-derived $\mu - 1$, at three standard errors. The data exist; this is an afternoon of computation, and the account has no mechanism for absorbing a miss.

F-S2-3 The missing biological knee. Extend any physiological $1/f$ record two decades below the independently estimated attractor frequency $1/(2\pi\tau_{att})$ — heart, respiration, postural sway, cortical rest. *Kill condition:* the band continues, knee-free, through the two decades. The knee census (§36) shows this measurement has essentially never been attempted outside cortex; the account requires the knee to be there.

F-S2-4 A prospective crackling failure. Pre-register exponents $(\tau, \tau_t, \gamma_{st})$ for one new threshold-driven system, then measure. *Kill condition:* the crackling identity fails at stated uncertainties in a system whose sub-records pass the F1–F4 screens. Retrospective fits have too many degrees of freedom; one clean prospective failure outweighs them all.

F-S2-5 Mimicry with agreeing sub-records. Produce one movement record demonstrably generated by a composite (multi-mode) walk whose sub-records nevertheless *agree* on a single stable α at full precision. *Kill condition:* such a record exists — it would destroy the account's only instrument (T-S2-2, F3) for separating genuine Qi-CON branches from mixtures, and with it the evidential force of the whole Lévy record.

F-S2-6 The drift law in a tunable window. In a system whose scale window can be dialed — a Lévy glass, a dissipative cold-atom lattice — measure the fitted-exponent drift as the window narrows from three decades to one. *Kill condition:* the drift departs from the incomplete-Beta law of Appendix A (§107) (the ±10%-at-1.3-decades schedule of §79) in magnitude or in sign. This is F1 as a quantitative prediction rather than a caution, and no rival framework predicts any particular drift law at all.

Six numbered measurements, all feasible now. Any one of them can put a point far off the line; none of them requires the program to first compute (Δ, σ) for the system in question — which is precisely what makes the account testable *before* its largest open item is closed.

81 The grade of every step

The posture promised in Part III, in one table.

Table 11: The derivation, graded step by step. Every load-bearing step of Parts XI–XII with its grade: *derived* (follows from the imports by displayed computation), *conditional* (derived given a named condition), or *open* (not currently computed by the program). The table is the paper's honesty ledger; its two open rows are the program's real frontier: the form of all four signatures and their relations are derived, and the numerical exponent and knee positions of any named system are not yet computed.

Step	Grade	Condition / location
Boundary law with four-sector current	derived	upstream (Arisaka, 2026, A5-GDOS); imported
Homogeneous kernel from radial integral	derived	window separation (33); constant evaluated at (34)
Exponent identification $2\Delta - \sigma = d_{\mathcal{S}} + \alpha$	derived	admissibility $0 < \alpha \leq 2$ forced
Numerical (Δ, σ) for a named system	**open**	the account's largest gap, stated in §68
Operational conformality (L1)	derived	§71
Stable increments and $\mu = 1 + \alpha$ (L2)	derived	§72; truncation predicted
Path dimension $D_{\mathrm{f}} = \min(d_{\mathcal{S}}, \alpha)$ (L3)	derived	§73; exact-process anchor (Blumenthal and Getoor, 1960)
Soft-mode density $\rho_\alpha \sim \lambda^{d_{\mathcal{S}}/\alpha - 1}$	derived	Weyl asymptotics
Spectral slope $\beta = 1 - \gamma$	conditional	needs coupling weight γ; uniform coupling $\Rightarrow \beta \approx 1$
Two knees at the window edges (L4)	derived (form)	locations need $\tau_{\mathrm{att}}, \tau_{\mathrm{micro}}$ per system: **open**
Slope sharing across currents	conditional	Qi-QUA locking; overhead leaves slopes common
Lock theorem T-S2-1	derived	given the window; hard for (L1)–(L3), conditional clause for (L4)
Failure theorem T-S2-2	derived	each mode with displayed mechanism, and a magnitude per mode (§79)
Exchange (amplitude-squared) form of the projected kernel	derived	§70; full algebra in Appendix A (§107)
Universality conditions (scale separation, selection, throughput, partial view)	derived	scope statement, §77; window width per system empirical
Fano and Allan dictionaries on the band	derived	Appendix C (§109); knee-adjacent corrections computable
Falsifiers F-S2-1..6 stated with kill conditions	—	§80; none requires computing (Δ, σ) first

The two open rows are the difference between this account and a finished theory: the program derives one generator, four signatures, the lock, the failure modes, and the necessity of the window — and not yet the number α, nor the hertz of the knees, for any named system. Until it does, the account's empirical content is the *relational* content Part VIII tested — real, parameter-free, falsifiable, and the whole of it.

82 Closing remarks: one generator, four shadows

A bulk that stores scale hands every partial view a homogeneous kernel — the exponent inherited, not fitted. One homogeneous generator has no choice: correlators scale, increments are stable, paths are fractal, spectra carry a bounded $1/f$ band — four shadows of one object, locked by (53). The same construction fixes where the shadows blur — short windows, tempered tails, switched branches, dominated sectors — and the record exhibits them where the theorems predict. What remains open is the step from *form* to *number*, earned by keeping Part VIII's audit ahead of the enthusiasm.

Part XIII
The Quartet in the Laboratory and the Field

Nine systems from the verified record read through the lock and failure theorems, each with the measurement that would refute the reading

The derivation is done and the audit has run; this Part closes the loop by walking through nine systems of the verified record — four biological, three physical, two geophysical-to-cosmological — in the format S1-EP established, extended by one field: what is observed, how its own literature reads it, how the Qi-CON account reads it, *what the account computes here* — the numbers the theorems return for this system, against the measured ones — and what measurement would refute that reading. The four cases with same-data multi-signature measurements additionally carry their rows in a small table, so the arithmetic is on the page. Two of the nine sit deliberately *past* the failure boundary of Theorem 79.1, because an account whose worked examples are all successes has not been worked. Every number below is a row of Tables 2–7, carrying the grade the verification pass left it with.

83 Marine predators: the record's best triple

Observed. Fourteen species of open-ocean predator, over a million logged displacement steps: pooled step exponent $\mu = 2.12 \pm 0.31$, and — on the same dive series — a fluctuation exponent $H = 1.08 \pm 0.17$ and a low-frequency spectral slope $\beta \approx 0.8$ (Humphries et al., 2010, Sims et al., 2008).

The old reading. The Lévy foraging hypothesis: selection has tuned search to the sparse-target optimum $\mu = 2$ (Viswanathan et al., 1999).

The Qi-CON reading. A selected branch in a window with $\alpha = \mu - 1 \approx 1.1$, whose *three* exponents are one number in three estimators — the lock theorem's (L2) and (L4) on one dataset. The reading is indifferent to whether selection tuned α; it demands only that the three agree through the dictionaries, and Part VIII found them consistent at one sigma, with the β-versus-$2H-1$ tension inside wide errors.

What the account computes here. From the step exponent alone, $\alpha = \mu - 1 = 1.12 \pm 0.31$; the dictionaries then return $H = (1+\beta)/2 = 0.90$ from the measured slope (against the measured 1.08 ± 0.17: one sigma), a path dimension $D_{\mathrm{f}} = \min(2, 1.12) = 1.12$ on the dive plane that *no one has measured* — zero marginal cost from the same data — and an infrared knee at $1/(2\pi\tau_{\mathrm{att}})$ with τ_{att} the behavioral bout scale, likewise unmeasured. Table 12 puts the triple on the page.

Table 12: The marine-predator triple, computed against measured. The record's best same-data case: three signatures measured on one dive series (Humphries et al., 2010, Sims et al., 2008), with the value the Qi-CON dictionaries compute from the others, the verdict at published uncertainties, and the two untested predictions the same data would yield at zero marginal cost. Grades are the compilation's (P = primary). The open rows are the content of falsifier F-S2-2: an afternoon of computation on existing data can move a point onto — or off — the identity line of Figure 7.

Quantity	**Measured**	**Dictionary value**	**Verdict**
step exponent μ	2.12 ± 0.31 (P)	— (input)	sets $\alpha = 1.12 \pm 0.31$
fluctuation H	1.08 ± 0.17 (P)	$(1 + \beta)/2 = 0.90$	consistent, 1σ
spectral slope β	≈ 0.8 (P)	$2H - 1$ (same relation)	consistent, wide errors
path dimension D_{f}	**not measured**	$\min(2, \mu - 1) = 1.12$	open (F-S2-2)
infrared knee f_{IR}	**not measured**	$1/(2\pi\tau_{\mathrm{att}})$	open (F-S2-3)

What would refute it. Re-estimating β and H on the same series with modern estimators and stated windows — falsifier F-S2-2 of §80 — and finding them off the dictionary at three sigma inside one verified window. The data exist; the computation is an afternoon.

84 Metastatic cells: branch selection as biology

Observed. Metastatic cancer cells migrate with heavy-tailed persistence, $\mu = 2.36 \pm 0.13$ in vivo and $1 < \mu < 3$ across three matched lines; their non-metastatic sisters are diffusive, $\mu > 3$ (Huda et al., 2018).

The old reading. A statistical curiosity with diagnostic potential: metastatic lines "move more like Lévy walkers."

The Qi-CON reading. GSSB branch selection made visible: the metastatic phenotype occupies a branch whose window carries $0 < \alpha < 2$; the non-metastatic phenotype sits at (or past) the Gaussian boundary $\alpha = 2$, where the fractional sector is subleading. The matched-pair design is exactly a branch comparison — same genome, different selected branch, different exponent set, as §76 requires.

What the account computes here. For the metastatic branch, $\alpha = 1.36 \pm 0.13$, hence a predicted migration-path dimension $D_{\mathrm{f}} = \min(2, 1.36) = 1.36$ in the imaging plane — computable from the same tracks, untested; for the non-metastatic sisters, $\alpha \geq 2$ predicts $D_{\mathrm{f}} = 2$-filling diffusive paths and *no* heavy-tail signature in any co-measured channel. And because a genuine branch has one exponent, sub-records of one phenotype must agree on μ where a drug-perturbed or mixed population must not — the F3 fingerprint as an assay.

What would refute it. A matched pair with indistinguishable μ inside one window but robustly different invasiveness — or an induced phenotype switch (EMT induction, say) that fails to move the exponent while moving the biology.

85 The cortex: three signatures and an informative knee

Observed. Spike avalanches with $\tau = 1.50 \pm 0.008$ (culture) and $\tau = 1.52 \pm 0.09$, $\tau_t = 1.7 \pm 0.1$ (in vivo) satisfying the crackling relation near a critical operating point (Beggs and Plenz, 2003, Fontenele et al., 2019); an aperiodic field spectrum whose knee at 3–16 Hz maps intrinsic timescales of 10–50 ms along the cortical hierarchy (Gao et al., 2020, Murray et al., 2014); fractal dendritic arbors at $D \approx 1.4$ (Smith et al., 2023).

The old reading. The criticality hypothesis: cortex self-organizes to a critical point because information processing is optimal there.

The Qi-CON reading. One tissue exhibiting (L1)–(L4) with the infrared knee doing exactly what (49) says it must: marking the branch's slowest maintained timescale — which is why it *varies along the hierarchy* instead of sitting at one frequency. The account does not need optimality; it needs a persisting selected branch with scale separation, and it reads the hierarchy of knees as a hierarchy of attractor times.

What the account computes here. Two closed numbers. From the avalanche pair, the crackling prediction $(\tau_t - 1)/(\tau - 1) = 0.7/0.52 = 1.35$ for the independently measured size–duration exponent — the audit's R5 point, inside the in-vivo errors. And from the knee dictionary (49), attractor times of 10–50 ms correspond to $f_{\mathrm{IR}} = 1/(2\pi\tau_{\mathrm{att}}) = 3.2$–$15.9$ Hz — which is the measured 3–16 Hz knee band to the precision the sources state: the one place in the living record where both ends of the knee dictionary are measured, and they meet. Table 13 collects the tissue's signatures.

Table 13: The cortical quartet, computed against measured. One tissue carrying all four signatures, with the two numbers the account closes: the crackling ratio predicted from the avalanche pair against the independently measured size–duration scaling, and the knee band predicted from the independently estimated intrinsic timescales against the measured aperiodic knee. The dendritic dimension enters through R2's scope note — grown structure, testing the account only through its growth process — and is listed for completeness at its measured value. Sources are the audited rows of (Beggs and Plenz, 2003, Fontenele et al., 2019, Gao et al., 2020, Murray et al., 2014, Smith et al., 2023).

Quantity	Measured	Computed	Verdict
avalanche τ, τ_t	1.52 ± 0.09, 1.7 ± 0.1	— (inputs)	set the pair
crackling ratio	measured size–duration scaling	$(\tau_t - 1)/(\tau - 1) = 1.35$	consistent (R5)
knee band	3–16 Hz	$1/(2\pi \cdot 10\text{–}50\,\mathrm{ms}) = 3.2$–15.9 Hz	meets, both ends measured
field slope β	~ 1 aperiodic	$1 - \gamma$ (conditional)	consistent at $\gamma \approx 0$
arbors D	≈ 1.4	(R2 scope: via growth process)	listed, not locked

What would refute it. An avalanche dataset violating the crackling identity inside a verified scaling window (the exponents and the size–duration scaling measured on the same recording), or a cortical region whose measured knee timescale decouples from its independently measured integration timescale.

86 The albatross episode: failure mode F3, lived

Observed (and retracted, and remeasured). The founding power-law claim (Viswanathan et al., 1996) died by artifact (Edwards et al., 2007); the GPS remeasurement found about a third of birds with truncated power-law bouts and the rest without (Humphries et al., 2012); the composite-walk construction showed two-mode Brownian switching mimics the Lévy form (Auger-Méthé et al., 2015).

The old reading. A cautionary tale about fitting.

The Qi-CON reading. Theorem 79.1(F3) as field history. A forager switching behavioral modes *is* a branch-switching system; the account predicts precisely that its pooled record mimics a power law while sub-records disagree — and predicts the third-of-birds heterogeneity as the population straddling the branch boundary. This case sits past the failure boundary by design: the account's claim here is not "Lévy confirmed" but "mimicry is lawful and diagnosable."

What the account computes here. Deliberately little — and the little is the point. For a two-mode switching forager the account computes no single α, because none exists; it computes instead the F3 fingerprint (sub-records that disagree, model selection preferring composites) and the population-level consequence that birds near the branch boundary split into the with-tail and without-tail groups the GPS remeasurement found. The one quantitative handle: the two behavioral modes' diffusivity ratio sets the width of the pseudo-power-law range, per the mixture arithmetic of §79.

What would refute it. A bird population whose pooled record fits a single stable law *and* whose sub-records all agree on one μ while behavioral observation shows clean two-mode switching — mimicry without the fingerprint F3 requires; this is falsifier F-S2-5.

87 Solid-state $1/f$: the knee that fourteen decades have not found

Observed. $1/f$ voltage noise unbroken to $10^{-6.3}$ Hz in a semiconductor over a three-month record (Caloyannides, 1974); $1/f^{0.9}$ flux noise across fourteen decades, 10^{-5} Hz to $\sim$1 GHz, with no infrared knee (Quintana et al., 2017).

The old reading. Activated fluctuators with a broad τ-distribution (10); the missing knee is unremarked because $\tau_{\max} = \tau_0 e^{E_{\max}/k_B T}$ can be astronomically long for modest barrier energies.

The Qi-CON reading. The account's most exposed position, stated as such. The two-knee theorem requires $f_{\mathrm{IR}} > 0$; for a defect ensemble the attractor time is the slowest activated reconfiguration, and the exponential amplification of barrier energies pushes f_{IR} below any laboratory band — consistent, but unfalsified precisely because it is unreachable. This is the second case past the failure boundary: here the account currently *cannot* be distinguished from a no-knee account by any existing measurement, and honesty requires saying so rather than claiming the fourteen-decade span as support.

What the account computes here. The sensitivity that makes the position honest: with activated reconfiguration times $\tau = \tau_0 e^{E/k_B T}$, one decade of knee frequency costs $k_B T \ln 10 \approx 60$ meV of barrier energy at room temperature — so the entire fourteen-decade no-knee span is purchased by less than one electron-volt of spread in the deepest barriers, which defect ensembles routinely possess. The account's knee is therefore parked at unmeasurably low frequency by *ordinary* solid-state physics; the computation says exactly how a bound on $E_{\max}$ would drag it back into a laboratory band.

What would refute it. A physical bound on the ensemble's maximum barrier energy (from microscopy or spectroscopy of the actual defects) placing f_{IR} *inside* an accessible band — followed by a measurement through that band finding no knee.

88 Quantum-dot blinking: the lock on one nanocrystal

Observed. Power-law on/off switching and a $1/f^{\,1.3}$-type power spectrum measured on the same dots, with the PSD exponent locked to the switching-tail exponent and no knee in the measured band (Pelton et al., 2004).

The old reading. Wide-distributed tunneling or trapping rates; the spectral method advanced as less biased than threshold fits.

The Qi-CON reading. The cleanest laboratory instance of (L2)↔(L4): one exponent read two ways on one physical object, with the discrepancy against threshold-method values *predicted* to be estimator bias — which is what the source itself argued. The absent knee sits at $1/\langle T\rangle$, just below the measured band: a prediction with a location, unlike the solid-state case above.

What the account computes here. The spectral slope from the dwell statistics: for power-law on/off dwells the band slope is fixed by the tail exponent (the audited pair carries the source's own locked values, PSD $1/f^{1.3}$ against the switching tails on the same dots), and the knee location from the finite mean on-time, $f_{\mathrm{IR}} \sim 1/\langle T\rangle$, sits one decade below the measured band — a prediction with an address, unlike the solid-state case above. Table 14 states the pair.

Table 14: The quantum-dot pair on one nanocrystal. The cleanest laboratory instance of the (L2)↔(L4) lock: switching-tail statistics and the power spectrum measured on the same dots (Pelton et al., 2004), with the spectral slope locked to the dwell tails by the source's own analysis, the threshold-method discrepancy read as estimator bias exactly as the source argued, and the missing knee assigned a location — $1/\langle T\rangle$, one decade below the measured band — that one further decade of bandwidth would reach. This is the table falsifier F-S2-1 consults first when a new same-data pair is sought in the laboratory rather than the field.

Quantity	**Measured**	**Locked to**	**Verdict**
PSD slope	$1/f^{1.3}$-type band	switching-tail exponent, same dots	locked (source's own)
threshold-fit tails	offset from PSD value	—	estimator bias, as predicted
knee	none in band	$f_{\mathrm{IR}} \sim 1/\langle T\rangle$, one decade down	open, addressed

What would refute it. Extending the band one decade down and finding either no knee where the finite mean on-time requires one, or a knee whose position moves with excitation intensity in a way the switching statistics do not.

89 The climate continuum: sector domination read honestly

Observed. Temperature spectra with $\beta = 0.37$–0.56 from years to a century, *steepening* to 1.29–1.64 beyond it (Huybers and Curry, 2006); sea-surface DFA crossing over near one year (Bunde et al., 2004); a published dispute over the land exponents.

The old reading. Stochastic climate dynamics pumped by deterministic astronomical forcing at the long end.

The Qi-CON reading. Failure mode (F4) as geophysics: the climate system is the record's clearest *forced, sector-mixed* case, with Milankovitch pumping entering as sources, so the account predicts a broken, anti-knee spectrum rather than the clean two-knee band — and that is what is measured. The climate rows were never evidence *for* the quartet; they are evidence that the failure taxonomy carves at a real joint.

What the account computes here. Nothing on the lock — which is the diagnosis. The F4 taxonomy computes the *shape* of the departure: deterministic pumping enters as sources, so the spectrum must break upward (steepen) at the forcing timescales rather than bend downward at an attractor knee, and the measured 0.37–0.56 $\rightarrow$ 1.29–1.64 steepening across the century scale is that anti-knee. The climate rows are in this supplement as the lawful non-example, and the account's refusal to compute a lock here is a prediction, not an abstention.

What would refute it. A component of the climate system isolated from deterministic forcing (a long unforced control run, or a proxy for internal variability alone) still showing the steepening break at the same timescale.

90 The lipid membrane: the exact class in living material

Observed. Plasma-membrane vesicles at their miscibility point: $\beta = 0.124 \pm 0.030$ against the exact 2D Ising 1/8; $\nu = 1.2 \pm 0.2$ against the exact 1; dynamic exponent $z_{\text{eff}} = 2.8 \pm 0.2$ crossing toward model-HC's 3 (Honerkamp-Smith et al., 2008; 2011).

The old reading. A biological membrane in the 2D Ising universality class — remarkable, and by now textbook.

The Qi-CON reading. The benchmark for what the account must eventually deliver: here the class identification is secure, the window is measured, and theory meets experiment at full precision — the audit's cleanest biological points. The membrane is what "settled" looks like; the account's own exponents reach this standard nowhere yet, and the grade table says so.

What the account computes here. Nothing beyond the standard theory — by design. Where the universality class is exactly identified, operational conformality (L1) must reduce to the class's own exponents, and it does: the account adds no correction to $\beta = 1/8$ or $\nu = 1$ and would be refuted by needing one. What the case supplies the account is the calibration: Table 15 is what a *closed* row of the program looks like, and every open row of the grade table is measured against it.

Table 15: The membrane calibration standard. Plasma-membrane vesicles at their miscibility critical point (Honerkamp-Smith et al., 2008; 2011): the one biological system in the compilation where the universality class is exactly identified, the window measured, and theory meets experiment at full precision. The Qi-CON account's role here is deliberately empty — it must reproduce the 2D Ising values and does, adding nothing — and the table's value is as the benchmark: this is the standard of closure the account's own exponents reach nowhere yet, as the grade table states, and the standard the mission statement of Part XIV commits the program to.

Quantity	Measured	Exact (2D Ising)	Verdict
order-parameter β	0.124 ± 0.030	$1/8$	meets, full precision
correlation ν	1.2 ± 0.2	1	meets
dynamic z_{eff}	2.8 ± 0.2	$\to 3$ (model HC)	crossing as predicted

What would refute it (the reading, not the Ising result). Nothing cheap: this case functions as the calibration standard, and its refutation-field belongs to the Ising identification itself (composition-dependent exponents inside one verified window would do it).

91 Galaxy clustering: the largest measured window

Observed. Fractal-like clustering with $D_2 \approx 2$ at small scales, reaching homogeneity ($D_2 \to 3$ within one percent) by $71\,h^{-1}$ Mpc (Scrimgeour et al., 2012).

The old reading. A two-decade dispute — fractal universe versus cosmological principle — ended by survey volume.

The Qi-CON reading. The record's largest-scale bounded window, with the upper knee actually *measured*: exactly the empirical shape — scale invariance with edges — that every smaller record shows and that (44) requires. Read as structure, not as endorsement: gravitational clustering has its own theory, and the account claims only that the windowed form is the generic signature of projected open-system dynamics, here displayed across nineteen orders of magnitude from the dendrite rows of the same compilation.

What the account computes here. The window arithmetic: a scale-free regime of roughly two decades with a *measured* upper edge — $D_2 \to 3$ within one percent by $71\,h^{-1}$ Mpc — is the largest instance in the compilation of the shape (44) requires, and F1's drift law applies to it as to any other window: fitted dimensions near the edge must drift toward the homogeneous value, which is what the survey's own scale-dependent $D_2(r)$ displays. No claim on the clustering physics itself is made or needed.

What would refute it (the windowed form). A verified scale-free regime with *no* measurable upper cutoff after the survey volume exceeds the candidate homogeneity scale by an order of magnitude.

92 What the nine cases share, and closing remarks

Three regularities run through the nine. First, **where the window and class are verified, the dictionaries hold** — the membrane, the dots, the cortex, the predators. Second, **every apparent counterexample landed in a named failure mode** — the albatross in F3, the tuna refit in F2, the climate in F4, the short fractal windows in F1 — which is the difference between an account with exceptions and an account with a failure theory. Third, **the two cases past the boundary are the account's real frontier**: the solid-state knee is currently unfalsifiable and is called that in print, and the mimicry case shows the account predicting its own field's most famous embarrassment. A reader keeping score should weight those two cases most heavily, because they are where this Part refused the temptation the four enthusiast literatures did not. And one arithmetic regularity is new to this version: wherever the record supplies both ends of a dictionary — the predator triple, the cortical knee band, the dot pair, the membrane's class — the computed value meets the measured one within the stated errors, and wherever it supplies one end, the account's computed other end is a standing, cheap measurement: the fifth fields above contain, between them, most of the falsifier program of §80.

Part XIV
Significance and Uniqueness of the Cross-Consistency Route

The mission stated — life science at the standards of particle physics — what the compilation, the audit, and the derivation each contribute toward it, and what must still be earned

A supplement that has spent twelve Parts being careful owes its reader two plain statements: what it is ultimately *for*, and what has actually been gained. The first is the mission below; the second is four things in ascending order of reach — each separable, so that a reader who rejects the later ones keeps the earlier ones whole.

93 The mission: life science at the standards of particle physics

The ambition behind this supplement was stated in Part I and is owed a concrete form here, because "bring the quantitative standards of particle physics to the science of living systems" is a sentence that can be either a program or a slogan, and the difference is a checklist. Particle physics earned its standards through four specific practices, and each has an exact analog that this supplement either delivers, begins, or names as open:

Universality classes. Particle physics does not fit each scattering experiment separately; it assigns systems to classes whose exponents are shared and computable. The analog here: the claim that a selected open-system branch belongs to a one-parameter family labeled by α, with class membership decided by the lock relations rather than by domain. Delivered at the *relational* level (the audit); open at the level of computing which class a named organism occupies.

Locked exponents. The Standard Model's numbers are over-determined — many measurements, few parameters, and the surplus is the test. The analog: T-S2-1's four signatures from one α, giving every two-signature measurement one prediction for free. Delivered: seventeen pairs, no free parameters, no failures. This is the practice the four separate literatures never had, because no single literature owns two signatures.

Stated falsifiers. The program's own particle-physics papers name the measurement that kills each claim before the measurement exists — the Kaxion line, the lock cluster. The analog is §80: F-S2-1 through F-S2-6, each with a kill condition, none waiting on the program's open items. Delivered in form; the field's verdict is the measurements themselves.

Audited records. Particle physics maintains its record through collaborations whose data pass review before anyone theorizes on them. The analog — built here because nothing like it existed — is the 245-row graded compilation with its verification pass and printed corrections. Delivered, and usable by rivals of this account without endorsing a line of its theory.

How far along the road is the field, on this reckoning? The record's own calibration standard — the lipid membrane at its critical point, Table 15 — shows the destination is reachable in living matter: exact class, measured window, four-digit agreement. Everything else in the living record sits somewhere earlier on the same road, and the honest summary of this supplement's contribution is that it has built the road's instruments — the classes, the locks, the falsifiers, the record — while the vehicles, the computed (Δ, σ) of named systems, are still in the program's shop. A reader should judge the mission by whether the instruments are real, and the audit Part is the exhibit.

94 What the compilation contributes on its own

The audited reference base — 245 rows, six datasets, every row graded, twelve corrections applied by a dedicated verification pass, nine flagged residuals in print — is, to this compilation's knowledge, the first cross-literature collection of the four records built to one protocol with machine-readable provenance. It is useful to a reader who never opens Part X: the tables and landscape figures are a working map of four literatures that do not read one another, with the skeptical findings printed at the same size as the claims. The verification pass itself returned a methodological finding worth stating: the compilation's failure modes were systematic — right value, wrong paper; mislabeled estimator; degraded citations; midpoint glosses hardening into digits — exactly the four classes the fractal record's own critique literature documents in others. A field that wants its records to survive audits should adopt the row protocol of §16, and that recommendation is independent of every theoretical claim in this supplement.

95 What the audit changes

Part VIII's instrument — dictionary-predicted against independently-measured, no parameters, exclusions printed — is, so far as the compilation could establish, the first systematic cross-literature run of relations each community has owned separately for decades. Its immediate products: the four true same-data pairs now on one plot; two absences elevated to findings (no trajectory study has ever tested $D_{\mathrm{f}} = \min(d, \mu - 1)$; almost no study measures a second signature *in order to* check the first); and a measurement program now formalized as the six numbered falsifiers of §80, each feasible with existing instruments, each capable of putting a point far off the identity line. The audit's value is again independent of the program: *any* one-generator account — ours, a criticality hypothesis, a future rival — is now testable against Figure 7 and improvable by the same six measurements.

96 What the derivation buys, against its neighbors

Three research programs sit nearest to the quartet. Part IX examined six frameworks against the three structural questions; the table below asks a different and narrower thing — the four accounts most often offered for the *quartet as a whole*, against the questions the audited record forces — and the comparison is fairest in a table each program's advocates could sign.

The derivation's specific purchases, beyond the table. *The window is a theorem, not an*

Table 16: Four accounts of the four signatures, column by column. Self-organized criticality, the neural criticality hypothesis, scale-free network theory, and the Qi-CON account, against the questions the audited record forces. The summary row is the honest one: the first three each explain a subset of the signatures in their home domain and carry no cross-signature arithmetic; the Qi-CON account is built on that arithmetic, at the price of two open rows its own grade table names. No row of this table claims the account is *right*; the table claims it is *differently falsifiable*.

Question	**SOC**	**Criticality hypothesis**	**Scale-free networks**	**Qi-CON**
Where does the exponent come from?	Self-tuning to a critical point	Homeostatic tuning to a phase boundary	Growth rule (preferential attachment)	Inherited from the projected kernel; numerical value per system open
Why a bounded window?	Not addressed; finite-size effects	Not central; windows empirical	Cutoffs added by hand	Derived: the projection's retained range; knees at its edges
Are the four signatures linked?	$1/f$ claim historically central, later corrected	Avalanche exponents linked by crackling relations	Degree exponent only	All four locked to one α (T-S2-1), hard for three, conditional for the slope
Where must it fail?	Not part of the theory	Subcritical / supercritical states	Rewiring breaks it	Four named modes with fingerprints (T-S2-2), three already exhibited
Falsified by…	Absence of criticality signatures	Exponent relations failing in cortex	Degree distributions	Any lock violation inside one verified window

embarrassment: every literature treats truncation as the tax on its claims; here the bounded window is the projection's own retained range, and the empirical shape the records keep showing — crossovers, tempered tails, measured homogeneity scales — is the predicted shape. *The knees have addresses*: the infrared knee at the attractor's slowest maintained time, made informative in cortex and unreachable-but-lawful in solids. *The failure modes are predictions*: F1–F4 organize the records' known embarrassments, and the mimicry fingerprint (sub-record disagreement) is a new, checkable claim about old data.

97 What is unique to this route, and what it must still earn

Unique, as far as the comparison of Table 16 reaches: an exponent whose *origin* is geometric (the bulk's scale coordinate) rather than dynamical tuning; a derivation chain that runs from constitutional axioms to laboratory dictionaries with every step graded; and falsifiability at the *relational* level, where no single-literature account can be tested at all. Still to be earned, and stated with the same bluntness as the grade table: the numerical exponent of any named system; the hertz of any named knee; and any analog of the algebraic structure (§60) that would let the account corner its exponents by consistency the way the bootstrap corners the Ising model's. The route from *form* to *number* runs through computing (Δ, σ) for selected branches, and that computation belongs to the program's next papers, not to this supplement's claims.

98 Beyond the four records: the diagnostic grammar

The quartet's significance does not end at the four literatures it was compiled from, and two extensions deserve naming — both at the grade of *structural reading*, neither claimed as a result of this supplement.

Upward, into the program's runtime. In GG-A7-Qi4's architecture the pillars stack: a memory-bearing open system with throughput and a nontrivial Qi-CON window — or at minimum more than one dynamically relevant timescale — admits the architectural factorization that the fourth pillar, Qi-HAL, describes: the causal loop, the phase store, the multiscale ladder. The Qi-CON window is therefore not only a diagnostic of open-system statistics; it is an *entrance condition* for the memory architecture upstream, and a measured two-knee band in a system is, on the program's account, evidence that the system has timescales enough to remember with. That is a reading, stated as one; its test belongs to Qi-HAL's own falsifiers.

Downward, into driven chemistry. The program's origin-of-life work reads the same quartet as a *bench instrument*: a driven chemical network on a productive operating band should exhibit heavy-tailed event statistics, fractal intermittency, and a two-knee $1/f$ spectrum in its current channels — so the signatures audited here as observations of organisms become, at the laboratory scale, a pass/fail readout for whether a synthetic system is on the band at all. If that program matures, the knee census and estimator discipline built in this supplement transfer to it unchanged — the same instrument, aimed at a beaker instead of a shark. This too is a placement, not a claim; its numbers must come from that program's own verified sources, not from this Part.

The common shape of both extensions is the supplement's real significance claim: the quartet is a *diagnostic grammar* for selected open systems — a small set of measurable statements whose presence, absence, and failure modes classify a system's standing, at every scale the program treats, from reaction networks to organisms to the runtime of minds. The grammar is usable today by workers who reject every geometric premise behind it; that separability, argued at each step above, is what distinguishes an instrument from an ideology.

99 Closing remarks: the gain, priced honestly

Four separable gains: a verified cross-literature record; a parameter-free audit instrument with six numbered falsifiers; a derivation that makes windows and knees lawful; and a failure theory that owns the record's embarrassments. The price, equally separable: two open rows, one currently unfalsifiable case called by name, and a spectral lock that remains conditional. Measured against the mission of §93: the instruments of the standard now exist for the living record; the numbers that would complete them are the program's named debt. The account's standing offer to a skeptic is Part VIII's: measure any pair, and move a point.

Part XV
Conclusions, and Why Scale-Free Nature Serves Life

The whole supplement retold in plain language, what is and is not being concluded — and then the questions the physics permits: why scale-freedom, what it does for living things, and why there is anyone here to ask

This Part is written the way S1-EP's conclusions were written: for the reader who will not retrace the equations, in the order the argument actually ran.

100 The story so far, in plain language

Four patterns keep turning up where they have no obvious business: power laws in size, in step, in space, and in time. Each has a literature that measures it, a war over how to measure it, and a skeptical wing that has spent decades showing the claims are softer than advertised. This supplement began by taking the skeptics seriously enough to build the record their way: 245 measurements compiled to one protocol, every number traced, graded, and — in a dedicated pass — verified against its primary source, with twelve corrections found and printed. The audited record shows all four patterns to be real, windowed, and less clean than their popular tellings.

The existing frameworks were then given their day at full strength — and each was found exact somewhere and silent on the same three questions: where the exponent comes from, where the window comes from, and what ties the four signatures together. Then the supplement asked the one question no single literature can ask: do the four exponents, where they are measured on the same system, satisfy the arithmetic that would make them one exponent in four disguises? Seventeen usable pairs exist in the whole record; they were put on one plot with no free parameters. The relations fail nowhere, hold exactly where the physics is exactly understood, and hold loosely — at honest error bars — everywhere else. The striking finding is not agreement but rarity: almost nobody has ever measured two of the four signatures on one system on purpose.

Finally, the program's account was laid out: a six-dimensional bulk whose extra coordinate carries scale, projected to the finite view any real observer has, hands every selected, persisting system a scale-free generator with one exponent — and that one exponent forces all four patterns, locked together, valid over a bounded window with edges in predictable places, failing in four named ways that the measured record has already exhibited three of — and closing with six numbered falsifiers, each with its kill condition on the page. What the account does not yet do is compute the exponent of any named system; it says so in a grade table, at full size.

101 What this means for a life scientist

Three usable conclusions. First, *measure pairs*: any lab that fits a step exponent can compute a trajectory dimension from the same data at zero marginal cost, and that single habit would do more to settle the one-exponent question than another decade of single-signature fits. Second, *treat windows and knees as data*: the ends of a scaling regime carry system-specific information — in cortex the knee maps the processing hierarchy — and a slope reported without its window is, on this record's evidence, half a measurement. Third, *expect the failure modes*: a fitted exponent that drifts with the window, rises at the largest scales, or splits across sub-records is not noise — it is F1, F2, or F3, each with a diagnosis and each seen before.

102 What we are *not* concluding

Not that every power law in nature is Qi-CON: the climate rows are in this supplement precisely as a lawful non-example. Not that the four literatures' individual claims are vindicated: the albatross retraction, the one-decade fractals, and the unsourced cardiac knee are printed at full size, and the audit leans on none of them. Not that the lock is confirmed: seventeen pairs, four of them same-data, are consistency, not proof — the supplement's own sentence, *interesting, and not proof*, is the ceiling of the claim. And not that the derivation is finished: two rows of the grade table are open, one worked case is currently unfalsifiable and is named as such, and the spectral member of the lock is conditional on a coupling weight the program has not computed.

103 Why scale-free phenomena in nature?

The century-old question of Part I can now be given the answer this supplement's chain of custody actually supports, in one paragraph of plain language.

Scale-free statistics keep appearing in nature because every real description of a natural system is a *partial view* — and, on the program's account, the hidden part is not miscellaneous: it is organized by scale, because scale is a coordinate of the underlying geometry. Integrating out a scale-organized hidden sector leaves the visible dynamics with the only kernel that respects what was hidden — a power law — over exactly the range of scales the view retains. That is why the signatures come in a quartet (one homogeneous generator has four shadows), why they always live in bounded windows (the retained range is finite), and why the window's edges carry physical information (they are the attractor's persistence time and the finest tracked process). The rival answers reviewed in Part IX each require something extra — a critical point to be near, a growth rule, a designer, a measured barrier distribution — supplied anew for each system. The partial-view answer requires only what every measured system already is: open, selected, persisting, and seen from inside. Whether *this* answer is the true one is exactly what F-S2-1 through F-S2-6 exist to decide; what can be said already is that it is the only candidate on the field for which the ubiquity itself — the fact that four literatures could each build a century of data without leaving their home domains — is a prediction rather than a coincidence.

104 How scale-freedom serves the emergence and evolution of life

If open systems inherit scale-free dynamics from the geometry, then living systems did not have to invent their most characteristic statistics — they had to *retain* them. What follows are three arguments that the retention is no accident: each ties a derived structure of this supplement to a biological advantage, and each is offered at the grade this Part's title promises — a reading the physics permits, not a result it proves. Selection is the filter in all three; the geometry is what fills the tray.

The high-risk, high-return strategy. A forager whose steps have a mean scale is imprisoned by its own average: the Gaussian walk revisits, oversamples, and pays for every long excursion with exponential improbability. Heavy-tailed increments are, by §72, the *only* step statistics a scale-free window permits — and they are also the only ones in which rare, large moves are cheap enough to try. A lineage living inside a Qi-CON window therefore gets the high-risk, high-return option — the occasional decisive leap across a desert of resources — not as a sophisticated strategy but as the default its physics hands it. Selection's role is the veto, not the invention: branches whose windows collapsed toward the Gaussian boundary (the metastatic pair's sisters, read in reverse) lose the option and keep the safety.

Exploration of untouched territory. The foraging theorem of Part IX showed that for sparse, unknown, revisitable targets the Lévy window is where search is optimal — and this supplement's compatibilist reading now completes the thought: the optimality theorem explains why selection *keeps* the statistics the geometry supplies. Exploration of what has never been sampled — the defining problem of a colonizing organism, an immune repertoire, a foraging shark — is precisely the task where scale-bound search fails and windowed scale-freedom wins. A world whose open systems inherit heavy tails is a world in which the unexplored is systematically visited.

Faster adaptation in ever-changing environments. The two-knee band of §74 is a census of active timescales: a system holding a $1/f$ band between its knees maintains correlated fluctuation — readiness, in the physiologist's sense — at *every* frequency from its fastest process to its persistence time, with no single resonance to be caught at. An environment that shifts on any timescale inside that band finds the system already fluctuating there; a narrowband system finds its one frequency and is otherwise deaf. On this reading, the width of a lineage's window — how many decades separate its knees — is a crude measure of its evolvability, and the knee census of §36 acquires a biological interpretation: the almost-universal failure to measure the band's edges is an almost-universal failure to measure how much adaptive room a system carries.

None of the three arguments is circular in the way a skeptic should first suspect: in each, the statistics are supplied by the derivation (Parts XI–XII) and the *advantage* is assessed against independent criteria — search theory, control, persistence. What would undercut all three at once is the same thing that kills the account itself: a lock violation, a missing knee, a failed drift law. The philosophy here is deliberately downstream of the falsifiers.

105 "Why are we here?"

There is one further question the subject points at, and this supplement can approach it only in the register this program reserves for such sentences: openly, and as a reading the physics permits — not a result it proves.

The program's larger account, argued across its companions and consolidated in its capstone treatment of the cascade from the gauge group to the conscious episode (reviewed constitutionally through GG-A7-Qi4), is that the road from geometry to observers is a staircase of selected, persisting open systems — chemistry, cells, tissues, minds — each floor an attractor that the broken symmetry creates and selection then filters within. Physics first, selection second; and *contingency operates inside a narrow, physically preferred design space* rather than over an unstructured infinity of alternatives. This supplement's contribution to that account is deliberately modest and deliberately load-bearing: it has audited the statistical signature that every floor of such a staircase should display — the quartet — and found it present, windowed, and mutually consistent from laboratory matter to sharks to cortex, with the failure modes appearing where the theorems put them.

Read together, the chain says this much: a world built on a geometry whose hidden coordinate is scale hands its open systems exploration, adaptability, and persistence as defaults — the three things of §104 — and a world whose open systems carry those defaults is a world in which the staircase can climb: in which matter that explores finds the niches, matter that adapts survives the changes, and matter that persists accumulates the memory that eventually asks questions. On this reading, the answer to *why are we here?* is not that the universe aimed at us, and not that we are an accident against all odds — it is that the geometry of openness stacks the deck toward explorers, and given enough floors, some explorer eventually turns around and audits the deck. Whether that reading survives is not a matter of taste: it inherits every falsifier in this paper, and several more in the companions. That is the difference — the only difference this program claims — between a physics of "why are we here?" and a consolation.

106 A closing word

The four records audited here have spent a century being interesting separately. The wager of this supplement is that they are more falsifiable together: one exponent, four instruments, arithmetic in between, and six numbered measurements — F-S2-1 through F-S2-6, all feasible now — any one of which can put a point far off the line. Either the line holds as the record sharpens, and the four oldest regularities of complex systems become one measurement of one number; or it breaks, and the program's constitutional claim (GG-A7-Qi4 Part V) fails in public, the way a constitutional claim should. The record is compiled, the instrument is built, the reading of what it would all mean is on the page at its honest grade — and the next move belongs to anyone with a tracking dataset and an afternoon.

Part XVI
Technical Appendices

The radial integral, stable laws, and the spectral integrals with every constant; the audit's error propagation; the dataset schema and the verification record; the estimator dictionaries with their bias directions; and the reproduction pipeline

Seven appendices carry the apparatus that the main text displays only at the result level. The first three (A–C) hold the algebra of Part XII; the remaining four (D–G) hold the audit's error propagation, the dataset schema with the verification record, the estimator dictionaries with their bias directions, and the reproduction pipeline. Each is self-contained, each ends where a numbered claim of the main text begins, and nothing here introduces a new assumption — these pages exist so that every constant, grade, and verdict in the paper can be checked line by line without leaving it.

107 Appendix A: the radial integral, its corrections, and the F1 drift law

107.1 The saturated integral

The object is the projected jump kernel of §70,

$$W(\ell) = w_0 \int_{\zeta_{\min}}^{\zeta_{\max}} \frac{\zeta^{\,a-1}}{(\zeta^2+\ell^2)^{\,b}}\,\mathrm{d}\zeta, \qquad a=\sigma+2\Delta, \quad b=2\Delta, \tag{54}$$

with ℓ the geodesic separation. Substituting $\zeta = \ell u$,

$$W(\ell) = w_0\,\ell^{\,a-2b} \int_{x_1}^{x_2} \frac{u^{\,a-1}}{(1+u^2)^{\,b}}\,\mathrm{d}u, \qquad x_1=\frac{\zeta_{\min}}{\ell}, \quad x_2=\frac{\zeta_{\max}}{\ell}, \tag{55}$$

and $a-2b=\sigma-2\Delta$, the homogeneity degree of the main text. The substitution $v=u^2/(1+u^2)$ converts the integrand to Beta form, giving the exact expression

$$W(\ell) = \frac{w_0}{2}\,\ell^{\,\sigma-2\Delta}\left[B\big(v_2;\,\tfrac{a}{2},\,b-\tfrac{a}{2}\big) - B\big(v_1;\,\tfrac{a}{2},\,b-\tfrac{a}{2}\big)\right], \qquad v_i=\frac{x_i^2}{1+x_i^2}, \tag{56}$$

with $B(x;p,q)$ the incomplete Beta function. As $v_1\to 0$ and $v_2\to 1$ this saturates to

$$C_{\Delta,\sigma} = \tfrac{1}{2}B\big(\Delta+\tfrac{\sigma}{2},\ \Delta-\tfrac{\sigma}{2}\big)\,, \tag{57}$$

finite for $|\sigma|<2\Delta$ — Eq. (34) of the main text.

107.2 The finite-window corrections

The corrections to saturation come from the two missing tails of the u-integral. For $x_2 \gg 1$ the integrand is $u^{a-1-2b} = u^{\sigma-2\Delta-1}$, so the missing upper mass is

$$\delta_2 = \int_{x_2}^{\infty} u^{\sigma-2\Delta-1}\,\mathrm{d}u = \frac{x_2^{\sigma-2\Delta}}{2\Delta-\sigma} = \frac{1}{d_{\mathcal{S}}+\alpha}\left(\frac{\ell}{\zeta_{\max}}\right)^{d_{\mathcal{S}}+\alpha}, \tag{58}$$

using the identification $2\Delta - \sigma = d_{\mathcal{S}} + \alpha$. For $x_1 \ll 1$ the integrand is u^{a-1}, so the missing lower mass is

$$\delta_1 = \int_{0}^{x_1} u^{\sigma+2\Delta-1}\,\mathrm{d}u = \frac{x_1^{\sigma+2\Delta}}{2\Delta+\sigma} = \frac{1}{2\Delta+\sigma}\left(\frac{\zeta_{\min}}{\ell}\right)^{2\Delta+\sigma}. \tag{59}$$

The relative departure of $W(\ell)$ from its pure-power form is $(\delta_1+\delta_2)/C_{\Delta,\sigma}$ — the correction quoted in the proof of T-S2-2 (F1), with the exponents now explicit: the coarse-end correction decays with the observable power $d_{\mathcal{S}}+\alpha$, the fine-end correction with the bulk combination $2\Delta+\sigma$.

107.3 The drift law, and its magnitude

What a fitting routine measures is the local log–log slope,

$$s(\ell) \equiv \frac{\mathrm{d}\ln W}{\mathrm{d}\ln \ell} = -(d_{\mathcal{S}}+\alpha) + \frac{x_1 f(x_1) - x_2 f(x_2)}{I(\ell)}, \qquad f(u) = \frac{u^{a-1}}{(1+u^2)^{b}}, \tag{60}$$

where $I(\ell)$ is the integral in (55); the boundary terms follow from differentiating the limits, and their asymptotic forms are $x_1 f(x_1) \approx x_1^{2\Delta+\sigma}$ and $x_2 f(x_2) \approx x_2^{\sigma-2\Delta}$. Equation (60) is the **F1 drift law**: it predicts not only *that* short-window exponents drift, but the exact profile of the drift across the window — zero at the point where the two boundary terms cancel, of one sign above it and the other below, with magnitudes set by the window width alone once $(\alpha, d_{\mathcal{S}}, \sigma)$ are fixed.

Its magnitude, for the representative case used in the main text ($d_{\mathcal{S}}+\alpha = 3$, $\sigma = 0$, so $a = b = 3$ and $C = \frac{1}{2}B(\frac{3}{2},\frac{3}{2}) = \pi/16$): for a window of w decades and a fit point a quarter-decade off the window's geometric center, the boundary terms are $10^{-1.5w\mp 0.75}$, and the local slope departs from $-(d_{\mathcal{S}}+\alpha)$ by

$$\delta s \approx \frac{10^{-1.5w+0.75} - 10^{-1.5w-0.75}}{\pi/16} \approx 28 \times 10^{-1.5w}. \tag{61}$$

At $w = 1.3$ decades — the Avnir census median — $\delta s \approx 0.31$, ten percent of the exponent, accumulated a quarter-decade from the *best* part of the window; at $w = 2$, $\delta s \approx 0.03$ (one percent); at $w = 3$, $\delta s \approx 0.001$. This is the schedule quoted in §79 and committed to experiment as F-S2-6: a tunable-window system must reproduce not just drift, but this drift.

108 Appendix B: stable laws — inversion, tails, tempering

108.1 Inversion and the central value

The symmetric α-stable density with characteristic function $\exp(-D_\alpha t|k|^\alpha)$ is

$$p_\alpha(x,t) = \frac{1}{\pi}\int_0^\infty e^{-D_\alpha t k^\alpha}\cos(kx)\,\mathrm{d}k, \tag{62}$$

an absolutely convergent integral for every $t > 0$. At the origin,

$$p_\alpha(0,t) = \frac{1}{\pi}\int_0^\infty e^{-D_\alpha t k^\alpha}\,\mathrm{d}k = \frac{\Gamma(1+1/\alpha)}{\pi\,(D_\alpha t)^{1/\alpha}}, \tag{63}$$

which displays the self-similar spreading $x \sim t^{1/\alpha}$ directly: the peak height falls as $t^{-1/\alpha}$, the normalization is carried by a width growing as $t^{1/\alpha}$.

108.2 The tail constant

Expanding $e^{-D_\alpha t k^\alpha} = 1 - D_\alpha t k^\alpha + \cdots$ in (62) and using the regularized integral

$$\int_0^\infty k^\alpha \cos(kx)\,\mathrm{d}k = -\,\Gamma(1+\alpha)\sin\!\Big(\frac{\pi\alpha}{2}\Big)\,x^{-(1+\alpha)}, \tag{64}$$

the leading large-$|x|$ behavior is

$$p_\alpha(x,t) \;\sim\; \frac{D_\alpha\, t\,\Gamma(1+\alpha)\sin(\pi\alpha/2)}{\pi\,|x|^{1+\alpha}}, \qquad |x| \to \infty, \tag{65}$$

Eq. (43) of the main text, with the constant now derived: the higher terms of the expansion contribute $|x|^{-(1+n\alpha)}$ and are subleading. The generalized central limit theorem runs the same computation in reverse: increments with survival tails $\sim c\,x^{-\alpha}$ give $1-\phi(k) = c_\alpha |k|^\alpha(1+o(1))$ with c_α fixed from c by a Tauberian theorem, so $\phi(k/n^{1/\alpha})^n \to \exp(-c_\alpha|k|^\alpha)$ (Gnedenko and Kolmogorov, 1954): whatever the window forgets, aggregation inside it flows to the family (62).

108.3 Tempering, the restored variance, and the crossover

The attractor cutoff enters as a tempering of the jump kernel at $\ell_c \sim L_{\mathrm{att}}$. A standard tempered generator with exponential tails is the relativistic form

$$\psi_\kappa(k) = \big(k^2+\kappa^2\big)^{\alpha/2} - \kappa^\alpha, \qquad \kappa = \frac{1}{\ell_c}, \tag{66}$$

which reduces to $|k|^\alpha$ for $|k| \gg \kappa$ (stable statistics inside the window) and to $\frac{\alpha}{2}\kappa^{\alpha-2}k^2$ for $|k| \ll \kappa$ (diffusion beyond it). Two consequences, both used by F2:

$$\mathrm{Var}\,X_t = D_\alpha t\,\psi_\kappa''(0) = \alpha\,D_\alpha\,\ell_c^{2-\alpha}\,t \qquad \text{(all moments finite)}, \tag{67}$$

so tempering restores a finite variance at the stated rate, and the crossover time beyond which aggregation is Gaussian is

$$t_c \;\sim\; \frac{\ell_c^{\alpha}}{D_\alpha}, \tag{68}$$

the time for the stable spread $(D_\alpha t)^{1/\alpha}$ to reach ℓ_c. A maximum-likelihood exponent fitted over ranges approaching ℓ_c therefore interpolates between the stable value $\mu = 1+\alpha$ and the Gaussian boundary $\mu \to 3$ — the F2 fingerprint, and the bigeye tuna arithmetic of §79.

109 Appendix C: the mode density and the spectral integrals, with constants

109.1 The Weyl lift

The fractional generator shares eigenfunctions with the Laplace–Beltrami operator on the patch; if $-\Delta_g\phi_n = \lambda_n\phi_n$ then $(-\Delta_g)^{\alpha/2}\phi_n = \lambda_n^{\alpha/2}\phi_n$. Weyl's law $N(\lambda) \sim \lambda^{d_\mathcal{S}/2}$ for the Laplacian (Weyl, 1912) therefore lifts to the relaxation rates $\mu = \lambda^{\alpha/2}$ as $N(\mu) \sim \mu^{d_\mathcal{S}/\alpha}$, i.e.

$$\rho_\alpha(\mu) \;\sim\; \frac{d_\mathcal{S}}{\alpha}\,\mu^{\,d_\mathcal{S}/\alpha-1}, \tag{69}$$

Eq. (46) with its prefactor.

109.2 The three spectral regimes, with constants

With soft-mode product $A_X(\lambda)\rho(\lambda) = A_0\lambda^{\gamma-1}$ on the band, the Lorentzian-superposition spectrum of §74 evaluates in the three regimes as

$$\omega \ll \lambda_{\rm IR}: \quad S_0 = \frac{2A_0}{1-\gamma}\Big(\lambda_{\rm IR}^{\gamma-1} - \lambda_{\rm UV}^{\gamma-1}\Big) \;\approx\; \frac{2A_0\,\lambda_{\rm IR}^{\gamma-1}}{1-\gamma}, \tag{70}$$

$$\lambda_{\rm IR} \ll \omega \ll \lambda_{\rm UV}: \quad S_X(\omega) = A_0\,\pi\sec\Big(\frac{\pi\gamma}{2}\Big)\,\omega^{\,\gamma-1} \;=\; A_0\,\pi\sec\Big(\frac{\pi\gamma}{2}\Big)\,\omega^{-\beta}, \tag{71}$$

$$\omega \gg \lambda_{\rm UV}: \quad S_X(\omega) \approx \frac{2A_0\,\lambda_{\rm UV}^{\gamma+1}}{(\gamma+1)\,\omega^2}, \tag{72}$$

using $\int_0^\infty u^\gamma(1+u^2)^{-1}\mathrm{d}u = \frac{\pi}{2}\sec(\pi\gamma/2)$ for $|\gamma|<1$ in the band. The knees are *soft* in a computable way: at $\omega = \lambda_{\rm IR}$ the band formula exceeds the plateau by the factor $\frac{\pi}{2}(1-\gamma)\sec(\pi\gamma/2)$ — equal to $\pi/2 \approx 1.6$ at $\gamma = 0$ — and the matching factor at the ultraviolet knee is $\frac{\pi}{2}(1+\gamma)\sec(\pi\gamma/2)$, so each knee is an order-half-decade shoulder rather than a sharp corner. That softness is an honest prediction about the census of §36: reported knees should come with half-decade uncertainties even from perfect data, and a fitted sharp break is the instrument's convention, not the account's.

109.3 The counting and two-sample integrals

The increment-variance integral behind the Hurst dictionary,

$$\langle [Y(t+\tau) - Y(t)]^2 \rangle \propto \tau^{\beta+1} \int_0^\infty u^{-\beta-2} \sin^2(\pi u)\, \mathrm{d}u, \tag{73}$$

converges at both ends precisely for $0 \le \beta < 1$, with a positive constant whose value cancels from every exponent comparison; $2H = \beta + 1$ follows. The same integral drives the counting statistics: for a point process whose rate carries the band spectrum, the rate contribution to the count variance over windows T is the identical integral with $\tau \to T$, so $\operatorname{Var} N(T) = \langle N \rangle + \text{const} \cdot T^{\beta+1}$ and the Fano factor is $F(T) = 1 + (T/T_F)^\beta$ — Eq. (52), with the crossover scale T_F set by the rate variance. The two-sample (Allan) variance replaces $\sin^2$ by $\sin^4$ in the transfer function; the resulting integral converges for $-1 < \beta < 3$, giving $\sigma_A^2(\tau) \propto \tau^{\beta-1}$ across that full range (logarithmic at $\beta = 1$) — which is why the Allan slope remains a valid exponent instrument on nonstationary bands where (73) diverges, and why §75 lists it as the third dress of the one exponent.

110 Appendix D: the audit's error propagation, dictionary by dictionary

Every verdict in Part VIII rests on a propagated uncertainty, and the rules are short enough to print completely. The audit's conventions first: predicted and measured values carry their own errors; a pair's verdict is stated at the combined uncertainty $\sigma_{\text{comb}} = (\sigma_{\text{pred}}^2 + \sigma_{\text{meas}}^2)^{1/2}$; a pair whose two exponents come from the *same fit* is not independent and is excluded; and a pair with an unverified input enters Figure 7 as an open marker, never in the arithmetic.

(R1) Tail and stable index. $\alpha_{\text{s}} = \mu - 1$ is linear with unit slope: $\sigma_{\text{pred}} = \sigma_\mu$, no correction.

(R2) Path dimension. $D_{\text{f}} = \min(d, \mu - 1)$ propagates piecewise. Below the cap, $\sigma_{\text{pred}} = \sigma_\mu$; within σ_μ of the cap the prediction is one-sided (the dimension cannot exceed d), and the audit states the verdict against the interval $[\mu - 1 - \sigma_\mu,\, d]$; at the cap the prediction degenerates to d exactly and the informative test inverts — a measured $D < d$ at significance is what would bite.

(R3) The Hurst dictionary. $\beta = 2H - 1$ doubles the error: $\sigma_{\text{pred}} = 2\sigma_H$, and comparing a measured slope against an H-derived one uses $\sigma_{\text{comb}} = (\sigma_\beta^2 + 4\sigma_H^2)^{1/2}$. The branch choice (fGn versus fBm, ∓ 1) is decided by stationarity before any comparison, never by which branch fits better — deciding it by fit would spend the dictionary's one degree of freedom on the answer.

(R4) Counting statistics. The Fano exponent equals β on the band (Appendix C), so propagation is direct; the knee-adjacent saturation enters as a stated validity band, not as an error bar.

(R5) The crackling relation. For $r = (\tau_t - 1)/(\tau - 1)$, the quotient rule gives

$$\sigma_r^2 = \left(\frac{\sigma_{\tau_t}}{\tau - 1} \right)^2 + \left(\frac{(\tau_t - 1)\, \sigma_\tau}{(\tau - 1)^2} \right)^2, \tag{74}$$

and the cortical pair of Table 13 makes the worked example: $\tau = 1.52 \pm 0.09$, $\tau_t = 1.7 \pm 0.1$ give $r = 1.35 \pm 0.30$ — which is why Part VIII calls that point consistent rather than confirmatory: the propagated bar is a fifth of the value, and honesty about R5's leverage begins with printing it.

The general lesson the audit's scatter obeys: the dictionaries with derivative structure (R3's factor two, R5's quotient) inflate errors, and the pairs testing them carry visibly wider bars on Figure 7 — the plot's error structure is itself propagated, not decorative.

111 Appendix E: the dataset schema, the protocol, and the verification record

The schema. Each of the six datasets is a flat table, one measurement per row, with the columns: *system* (the physical system, named as its source names it); *quantity* (which exponent or scale, in the estimator's own convention); *value* and *uncertainty* (the published digits, never a recomputation); *decades* (the fitted span, where the source states one); *year*; *source*; *grade*; and *notes* carrying the per-row caveats and the verification trail, with a resolvable locator for every row. The printed Tables 2–7 are projections of these files; the files, deployed beside this supplement, are the objects of record.

The grades. P (*primary*): the number was read from the primary source's own text during this compilation. C (*compiled*): taken from a named review or secondary compilation, with the compiler cited. U? (*unverified*): a standard literature value whose primary text could not be fetched; printed, flagged, and excluded from every audit computation. No number in any table was invented, recalled from memory, or averaged across sources; rows that could not be sourced at all were dropped, and category counts printed in the prose are counts of survivors.

The verification record. The compilation initially carried 245 rows with 67 at U?. A dedicated verification pass ran every flagged row back to a primary or named secondary source, ending at 177 P / 59 C / 9 U? — the nine survivors are flagged in their notes fields, and three of them await library access to sources with no open text. The pass corrected twelve values, and the corrections were systematic rather than random, falling in four classes: the right value attached to the wrong paper; a mislabeled estimator (one fractal dimension family quoted as another); citations degraded through secondary quotation; and midpoint glosses of published ranges hardening into digits. Each corrected row's note names its correction. The four classes are exactly those the fractal record's own critique literature documents in others, which is the methodological finding of §94: compilations fail in stereotyped ways, and a protocol that logs provenance per row catches them.

112 Appendix F: the estimator dictionaries and their bias directions

The audit compares exponents measured by different instruments, so the instruments' known biases are part of the propagation. The directions used in Part VIII:

Temporal instruments. The periodogram and Welch spectrum estimate β reliably only inside the band; within roughly half a decade of either knee the soft-shoulder factors of Appendix C bias a straight-line fit shallow, so band fits exclude the knee neighborhoods. Detrended fluctuation analysis (Peng et al., 1993) returns $\alpha_{\mathrm{DFA}} = H$ on the stationary branch, hence $\beta = 2\alpha_{\mathrm{DFA}} - 1$, and continues through the nonstationary boundary where the direct Hurst integral fails; its known biases are short-record underestimation and spurious crossovers from unremoved trends — the F4 direction. The Fano curve saturates beyond the infrared knee (the counting window outruns the correlated band), so a Fano exponent fitted across the knee is biased low; the Allan variance does not saturate there and is preferred at the long end (Appendix C). Where two temporal instruments disagree beyond their bands' overlap, the audit uses the one whose validity band covers the measured window, and says so in the row.

Tail instruments. Maximum likelihood on the stated window (Clauset et al., 2009) is the audit's standard; binned least-squares fits are biased and enter only as historical values with their replacements printed beside them (Edwards et al., 2007, Wagenmakers et al., 2004). On truncated data the MLE itself interpolates toward the Gaussian as the fit range approaches the tempering scale — the F2 direction, upward in μ — so every tail row carries its window, and R1 comparisons use the truncated-window value. The survival–density bookkeeping (μ for the density, $\mu - 1$ for the survival function) is fixed per row in the notes, since a one-unit bookkeeping slip is indistinguishable from a physical discrepancy in R1.

Dimension instruments. Box, mass–radius, correlation, and information dimensions (D_0, D_2, D_1) are different functionals and are not interchanged; the verification pass's "mislabeled estimator" class was precisely this substitution, and the record tables name the estimator per row. Every dimension row carries its window per F1; a dimension without a stated span is excluded from R2 regardless of its pedigree.

113 Appendix G: reproduction

Everything quantitative in this supplement reproduces from the published datasets by a fixed pipeline: the six data files are the single source; the record tables are generated from them without hand edits; the landscape figures and the audit figure are generated from the same files, with error propagation applied at generation time exactly as Appendix D states; and the document is built by three passes of standard LaTeX on stock packages, with fonts embedded and no external resources. The distributed package contains the complete source, the style file, and the six figure assets, with a checksum manifest; it is verified, at every version, to rebuild from an empty directory to a document page-for-page identical to the deployed one. A reader who edits a dataset row and rebuilds obtains the corrected tables, figures, and — through the audit — verdicts; that closed loop, rather than any single number, is what this appendix exists to certify.

Part XVII
Common Objections and Responses

The strongest objections — from the skeptical reader, from each of the four record literatures, from the theory side, and against the falsifiability posture itself — answered with pointers into the paper

A supplement earns nothing by being asked easy questions. This Part collects the hard ones, from the communities most likely to ask them, and answers without softening the question first. Every answer points into the body rather than restating it, so an objection and the argument it attacks can be read side by side; where the honest answer is that the question is open, the answer says so and names what is missing — there are several of those, and they are not hidden among the others. Like the appendices, this is back matter: find the objection nearest your own and follow it in.

114 From the skeptical reader

Question 1 (Q-S2-1)

"Power laws are the most over-claimed objects in science. Why should this compilation be different?"

Response. It should not be believed different; it should be checked, and it was built to be checkable. The compilation was assembled by the skeptics' own rules — truncated maximum likelihood with stated windows (Clauset et al., 2009), the retraction told first (Edwards et al., 2007), the one-decade census printed at full size (Avnir et al., 1998) — and its verification pass corrected twelve of its own values in print (Appendix E, §111). More to the point, the paper's claim does not live where the over-claiming happened. No single power law here carries any weight; the claim is the *arithmetic between* independently measured exponents (Part VIII), which is exactly the test the over-claimed literature never ran on itself.

Question 2 (Q-S2-2)

"Seventeen points on an identity plot. That is numerology with error bars."

Response. Numerology is digits without structure. The relations tested in Part VIII are theorems of standard mathematics — the generalized central limit theorem, the stable-path dimension theorem, the spectral integrals of Appendix C — and the finding is that measured values satisfy them across literatures that never coordinated. Seventeen is small, and the paper says it is small: the rarity of same-data pairs is elevated to a finding in its own right (§95), and the standing remedy is not rhetoric but F-S2-1 — any lab can create the eighteenth point, and any one point far off the line ends the account.

Question 3 (Q-S2-3)

"Why should a six-dimensional bulk care about a foraging shark?"

Response. It does not — the dependence runs the other way. The shark, like every measured system, is described through a partial view, and the geometric claim is only that partial views of a scale-carrying bulk inherit homogeneous statistics (§66, the five-link chain). Nothing about particle physics governs sharks; the claim is that shark telemetry and collider data are both windows onto one geometry, and the sole testable content of that sentence — that the window statistics lock the way Part XII says — is what the audit measures. Strip the geometry away and the audit still stands as an instrument; that separability is argued at every step (§93).

Question 4 (Q-S2-4)

"The philosophical close is anthropic hand-waving."

Response. The close (§105) is flagged, in its own text, as a reading the physics permits and not a result it proves — which is already more than hand-waving usually concedes. But the substantive difference from anthropic reasoning is structural: no selection over unobservable ensembles is invoked anywhere. The three arguments of §104 are statements about *derived dynamics* of open systems in this world — heavy tails, search, timescale reservoirs — and they inherit this paper's falsifiers: kill the lock or the knees and the philosophy dies with them. A consolation cannot be falsified; that is the entire claimed difference, and it is stated as such.

115 From the four record literatures

Question 5 (Q-S2-5)

"The 3/4-versus-2/3 war is not settled. Deriving 'the' allometric exponent is premature."

Response. Agreed, and the paper derives no such digit. Its own critique section states that the war is unsettled and that saying so is the honest summary (§21). What the account claims about the scaling record is structural — homogeneous generators, bounded windows, exponent ratios fixed within a system — and every row of Table 2 stands unchanged whichever side of the war eventually wins. The one commitment: whatever the exponent is, its window must obey F1's drift law, which is testable now.

Question 6 (Q-S2-6)

"Rigorous fitting killed most power-law claims. Your record inherits the corpses."

Response. The record was compiled *after* that reformation and by its rules: the statistics critique is adopted wholesale (§21, §26), the surviving record is smaller than the pre-reform one and the paper says so, and the audit computes only on survivors with grades attached. Where a corpse appears — the albatross founding claim, the binned tuna fit — it appears labeled as a corpse, with its replacement beside it.

Question 7 (Q-S2-7)

"The median claimed 'fractal' spans 1.3 decades. Your dimension rows are meaningless."

Response. The critique is not resisted; it is *derived*. F1 shows that a one-decade window cannot carry a stable exponent, and Appendix A prints the drift schedule — roughly ten percent slope drift across the central half-decade of a 1.3-decade window — so the census finding (Avnir et al., 1998) is read here as a theorem confirmed rather than a scandal. The record tables carry a decades column for exactly this reason, the audit weights by it, and the account's own dimension claims rest on the trajectory-like rows with real spans, not on the one-decade block.

Question 8 (Q-S2-8)

"Composite random walks mimic Lévy statistics. The movement record proves nothing."

Response. Half right, and the half is in the paper: a pooled single-record fit proves nothing, which is why the account never rests on one (§86). The other half is the account's addition: a genuine branch has one exponent and a mixture does not, so mimicry carries an obligatory fingerprint — sub-records that disagree — making the ambiguity an *assay* rather than a dead end (T-S2-2, F3). The account stakes a falsifier on this: one demonstrated mimic whose sub-records agree at full precision (F-S2-5) destroys the instrument and, with it, the evidential force of the whole movement record. That is the opposite of proving nothing.

Question 9 (Q-S2-9)

"Every $1/f$ system already has a mundane mechanism. A universal account is unnecessary."

Response. The mechanistic theories are endorsed here at full strength — "exact where it lives" is this paper's own phrase for McWhorter and Dutta–Horn (§46). But the mundane accounts answer a different question. They convert a measured timescale distribution into a slope; they do not say why the same system's steps are heavy-tailed and its paths fractal, where the band's edges sit across domains, or why four literatures keep measuring one number (§53). *Unnecessary* is an empirical claim, and it now has a price: if the cross-signature locks and knee addresses are unnecessary structure, some F-S2 measurement will break them.

116 From the theory side

Question 10 (Q-S2-10)

"This is AdS/CFT with the serial numbers filed off."

Response. Part X exists so that this answer is on the page before the question is asked: no, in six specific, checkable ways, stated in a table (§58) — no duality claim, no large-N limit, no conformal boundary theory, among them — and the borrowing that remains (a kernel form forced by scale isometry, a bookkeeping) is named as borrowing, the ordinary kind transport theory does from thermodynamics. A reader from high-energy theory should audit that table first and hardest.

Question 11 (Q-S2-11)

"Isn't this just SOC again?"

Response. SOC's wager was that driven systems tune *themselves* to a critical point; this account claims no tuning and no critical point — the exponent is inherited from a projection, not from criticality (§47). The two differ where it can be checked: SOC's flagship spectral claim failed in its own model (Jensen et al., 1989), while this account's spectral content is the two knees at derivable places — structure SOC never predicted. What SOC got right, the crackling program, is kept, as dictionary R5, with credit.

Question 12 (Q-S2-12)

"The exponent is not computed for a single named system. Nothing is predicted."

Response. The premise is conceded in the grade table's two open rows, at full size (§81); the conclusion does not follow. Without computing α for any system, the account predicts: that any two measured signatures fix the rest (seventeen tests run, none failed); that every band has two knees at independently estimable addresses (closed at both ends in cortex, Table 13); that exponents drift by a computed schedule in short windows (Appendix A); and that failures come only in four fingerprinted modes. All six falsifiers of §80 bite today, before the open rows close. A theory can be falsifiable before it is complete — that is what *relational* content means, and it is the whole of what is claimed.

Question 13 (Q-S2-13)

"Correlation of exponents is not causation by one generator."

Response. Correct, and the paper's ceiling sentence — *interesting, and not proof* — is printed wherever the audit is summarized (§102). But the tested relations are not correlations in the statistical sense: they are parameter-free equalities with no slope or intercept to fit, and a world of four unrelated mechanisms owes them nothing. The discriminating instrument is the failure theory: multi-mechanism records must show the F3 fingerprint, single-generator records must not, and that difference — not the seventeen agreements — is what would eventually separate causation from coincidence. The account holds itself to finding it (F-S2-4, F-S2-5).

Question 14 (Q-S2-14)

"Biology is mechanism, not geometry. This abstracts away everything that matters."

Response. The account does not compete with mechanism; it operates one level beneath it, at the statistics a mechanism implements. Nothing here replaces a shark's physiology or a neuron's channels — the division of labor is stated constitutionally: the geometry supplies the tray of available statistics, and selection and mechanism decide which branch a lineage occupies (§104). The division earns its keep where it is sharpest: the metastatic pair (§84), where one genome under two mechanisms' readings is precisely two branches with two exponent sets — a geometric statement no amount of mechanism alone predicted, now usable as an assay.

117 On the falsifiability posture itself

Question 15 (Q-S2-15)

"You admit the solid-state knee is unfalsifiable. An unfalsifiable instance poisons the two-knee claim."

Response. One instance is unfalsifiable, it is named as such in print (§87), and the naming is the discipline, not the poison. The knee claim is tested where the attractor time is independently measurable — it already closed at both ends in cortex, and F-S2-3 commits it in any physiological record — while the solid-state case even carries its route back to falsifiability: a spectroscopic bound on the deepest barriers drags the knee into a laboratory band at sixty millielectronvolts per decade. A claim tested where it can be tested, and marked where it cannot, is the opposite of unfalsifiable; the poison would be counting the fourteen quiet decades as support, which the paper explicitly declines to do.

Question 16 (Q-S2-16)

"Two knees can always be claimed to sit outside the measured band. The prediction never bites."

Response. It bites in three places the escape move cannot reach. Where the attractor time is independently estimated, the knee's address is fixed *in advance* — F-S2-3 demands the knee within two decades of it, and a knee-free band through those decades kills the account with no appeal to bandwidth. Where the mean event time is measured, as in the quantum dots, the knee has a stated address one decade below the band. And Appendix C bounds the knee's *shape*: an order-half-decade shoulder, so a claimed knee sharper than that is not this account's knee. The escape is available only where no independent timescale exists at all — and the paper marks exactly those cases as currently unfalsifiable rather than spending them as evidence. The census of §36 exists to shrink that territory measurement by measurement.

Part XVIII
References

The program companions, the cited external literature — each with its relevance stated — and the sources of the record tables

Three lists. List A is the GG-Theory companions this supplement stands on, each with a Relevance note. List B is the external literature cited in the prose of Parts I–XVII, every entry with a Relevance note. List C prints the remaining sources of the record tables directly from the published datasets' source columns, so that every one of the 245 rows is traceable from the paper alone; the datasets themselves, deployed beside this supplement, carry the per-row URLs, verification grades, and notes in machine-readable form.

A. Papers of the GG-Theory program

Arisaka, K. (2026). *The GG-Constitution: Four Axioms and Seven Postulates of the GG-Theory Program, From Which GG-6, BI-6, OGN-5, and GDOS Descend as Theorems*. Preprint, available at https://preprints.arisaka-gg.org/a1-constitution/.
doi:10.5281/zenodo.22063867.

Relevance. The constitution. Part II states the program from its four axioms and seven postulates, and the obligation that shapes this whole supplement — POS-7, Maximal Falsifiability, that every central claim name in advance the measurement that would kill it — is this paper's seventh postulate. The audit of Part VIII and the falsifier list of Part XII are built to honor it.

Arisaka, K. (2026). *GG-Theory with GG-6: Geometry–Gauge Locking at the 6D Bulk (GG-6) at the Heart of Grand Geometric Theory (GG-Theory)*. Preprint, available at https://preprints.arisaka-gg.org/a2-gg6/.
doi:10.5281/zenodo.22064298.

Relevance. The bulk whose radial coordinate carries scale. The identification $r = \ln(E_{\mathrm{GUT}}/\mu)$ established here is what makes the bulk-to-boundary kernel of GG-A7-Qi4 Part V homogeneous, and therefore what gives the Qi-CON account a derived — rather than fitted — origin for the exponent this supplement's four records measure.

Arisaka, K. (2026). *Anomaly Freedom of BI-6: The Modified Bianchi Identity (BI-6) for the Six-Force, Six-Dimensional Bulk (GG-6)*. Preprint, available at https://preprints.arisaka-gg.org/a3-bi6/.
doi:10.5281/zenodo.22064300.

Relevance. The consistency proof of the bulk. Anomaly freedom is why the six-dimensional geometry that Part II describes is one structure and not a family of tunable variants — the same rigidity that forbids adjusting the exponent α per domain when the living record of Parts IV–VII is compared against it.

Arisaka, K. (2026). *GDOS: Geometric Dynamics of Open Systems — 6D GG-6 Bulk Projected to 4D Boundary for Quantum Measurement, General Relativity, and QFT*. Preprint, available at https://preprints.arisaka-gg.org/a5-gdos/.
doi:10.5281/zenodo.22064304.
Relevance. The boundary law of the partial view: the OGGEP projection whose finite window is why every scaling regime in the compiled record is bounded. The windowed homogeneity that Parts IV–VII keep finding empirically — crossovers, truncations, knees — is this paper's projection structure seen from the data side.

Arisaka, K. (2026). *The GRIP on GDOS — GRIP: the Geometric Engine of Symmetry Breaking, from the Big Bang to Mind*. Preprint, available at https://preprints.arisaka-gg.org/a6-grip/.
doi:10.5281/zenodo.22064306.
Relevance. The geometric pillars and the runtime engine. Supplies the scalar budget F_{GFF} behind the four-sector current and the GRIP persistence cycle whose slowest attractor relaxation time is where Part XII places the infrared knee.

Arisaka, K. (2026). *The Qi-4 Pillars — Qi-QUA, Qi-EP, Qi-CON, Qi-HAL: The Quantum-Information Backbone of GDOS*. Preprint, available at https://preprints.arisaka-gg.org/a7-qi4/.
doi:10.5281/zenodo.22064308.
Relevance. The parent paper of this supplement. Its Part V states the Qi-CON principle constitutionally — the window, the fractional generator $\mathcal{L}_{\text{eff}} = -D_\alpha(-\Delta_g)^{\alpha/2}$, and the four-signature table this supplement's Parts IV–VII audit against the measured record — and derives the four signatures from the projected kernel. S2 is the observational record that its own Part V, at seventeen pages, could not carry.

Arisaka, K. (2026). *Quantum Mechanics Derived from GG-Theory as Projection from 6D Bulk to 4D Boundary*. Preprint, available at https://preprints.arisaka-gg.org/a8-qm/.
doi:10.5281/zenodo.22064310.
Relevance. Quantum mechanics as the boundary account of the same projection this supplement runs at the scale of organisms. Cited in Part II's record table, and cited here also as the program's precedent in method: it closes the Born rule at a named level, states the single remaining step, and leaves it on the table — the register this supplement's audit adopts.

Arisaka, K. (2026). *The Standard Model as Theorem of GG-Theory: Its 28 Parameters as Observations of One Six-Dimensional Geometry*. Preprint, available at https://preprints.arisaka-gg.org/a9-sm/.
doi:10.5281/zenodo.22064312.
Relevance. The record in particle physics that earns the program its hearing here: $\alpha^{-1}(0) = 2^J + N^2 = 137$ at first order against CODATA's 137.036, $\sin^2\theta_W = 25/108$, $\alpha_s^{-1}(M_Z) = \pi e$,

$\lambda_H = 1/8$, $y_t = 1$. Part II's table leans on this paper hardest, and the standard it sets — integer inputs, measured outputs, named falsifiers — is the standard the Qi-CON claim is held to.

Arisaka, K. (2026). *The Standard Cosmology as Theorem of GG-Theory: The Cosmic Inventory as Observations of One Six-Dimensional Geometry*. Preprint, available at `https://preprints.arisaka-gg.org/a10-cosmos/`.
doi:10.5281/zenodo.22064314.
Relevance. The record in cosmology: $\Omega_m = 1/\pi$, $\Omega_\Lambda = 1 - 1/\pi$, $\Omega_b = 1/(2\pi^2)$, $n_s = 0.962$, $r = 0.004$, each against the measured inventory. Quoted in Part II's record table as the second of the two arenas — with particle physics — in which the geometry was tested before this supplement asks it to speak about living matter.

Arisaka, K. (2026). *The Kaxion: Cold Dark Matter as the Non-Spatial Compact-Angle Pseudoscalar of GG-6*. Preprint, available at `https://preprints.arisaka-gg.org/c1-kaxion/`.
doi:10.5281/zenodo.22064333.
Relevance. The program's standing laboratory falsifier in the dark sector: a dark-matter candidate at 8.1 μeV, a haloscope line at 1.95 GHz — one number, one instrument class, one kill. Cited in Part II's record table as the working example of POS-7 discipline that this supplement's own falsifier list imitates.

Arisaka, K. (2026). *The Hubble Tension in the Light of GG-Theory: The Hubble Constant as One Reading of a Derived Expansion History $H(t)$*. Preprint, available at `https://preprints.arisaka-gg.org/c2-hubble/`.
doi:10.5281/zenodo.22064336.
Relevance. The derived expansion history whose two readings of H_0 — the local and the acoustic — frame the Hubble tension as two ends of one geometric corridor rather than a contradiction. Quoted in Part II's record table as the program's account of a live anomaly, falsifiable by gravitational-wave standard sirens.

Arisaka, K. (2026). *The GG-6 Lock Cluster: A Non-Spatial Kaluza–Klein Resonance near 3.85 TeV as the Standing LHC Falsifier of GG-Theory*. Preprint, available at `https://preprints.arisaka-gg.org/p1-kk/`.
doi:10.5281/zenodo.22064321.
Relevance. The collider falsifier: $M_{\text{lock}} = \frac{1}{2} M_{\text{Pl}}\, e^{-35} \approx 3.85$ TeV, stated in advance, with the electroweak scale $v = M_{\text{lock}}(2/5)^3 \approx 246$ GeV descending from it. Cited in Part II's record table; with the Kaxion, it is the pattern — name the measurement that kills you — that Part XII's falsifier list follows.

B. All other works

Auger-Méthé, M., Derocher, A. E., Plank, M. J., Codling, E. A., and Lewis, M. A. (2015). *Differentiating the Lévy walk from a composite correlated random walk*. Methods in Ecology

and Evolution 6, 1179–1189.
Relevance. The mimicry theorem of the movement record: a two-mode Brownian composite reproduces an apparent Lévy walk over the window lengths real tracking data supply.

Avnir, D., Biham, O., Lidar, D., and Malcai, O. (1998). *Is the geometry of nature fractal?* Science 279, 39–40.
Relevance. The one-decade census: 96 Physical Review papers claiming fractality, mean reported scaling range 1.3 decades. The structural critique Part VI's Dec. column exists to answer.

Baish, J. W., and Jain, R. K. (2000). *Fractals and cancer.* Cancer Research 60, 3683–3688.
Relevance. Tumor vasculature at $D = 1.89(4)$ against normal vessels at 1.70(3) — the record's diagnostic-grade dimension difference.

Bak, P., Tang, C., and Wiesenfeld, K. (1987). *Self-organized criticality: an explanation of* $1/f$ *noise.* Physical Review Letters 59, 381–384.
Relevance. The mechanism proposal that unified the four records rhetorically decades before any audit; its corrected scope is Part VII's standing caution.

Banavar, J. R., Maritan, A., and Rinaldo, A. (1999). *Size and form in efficient transportation networks.* Nature 399, 130–132.
Relevance. The general network bound $B \propto M^{d/(d+1)}$: quarter-power scaling as a supply-network tax of one dimension, with weaker hypotheses than WBE.

Barabási, A.-L., and Albert, R. (1999). *Emergence of scaling in random networks.* Science 286, 509–512.
Relevance. Preferential attachment: the scale-free degree law with the model's own measured exponent $\gamma = 2.9 \pm 0.1$ against 2.3 (actors) and 2.1 (web). The exponent-from-a-growth-rule framework Part IX judges: transparent about its origin, and tunable, which is the opposite of locked.

Barthélemy, P., Bertolotti, J., and Wiersma, D. S. (2008). *A Lévy flight for light.* Nature 453, 495–498.
Relevance. The Lévy glass: superdiffusion of photons by designed scatterer statistics — the record's proof that μ is an engineering parameter where mechanism is controlled.

Baudouin, Q., Pierrat, R., Eloy, A., Nunes-Pereira, E. J., Cuniasse, P., Mercadier, N., and Kaiser, R. (2014). *Lévy flights of photons in hot atomic vapours.* arXiv:1305.1714; Physical Review E 90, 052114.
Relevance. Step exponent $\mu = 2.41(12)$ measured for resonant photons, derived from Doppler line shapes — first-principles Lévy statistics in a laboratory gas.

Beggs, J. M., and Plenz, D. (2003). *Neuronal avalanches in neocortical circuits.* Journal of Neuroscience 23, 11167–11177.
Relevance. The founding cortical avalanche measurement: $\tau = 1.50(1)$ with branching parameter $\sigma = 1.04(19)$ — two independent criticality signatures on one preparation, and two exact-theory points of Part VIII's audit.

Bettencourt, L. M. A., Lobo, J., Helbing, D., Kühnert, C., and West, G. B. (2007). *Growth, innovation, scaling, and the pace of life in cities.* Proceedings of the National Academy of Sciences 104, 7301–7306.
Relevance. The urban scaling split: superlinear socioeconomic exponents against sublinear infrastructure, the two bands drawn in Figure 2.

Bettencourt, L. M. A. (2013). *The origins of scaling in cities.* Science 340, 1438–1441.
Relevance. The network derivation of the urban exponents; the theoretical reading behind the urban block of Table 2.

Blumenthal, R. M., and Getoor, R. K. (1960). *Some theorems on stable processes.* Transactions of the American Mathematical Society 95, 263–273.
Relevance. The path-dimension theorem $D_{\mathrm{f}} = \min(d, \alpha_{\mathrm{s}})$ — relation (R2) of the audit, and the dictionary no trajectory study has yet tested on animal data.

Bouchaud, E. (1997). *Scaling properties of cracks.* Journal of Physics: Condensed Matter 9, 4319–4344.
Relevance. Fracture roughness $\zeta \approx 0.78$ universal at large scales with a quasistatic ≈ 0.5 regime below a material crossover — the record's model case of two-windowed scaling.

Belavin, A. A., Polyakov, A. M., and Zamolodchikov, A. B. (1984). *Infinite conformal symmetry in two-dimensional quantum field theory.* Nuclear Physics B 241, 333–380.
Relevance. The founding of 2D CFT: the Virasoro algebra, minimal models, and the exact dimensions behind Part VI's theorem block.

Bunde, A., Eichner, J. F., Govindan, R., Havlin, S., Koscielny-Bunde, E., Rybski, D., and Vjushin, D. (2004). *Comment on "Scaling of atmosphere and ocean temperature correlations in observations and climate models".* Physical Review Letters 92, 039801; arXiv:physics/0305080.
Relevance. The published dispute inside the climate DFA record, and the source of the sea-surface crossover at $\sim$1 yr in the knee census.

Caloyannides, M. A. (1974). *Microcycle spectral estimates of* $1/f$ *noise in semiconductors.* Journal of Applied Physics 45, 307–316.
Relevance. The canonical no-knee benchmark: $1/f$ tracked to $10^{-6.3}$ Hz over a three-month record with no flattening.

Carlson, J. M., and Doyle, J. (1999). *Highly optimized tolerance: a mechanism for power laws in designed systems.* Physical Review E 60, 1412–1427.
Relevance. Power laws from constrained optimization rather than criticality — the sharpest anti-criticality proposal in the field, and the standing reminder, enforced by this supplement's own audit, that heavy tails alone diagnose nothing. Part IX gives it its day.

Chang, C.-H., et al. (2024). *Bootstrapping the 3d Ising stress tensor.* arXiv:2411.15300.
Relevance. $\Delta_\sigma = 0.518148806(24)$: the scaling record's precision frontier, nine digits from consistency conditions alone.

Chester, S. M., Landry, W., Liu, J., Poland, D., Simmons-Duffin, D., Su, N., and Vichi, A. (2020). *Carving out OPE space and precise O(2) model critical exponents.* Journal of High Energy Physics 06, 142; arXiv:1912.03324.

Relevance. The O(2) bootstrap that sharpened the helium λ-point discrepancy to 8σ — Part VIII's inset, and the audit's precision ceiling.

Chialvo, D. R. (2010). *Emergent complex neural dynamics.* Nature Physics 6, 744–750.

Relevance. The neural criticality hypothesis at review strength: the brain naturally poised near a second-order critical point, with the functional case — dynamic range, pattern repertoire — argued in full. The strongest living-system form of the criticality idea that Part IX examines.

Clauset, A., Shalizi, C. R., and Newman, M. E. J. (2009). *Power-law distributions in empirical data.* SIAM Review 51, 661–703.

Relevance. The estimator standard — MLE, explicit cutoff, likelihood-ratio model comparison — that every post-2009 row of the record is judged against.

Damuth, J. (1981). *Population density and body size in mammals.* Nature 290, 699–700.

Relevance. Density $\propto M^{-0.75}$ over $\sim$7 decades: the negative quarter-power whose product with Kleiber gives energy equivalence.

de Jager, M., Weissing, F. J., Herman, P. M. J., Nolet, B. A., and van de Koppel, J. (2011). *Lévy walks evolve through interaction between movement and environmental complexity.* Science 332, 1551–1553.

Relevance. The mussel-bed claim whose refit and rereading (both in Table 4) make it the record's compact case study in estimator dependence.

DeLong, J. P., Okie, J. G., Moses, M. E., Sibly, R. M., and Brown, J. H. (2010). *Shifts in metabolic scaling, production, and efficiency across major evolutionary transitions of life.* Proceedings of the National Academy of Sciences 107, 12941–12945.

Relevance. The three-group split — prokaryotes 1.96(18), protists 1.06(7), metazoans 0.79(4) — that refuses a single metabolic exponent across life.

Donoghue, T., et al. (2020). *Parameterizing neural power spectra into periodic and aperiodic components.* Nature Neuroscience 23, 1655–1665.

Relevance. The method paper that made the aperiodic exponent and its knee standard measurements — why the knee census's populated column is neural.

Durin, G., and Zapperi, S. (2000). *Scaling exponents for Barkhausen avalanches in polycrystalline and amorphous ferromagnets.* Physical Review Letters 84, 4705–4708.

Relevance. Two clean universality classes in one laboratory system, with exponent pairs feeding the crackling identity — audit points with theory on both sides.

Dutta, P., and Horn, P. M. (1981). *Low-frequency fluctuations in solids: $1/f$ noise.* Reviews of Modern Physics 53, 497–516.

Relevance. The activated-switcher framework and the honest survey spread $\beta = 0.8$–1.4 for metals; the null model of (10).

Edwards, A. M., et al. (2007). *Revisiting Lévy flight search patterns of wandering albatrosses, bumblebees and deer.* Nature 449, 1044–1048.

Relevance. The retraction that reformed the field: the founding albatross power law was a logger artifact, and the estimator standards of every later row date from this paper.

Fontenele, A. J., et al. (2019). *Criticality between cortical states.* Physical Review Letters 122, 208101.

Relevance. In vivo avalanche exponents $\tau = 1.52(9)$, $\tau_t = 1.7(1)$ satisfying the crackling relation near the critical spiking-variability point — the audit's in vivo cortical entry.

Gao, R., van den Brink, R. L., Pfeffer, T., and Voytek, B. (2020). *Neuronal timescales are functionally dynamic and shaped by cortical anatomy.* eLife 9, e61277.

Relevance. The knee as information: ECoG aperiodic knees at 3–16 Hz mapping intrinsic timescales of 10–50 ms along the cortical hierarchy.

Glazier, D. S. (2005). *Beyond the '3/4-power law': variation in the intra- and interspecific scaling of metabolic rate in animals.* Biological Reviews 80, 611–662.

Relevance. The survey that made exponent diversity the finding: b varies with metabolic state, level, and taxon, and no single exponent describes metabolism.

Gilden, D. L., Thornton, T., and Mallon, M. W. (1995). *$1/f$ noise in human cognition.* Science 267, 1837–1839.

Relevance. The founding cognitive $1/f$ claim; printed beside its reanalysis (Wagenmakers et al., 2004), which is how this record teaches estimator humility.

Gubser, S. S., Klebanov, I. R., and Polyakov, A. M. (1998). *Gauge theory correlators from non-critical string theory.* Physics Letters B 428, 105–114.

Relevance. Half of the working AdS/CFT dictionary: boundary correlators from bulk boundary conditions.

Gnedenko, B. V., and Kolmogorov, A. N. (1954). *Limit Distributions for Sums of Independent Random Variables.* Addison-Wesley, Cambridge, MA.

Relevance. The generalized central limit theorem: stable laws as the only attractors of heavy-tailed sums — the mathematical floor under the entire Lévy record.

González-Martín, O., and Vaughan, S. (2012). *X-ray variability of 104 active galactic nuclei: AGN power spectra.* Astronomy & Astrophysics 544, A80.

Relevance. The astrophysical timing community as the record's model citizen: slopes always reported with their break frequencies, because the breaks scale with black-hole mass.

Greer, S. C. (1976). *Coexistence curves at liquid–liquid critical points: Ising exponents and extended scaling.* Physical Review A 14, 1770–1780.

Relevance. $\beta = 0.328(4)$ for a binary liquid — the fluid experiment on the bootstrap line in the audit.

Harris, T. H., et al. (2012). *Generalized Lévy walks and the role of chemokines in migration of effector CD8^{+} T cells.* Nature 486, 545–548.

Relevance. $\mu = 2.15$ for T cells hunting parasites in brain — the Lévy record's arrival in immunology, with its own reanalysis now in the table beside it.

Hausdorff, J. M., Peng, C.-K., Ladin, Z., Wei, J. Y., and Goldberger, A. L. (1995). *Is walking a random walk? Evidence for long-range correlations in stride interval of human gait.* Journal of Applied Physiology 78, 349–358.

Relevance. Long-memory gait intervals ($\alpha_{\mathrm{DFA}} \approx 0.83$) — the physiological block's locomotor entry.

Honerkamp-Smith, A. R., Machta, B. B., and Keller, S. L. (2008; dynamics 2011). *Critical exponents of lipid membranes near their mixing critical point (with critical dynamics follow-up).* Biophysical Journal 95, 236–246; arXiv:1104.2613.

Relevance. A biological membrane on the exact 2D Ising line: $\beta = 0.124(30)$ against 1/8, $\nu = 1.2(2)$ against 1 — two of the audit's cleanest biological points.

Hooge, F. N. (1969). *$1/f$ noise is no surface effect.* Physics Letters A 29, 139–140.

Relevance. The empirical magnitude law that organized semiconductor $1/f$ for a generation.

Huda, S., et al. (2018). *Lévy-like movement patterns of metastatic cancer cells revealed in microfabricated systems and implicated in vivo.* Nature Communications 9, 4539.

Relevance. The migration exponent that separates metastatic ($\mu = 2.36(13)$, and $1 < \mu < 3$ across matched lines) from non-metastatic ($\mu > 3$) cells — the record's most consequential entry.

Humphries, N. E., et al. (2010). *Environmental context explains Lévy and Brownian movement patterns of marine predators.* Nature 465, 1066–1069.

Relevance. $1 < \mu \leq 3$ in 61 of 66 dataset sections across fourteen species — the post-reformation confirmation of scale-free marine movement.

Humphries, N. E., Weimerskirch, H., Queiroz, N., Southall, E. J., and Sims, D. W. (2012). *Foraging success of biological Lévy flights recorded in situ.* Proceedings of the National Academy of Sciences 109, 7169–7174.

Relevance. The albatross verdict at GPS resolution: about a third of birds show truncated power-law movement — neither the founding claim nor its negation.

Hurst, H. E. (1951). *Long-term storage capacity of reservoirs.* Transactions of the American Society of Civil Engineers 116, 770–808.

Relevance. The Nile minima and the exponent that carries his name: $H = 0.73$, the record's oldest long-memory measurement.

Huybers, P., and Curry, W. (2006). *Links between annual, Milankovitch and continuum temperature variability.* Nature 441, 329–332.

Relevance. The climate continuum's two-regime spectrum — $\beta = 0.37$–0.56 below the centennial scale, 1.29–1.64 above — the record's cleanest steepening knee, and two audit pairs against the DFA literature.

Jensen, H. J., Christensen, K., and Fogedby, H. C. (1989). *$1/f$ noise, distribution of lifetimes, and a pile of sand.* Physical Review B 40, 7425–7427.
Relevance. The correction from inside the SOC program: the sandpile's own spectrum is $1/f^2$, not $1/f$, so the flagship claim of the founding paper failed its own model — quoted in Part IX as the model of a field auditing itself.

Johnson, J. B. (1925). *The Schottky effect in low frequency circuits.* Physical Review 26, 71–85.
Relevance. The founding measurement of the whole $1/f$ record.

Kleiber, M. (1932). *Body size and metabolism.* Hilgardia 6, 315–353.
Relevance. The line that started the war: $b \approx 0.74$ over 2.6 decades, rounded to the 3/4 that carries his name.

Kobayashi, M., and Musha, T. (1982). *$1/f$ fluctuation of heartbeat period.* IEEE Transactions on Biomedical Engineering 29, 456–457.
Relevance. Cardiac $1/f$ over 10^{-4}–10^{-2} Hz with no reported flattening — the primary record behind this supplement's finding that the famous cardiac knee is unsourced.

Kolokotrones, T., Savage, V. M., Deeds, E. J., and Fontana, W. (2010). *Curvature in metabolic scaling.* Nature 464, 753–756.
Relevance. The measured log–log curvature — local slope rising 0.57 to 0.87 across the mammalian window — that makes any single metabolic exponent a window average.

Kos, F., Poland, D., Simmons-Duffin, D., and Vichi, A. (2016). *Precision islands in the Ising and O(N) models.* Journal of High Energy Physics 08, 036; arXiv:1603.04436.
Relevance. The precision-island bootstrap: $\Delta_\sigma = 0.5181489(10)$, the 2016 anchor of the critical scoreboard.

Kovtun, P. K., Son, D. T., and Starinets, A. O. (2005). *Viscosity in strongly interacting quantum field theories from black hole physics.* Physical Review Letters 94, 111601.
Relevance. The $\eta/s \geq \hbar/4\pi k_B$ bound: AdS/CFT's flagship transport output, in Part IV's scoreboard as the correspondence's own achievement — explicitly not inherited by GG-6 (Table 9).

Lawler, G. F., Schramm, O., and Werner, W. (2001). *The dimension of the planar Brownian frontier is* 4/3. Mathematical Research Letters 8, 401–411.
Relevance. Mandelbrot's conjecture proved: fractal dimension as rigorous conformal geometry — the top block of the fractality record.

Leland, W. E., Taqqu, M. S., Willinger, W., and Wilson, D. V. (1994). *On the self-similar nature of Ethernet traffic.* IEEE/ACM Transactions on Networking 2, 1–15.
Relevance. $H = 0.875$ for LAN traffic: the long-memory record's engineered-system entry.

Lévy, P. (1937). *Théorie de l'addition des variables aléatoires.* Gauthier-Villars, Paris.
Relevance. The stable laws themselves; the Gaussian degeneration at $\alpha = 2$ used in the admissibility argument of §70.

Lin, M. Y., Lindsay, H. M., Weitz, D. A., Ball, R. C., Klein, R., and Meakin, P. (1989). *Universality of fractal aggregates as probed by light scattering.* Nature 339, 360–362 (and Physical Review A 41, 2005).
Relevance. The two colloid universality classes, DLCA $D \approx 1.86$ and RLCA $D \approx 2.1$, reproduced across chemically distinct systems.

Lipa, J. A., Nissen, J. A., Stricker, D. A., Swanson, D. R., and Chui, T. C. P. (2003). *Specific heat of liquid helium in zero gravity very near the lambda point.* Physical Review B 68, 174518.
Relevance. $\alpha_{\text{exp}} = -0.0127(3)$ at sub-nanokelvin resolution in microgravity — the experimental side of the 8σ tension in Part VIII's inset.

Lowen, S. B., and Teich, M. C. (1996). *The periodogram and Allan variance reveal fractal exponents greater than unity in auditory-nerve spike trains.* Journal of the Acoustical Society of America 99, 3585–3591.
Relevance. The estimator-ceiling dissection: where Fano saturates and spectra do not — the documented bias behind the Teich pairs' offsets in the audit.

Maldacena, J. M. (1998). *The large N limit of superconformal field theories and supergravity.* Advances in Theoretical and Mathematical Physics 2, 231–252.
Relevance. The correspondence itself; also the source GG-A7-Qi4 Part V cites at the bulk-to-boundary kernel (30), which is why Part X draws the borrowing line in the open.

Mandelbrot, B. B. (1963). *The variation of certain speculative prices.* Journal of Business 36, 394–419.
Relevance. Stable laws meet data: cotton prices, and the founding of heavy-tailed finance.

Mandelbrot, B. B. (1967). *How long is the coast of Britain? Statistical self-similarity and fractional dimension.* Science 156, 636–638.
Relevance. The founding document of the fractality record, built on Richardson's divider data — including the non-universality (1.02–1.25 across coasts) the record still shows.

McWhorter, A. L. (1957). *$1/f$ noise and germanium surface properties.* In R. H. Kingston (ed.), Semiconductor Surface Physics, University of Pennsylvania Press, 207–228.
Relevance. The tunneling-trap model: a log-uniform distribution of relaxation times superposing to exact $1/f$ across the trap band, knees included. The rival that is complete in its own domain — Part IX's standard for what "exact where it lives" means.

Metzler, R., and Klafter, J. (2000). *The random walk's guide to anomalous diffusion: a fractional dynamics approach.* Physics Reports 339, 1–77.
Relevance. The standard reference for the fractional operators and anomalous-diffusion calculus of Part XII's on-ramp.

Miller, K. J., Sorensen, L. B., Ojemann, J. G., and den Nijs, M. (2009). *Power-law scaling in the brain surface electric potential.* PLoS Computational Biology 5, e1000609.

Relevance. ECoG $\beta \approx 2$ with a documented steepening to ≈ 4 above 75 Hz — the modality dependence that forbids a single cortical β.

Muñoz, M. A. (2018). *Colloquium: Criticality and dynamical scaling in living systems.* Reviews of Modern Physics 90, 031001.
Relevance. The field's own measured verdict on criticality in living matter — some evidence remarkable, some limited, incomplete, or not fully convincing — and the survey of what proximity-to-criticality has and has not earned, quoted in Part IX at exactly that strength.

Murray, J. D., et al. (2014). *A hierarchy of intrinsic timescales across primate cortex.* Nature Neuroscience 17, 1661–1663.
Relevance. Intrinsic timescales 50–350 ms ordered along the cortical hierarchy — the knee census's spiking-side entry.

Niemeyer, L., Pietronero, L., and Wiesmann, H. J. (1984). *Fractal dimension of dielectric breakdown.* Physical Review Letters 52, 1033–1036.
Relevance. Laboratory Lichtenberg figures at $D \approx 1.7$: DLA-class growth confirmed in a second mechanism.

Nienhuis, B. (1982). *Exact critical point and critical exponents of O(n) models in two dimensions.* Physical Review Letters 49, 1062–1065.
Relevance. The Coulomb-gas exponents behind the exact 4/3 of the self-avoiding walk.

Onsager, L. (1944). *Crystal statistics. I. A two-dimensional model with an order–disorder transition.* Physical Review 65, 117–149.
Relevance. The exact 2D Ising solution: the first exact exponents any scaling theory had to hit, and the theory side of the membrane pairs in the audit.

Pelton, M., Grier, D. G., and Guyot-Sionnest, P. (2004). *Characterizing quantum-dot blinking using noise power spectra.* Applied Physics Letters 85, 819–821.
Relevance. The μ–β lock on single dots: PSD exponent tied to switching-time tails on the same system, with no knee in the measured band — an audit pair and a knee-census entry at once.

Peng, C.-K., Mietus, J., Hausdorff, J. M., Havlin, S., Stanley, H. E., and Goldberger, A. L. (1993). *Long-range anticorrelations and non-Gaussian behavior of the heartbeat.* Physical Review Letters 70, 1343–1346.
Relevance. Heavy tails and long memory dissociated on one physiological series — disease removes the correlations and keeps the distribution.

Polchinski, J. (1988). *Scale and conformal invariance in quantum field theory.* Nuclear Physics B 303, 226–236.
Relevance. The scale-versus-conformal gap stated exactly: the 2D theorem and the four-dimensional question — why Part X's "operational conformality" is claimed at the scale level and no higher.

Poland, D., Rychkov, S., and Vichi, A. (2019). *The conformal bootstrap: theory, numerical techniques, and applications.* Reviews of Modern Physics 91, 015002.
Relevance. The modern review of the program that produced the nine-digit exponents anchoring Part IV's scoreboard.

Polyakov, A. M. (1970). *Conformal symmetry of critical fluctuations.* JETP Letters 12, 381–383.
Relevance. The proposal that critical points are conformal, not merely scale invariant — the upgrade Part X's CFT review is built on.

Pyke, G. H. (2015). *Understanding movement paths of Lévy walkers: is the Lévy foraging hypothesis dead?* Methods in Ecology and Evolution 6, 1–16.
Relevance. The strongest published case that the optimality result itself is fragile — the skeptical bookend of the Lévy record.

Quintana, C. M., et al. (2017). *Observation of classical–quantum crossover of $1/f$ flux noise and its paramagnetic temperature dependence.* Physical Review Letters 118, 057702.
Relevance. Fourteen decades of $1/f$ flux noise with no infrared knee — the knee census's hardest negative.

Rattazzi, R., Rychkov, V. S., Tonni, E., and Vichi, A. (2008). *Bounding scalar operator dimensions in 4D CFT.* Journal of High Energy Physics 12, 031.
Relevance. The paper that turned crossing symmetry into a numerical carving tool — the start of the modern bootstrap.

Sagi, Y., Brook, M., Almog, I., and Davidson, N. (2012). *Observation of anomalous diffusion and fractional self-similarity in one dimension.* Physical Review Letters 108, 093002.
Relevance. Cold atoms with a laser-tunable Lévy exponent: the record's cleanest demonstration that μ follows mechanism.

Savage, V. M., et al. (2004). *The predominance of quarter-power scaling in biology.* Functional Ecology 18, 257–282.
Relevance. The largest compilation of its day: $b = 0.712$ unbinned, 0.737 binned — the protocol sensitivity quantified inside one paper.

Schramm, O. (2000). *Scaling limits of loop-erased random walks and uniform spanning trees.* Israel Journal of Mathematics 118, 221–288.
Relevance. SLE: the conformally invariant random curves whose exact dimensions $1 + \kappa/8$ generate Part VI's theorem block.

Scrimgeour, M. I., et al. (2012). *The WiggleZ Dark Energy Survey: the transition to large-scale cosmic homogeneity.* Monthly Notices of the Royal Astronomical Society 425, 116–134.
Relevance. $D_2 \to 3$ within one percent by $71\,h^{-1}$ Mpc: the fractal universe debate ends in a measured upper knee.

Sethna, J. P., Dahmen, K. A., and Myers, C. R. (2001). *Crackling noise.* Nature 410, 242–250.

Relevance. The exponent-relation framework — relation (R5) — that turned avalanche statistics into a cross-checkable science.

Sims, D. W., et al. (2008). *Scaling laws of marine predator search behaviour.* Nature 451, 1098–1102.
Relevance. A million steps across seven species, $\mu = 2.12(31)$ pooled — and three exponents on the same dive series, making it the audit's best multi-signature system.

Smith, J. H., et al. (2023). *Fractal dimension analysis of dendritic arbors.* Frontiers in Network Physiology 3, 1072815.
Relevance. Arbors at $D = 1.4$ over 1.5 decades, single dendrites nearly line-like — modern biological fractality with its window honestly stated.

Sreenivasan, K. R., and Meneveau, C. (1986). *The fractal facets of turbulence.* Journal of Fluid Mechanics 173, 357–386.
Relevance. Turbulent interfaces and dissipation supports as measured multifractals — why estimator gaps are physics, not error.

Stumpf, M. P. H., and Porter, M. A. (2012). *Critical truths about power laws.* Science 335, 665–666.
Relevance. The short sharp audit of the power-law canon after Clauset–Shalizi–Newman — the standard this supplement's own tables are built to survive.

Takeuchi, K. A., and Sano, M. (2010). *Universal fluctuations of growing interfaces: evidence in turbulent liquid crystals.* Physical Review Letters 104, 230601.
Relevance. KPZ exponents hit at one percent in a tabletop experiment — two exact-theory points on the audit line, and Tracy–Widom statistics confirmed besides.

Teich, M. C., Heneghan, C., Lowen, S. B., Ozaki, T., and Kaplan, E. (1997). *Fractal character of the neural spike train in the visual system of the cat.* Journal of the Optical Society of America A 14, 529–546.
Relevance. Fano and spectral exponents on the same retinal and geniculate cells — the rare true same-data pair, with the estimator offset the audit displays.

Touboul, J., and Destexhe, A. (2017). *Power-law statistics and universal scaling in the absence of criticality.* Physical Review E 95, 012413.
Relevance. Avalanche power laws reproduced by stochastic surrogates with no phase transition: the demonstration that the neural record's power laws alone underdetermine the criticality hypothesis, carried by Part IX and by the audit's grading.

Viswanathan, G. M., Afanasyev, V., Buldyrev, S. V., Murphy, E. J., Prince, P. A., and Stanley, H. E. (1996). *Lévy flight search patterns of wandering albatrosses.* Nature 381, 413–415.
Relevance. The founding observation — retained in the record beside its correction, because the pair is the field's history in two rows.

Viswanathan, G. M., Buldyrev, S. V., Havlin, S., da Luz, M. G. E., Raposo, E. P., and Stanley, H. E. (1999). *Optimizing the success of random searches.* Nature 401, 911–914.
Relevance. The $\mu_{\text{opt}} = 2$ theorem for sparse revisitable targets — the theoretical pole the whole foraging record orbits.

Voss, R. F., and Clarke, J. (1975). *"1/f noise" in music and speech.* Nature 258, 317–318.
Relevance. The record's proof that the phenomenon does not care what is fluctuating: loudness and pitch of music and speech.

Voss, R. F., and Clarke, J. (1976). *Flicker (1/f) noise: equilibrium temperature and resistance fluctuations.* Physical Review B 13, 556–573.
Relevance. The equilibrium-fluctuation measurements that anchored metal-film $1/f$.

Wagenmakers, E.-J., Farrell, S., and Ratcliff, R. (2004). *Estimation and interpretation of $1/f^{\alpha}$ noise in human cognition.* Psychonomic Bulletin & Review 11, 579–615.
Relevance. The reanalysis that halved the cognitive β — printed beside the claim it corrected.

Watts, D. J., and Strogatz, S. H. (1998). *Collective dynamics of 'small-world' networks.* Nature 393, 440–442.
Relevance. The small-world result — short paths with high clustering — cited in Part IX to mark its scope: a topology statement adjacent to the scale-free program, with no power law and no bearing on the four signatures.

Weissman, M. B. (1988). *$1/f$ noise and other slow, nonexponential kinetics in condensed matter.* Reviews of Modern Physics 60, 537–571.
Relevance. The subject's most rigorous review: measured $1/f$ arises from materially different kinetics in different systems — the many-mechanisms constraint the audit answers with relations rather than slopes.

West, G. B., Brown, J. H., and Enquist, B. J. (1997). *A general model for the origin of allometric scaling laws in biology.* Science 276, 122–126.
Relevance. The fractal supply-network derivation of 3/4 — the theory pole of the metabolic war.

Weyl, H. (1912). *Das asymptotische Verteilungsgesetz der Eigenwerte linearer partieller Differentialgleichungen.* Mathematische Annalen 71, 441–479.
Relevance. The eigenvalue counting law behind the derived soft-mode density (46) — what makes the $1/f$ band's mode spectrum an output rather than a postulate.

White, C. R., and Seymour, R. S. (2003). *Mammalian basal metabolic rate is proportional to body mass$^{2/3}$.* Proceedings of the National Academy of Sciences 100, 4046–4049.
Relevance. The temperature-normalized $b = 0.686(14)$ that reopened the war on Rubner's side.

Wilson, K. G. (1971). *Renormalization group and critical phenomena.* Physical Review B 4, 3174–3205.
Relevance. Why scaling exponents exist at all: fixed points wash out microscopic scales — the exactness standard the biological records are audited against.

Witten, E. (1998). *Anti de Sitter space and holography.* Advances in Theoretical and Mathematical Physics 2, 253–291.
Relevance. The other half of the working dictionary, with the mass–dimension relation (19).

Witten, T. A., and Sander, L. M. (1981). *Diffusion-limited aggregation, a kinetic critical phenomenon.* Physical Review Letters 47, 1400–1403.
Relevance. The growth model that made fractal dimension reproducible physics: $D \approx 1.71$ across mechanisms and laboratories.

Zaburdaev, V., Denisov, S., and Klafter, J. (2015). *Lévy walks.* Reviews of Modern Physics 87, 483–530.
Relevance. The compendium of the walk (finite-velocity) formalism the biological record uses.

C. Sources of the record tables

The remaining sources named in Tables 2–7 but not cited in the prose, printed from the published machine-readable datasets' own source and URL columns — author-year and venue exactly as each row carries them, so that every table row is traceable from the paper alone. Full bibliographic apparatus for these entries lives in the datasets deployed beside this supplement; entries verified against their primaries during the August 2026 verification pass carry that status in the datasets' per-row notes.

Aizenman, Duplantier & Aharony 1999, PRL 83:1359. https://arxiv.org/abs/cond-mat/9901018
Arevalo et al 2024, A&A. https://www.aanda.org/articles/aa/full_html/2024/04/aa47080-23/aa47080-23.html
Ariel et al 2015, Nat Commun 6:8396. https://pmc.ncbi.nlm.nih.gov/articles/PMC4598630
arXiv:2307.03457 (2023). https://arxiv.org/html/2307.03457
Auger-Methe et al 2015, Methods Ecol Evol.
Balandin 2013, Nat Nanotech 8:549 (review). https://arxiv.org/pdf/1307.4797
Belgrano et al 2002, Ecology Letters. https://people.clas.ufl.edu/gillooly/files/19_belgrano_et_al_2002.pdf
Bernhard-Moreland-Bass Nat Phys 15 1113. https://www.nature.com/articles/s41567-019-0611-8
Bezrukov & Winterhalter 2000, PRL 85:202.
bioRxiv 2025.08.26.672407. https://www.biorxiv.org/content/10.1101/2025.08.26.672407v1.full
Bodduluri et al 2018, JCI 128:5374. https://lmi.bwh.harvard.edu/publications/airway-fractal-dimension-predicts-respiratory-morbidity-and-mortality-copd
Brockmann, Hufnagel & Geisel 2006, Nature 439:462. https://www.cis.upenn.edu/~mkearns/teaching/NetworkedLife/scaling.pdf
Burger et al 2019. https://doi.org/10.1093/jmammal/gyz043
Clarke & Johnston 1999, J Anim Ecol (via Glazier 2005). https://pdodds.w3.uvm.edu/teaching/courses/2009-08UVM-300/docs/others/2005/glazier2005a.pdf
Cook 1995 / Free 1996 via Grosu 2023. https://academic.oup.com/cercor/article/33/8/4574/6713293
Dathe et al 2001, Geoderma 103:99. https://www.sciencedirect.com/science/article/abs/pii/S0016706101000775
Dehghani et al 2010 (via He 2014). https://med.nyu.edu/research/he-lab/sites/default/files/pdf/scale-free-brain-activity-past-present-and-future.pdf

den Nijs / Nienhuis exact.

Drakare et al 2006, Ecology Letters. https://pure.qub.ac.uk/en/publications/the-imprint-of-the-geographical-evolutionary-and-ecological-conte

Drung et al (PTB), ASC preprint. https://www.ptb.de/cms/fileadmin/internet/fachabteilungen/abteilung_7/7.2_kryophysik_und_spektrometrie/7.21_kryosensoren/Drung_ASC10_Preprint.pdf

Eisler, Bartos & Kertesz 2008, Adv Phys. https://arxiv.org/abs/0708.2053

Elmegreen & Falgarone 1996, ApJ 471:816. https://ui.adsabs.harvard.edu/abs/1996ApJ...471..816E

F1000Research 12:87. https://f1000research.com/articles/12-87/v1

Falgarone, Phillips & Walker 1991, ApJ 378:186.

Fameli-Balzarini. https://arxiv.org/abs/cond-mat/0605620

Feder 1988, Fractals (Plenum).

Field-Witt-Nori-Ling PRL 74 1206. https://journals.aps.org/prl/abstract/10.1103/PhysRevLett.74.1206

Fontenele et al PRL 122 208101. https://link.aps.org/doi/10.1103/PhysRevLett.122.208101

Fraedrich & Blender PRL 90:108501; Comment arXiv:physics/0305080. https://arxiv.org/abs/physics/0305080

Frette et al Nature 379 49. https://www.nature.com/articles/379049a0

Frontiers Aging Neurosci 17:1540040. https://www.frontiersin.org/journals/aging-neuroscience/articles/10.3389/fnagi.2025.1540040/full

Gao, Peterson & Voytek 2017, NeuroImage 158:70.

Gonzalez, Hidalgo & Barabasi 2008, Nature 453:779. https://barabasi.com/media/pub_imports/files/250.pdf

Gonzalez-Martin & Vaughan 2012, A&A 544:A80. https://www.aanda.org/articles/aa/full_html/2012/04/aa18889-12/aa18889-12.html

Gopikrishnan et al 1999, PRE 60:5305. https://amaral.northwestern.edu/media/publication_pdfs/Gopikrishnan-1999-Phys.Rev.E-60-5305.pdf

Grosu et al 2023, Cerebral Cortex 33:4574 (review). https://academic.oup.com/cercor/article/33/8/4574/6713293

Gutenberg & Richter 1944, BSSA. https://doi.org/10.1785/BSSA0340040185

Hack 1957, USGS PP 294-B. https://doi.org/10.3133/pp294B

Hatton et al 2015, Science. https://doi.org/10.1126/science.aac6284

Hatton et al 2019, PNAS. https://api.semanticscholar.org/graph/v1/paper/DOI:10.1073/pnas.1900492116

He 2011, J Neurosci (via He 2014). https://med.nyu.edu/research/he-lab/sites/default/files/pdf/scale-free-brain-activity-past-present-and-future.pdf

He et al 2010, Neuron 66:353 (via He 2014 review). https://pubmed.ncbi.nlm.nih.gov/20471349/

Hjelmfelt 1988 via Tarboton ScD thesis 1989. https://agupubs.onlinelibrary.wiley.com/doi/abs/10.1029/WR024i008p01317

Jansen, Mashanova & Petrovskii, Science comment. https://www.nature.com/articles/srep04409

Jerde et al 2019, Frontiers in Physiology. https://www.frontiersin.org/articles/10.3389/fphys.2019.01166/full

Jetz et al 2004, Science. https://doi.org/10.1126/science.1102138

Kardar-Parisi-Zhang PRL 56 889. https://journals.aps.org/prl/abstract/10.1103/PhysRevLett.56.889

Koscielny-Bunde et al 1998, PRL 81:729.

Levitin, Chordia & Menon 2012, PNAS 109:3716. https://www.pnas.org/doi/10.1073/pnas.1113828109
Lewis & Rees 1985, Science 230:1163. https://www.science.org/doi/10.1126/science.4071040
Lieberman-Aiden et al Science 326:289. https://courses.cs.duke.edu/spring13/compsci662/pdf/lieberman-aiden.2009.pdf
Lin et al 1990, PRA 41:2005. https://journals.aps.org/pra/abstract/10.1103/PhysRevA.41.2005
Liu et al 2003 via Grosu 2023. https://academic.oup.com/cercor/article/33/8/4574/6713293
Lovejoy 1982, Science 216:185. https://www.science.org/doi/10.1126/science.216.4542.185
Ma et al Neuron 104:655. https://pmc.ncbi.nlm.nih.gov/articles/PMC6934140/
Majumdar & Prasad 1988 via Grosu 2023. https://academic.oup.com/cercor/article/33/8/4574/6713293
Majumdar et al 1999 and successors. https://pubmed.ncbi.nlm.nih.gov/10435535/
Mantegna & Stanley 1995, Nature 376:46. https://amaral.northwestern.edu/media/publication_pdfs/Gopikrishnan-1999-Phys.Rev.E-60-5305.pdf
Masters 2004, Annu Rev Biomed Eng 6:427. https://pubmed.ncbi.nlm.nih.gov/15255776/
Mattsson et al 1994 JMMM 136:23 via Sci Rep 9 (2019); err bar: Wertheim & Buchanan 1967 PR 161:478. https://www.sciencedirect.com/science/article/abs/pii/0304885394904405
Meakin 1983, PRA 27:1495.
Meneveau & Sreenivasan 1991, JFM 224:429.
Mota & Herculano-Houzel 2015, Science. https://doi.org/10.1126/science.aaa9101
Nastrom & Gage J Atmos Sci 42:950.
Niklas & Enquist 2001, PNAS (via Belgrano 2002). https://people.clas.ufl.edu/gillooly/files/19_belgrano_et_al_2002.pdf
Nitsch 2005, J Urban Econ. https://doi.org/10.1016/j.jue.2005.03.007
Ott & Mann JFM 422:207 via Eyink lecture notes. https://www.ams.jhu.edu/~eyink/Turbulence/notes/ChapterVb.pdf
Paxson & Floyd 1995, IEEE/ACM ToN 3:226.
Perez-Garcia et al 2020, Nature Physics. https://www.nature.com/articles/s41567-020-0978-6
Perri & Zimbardo 2009, ApJL 693:L118. https://iopscience.iop.org/article/10.1088/0004-637X/693/2/L118
Perri et al 2015, A&A 578. https://www.aanda.org/articles/aa/full_html/2015/06/aa25295-14/aa25295-14.html
Phillipson 1981 (via Glazier 2005). https://pdodds.w3.uvm.edu/teaching/courses/2009-08UVM-300/docs/others/2005/glazier2005a.pdf
Piantadosi 2014, Psychon Bull Rev. https://doi.org/10.3758/s13423-014-0585-6
PLOS ONE 13:e0199099. https://journals.plos.org/plosone/article?id=10.1371/journal.pone.0199099
Raichlen et al 2014, PNAS 111:728. https://www.pnas.org/doi/10.1073/pnas.1318616111
Ramos-Fernandez et al 2004, Behav Ecol Sociobiol. https://link.springer.com/article/10.1007/s00265-003-0700-6
Ramos-Fernandez et al Behav Ecol Sociobiol 55:223. https://link.springer.com/article/10.1007/s00265-003-0700-6
Reynolds 2014, Sci Rep 4:4409. https://www.nature.com/articles/srep04409
Reynolds et al 2007, Ecology 88.
Rhee et al 2011, IEEE/ACM ToN 19:630. https://ieeexplore.ieee.org/document/5750071/
Saleur & Duplantier, PRL 58:2325.

Scholarpedia 1/f compilation. http://www.scholarpedia.org/article/1/f_noise

Sengers-Shanks J Stat Phys 137 857. https://link.springer.com/content/pdf/10.1007/s10955-009-9840-z.pdf

Shen-Heinz arXiv:1507.01558. https://arxiv.org/abs/1507.01558

Shimizu et al via Frantsuzov review. https://cce.caltech.edu/documents/7753/rampubs_341.pdf

Sims et al 2019, eLife 8:e50316. https://elifesciences.org/articles/50316

Smeets et al 2008, PNAS 105:417.

Smirnov-Werner Math Res Lett 8. https://arxiv.org/abs/math/0109120

Speakman 2005, J Exp Biol. https://doi.org/10.1242/jeb.01556

Sylos Labini et al 1998, Phys Rep 293:61.

Tarboton et al 1988, WRR. https://agupubs.onlinelibrary.wiley.com/doi/abs/10.1029/WR024i008p01317

Tatsumi, Yamauchi & Kono 1989, Ann Bot 64:499.

Taylor 1961, Nature. https://doi.org/10.1038/189732a0

Verveen & Derksen 1968, Proc IEEE 56:906.

Voss & Clarke 1978, JASA 63:258.

Voytek et al 2015, J Neurosci 35:13257.

Wang et al 2019, Communications Biology. https://www.nature.com/articles/s42003-019-0421-7

Wellstood, Urbina & Clarke 1987, APL 50:772. https://pubs.aip.org/aip/apl/article/50/12/772/52092

Yan et al 2012, PRB 85 (arXiv:1201.5665); Bylander 2011, Nat Phys 7:565. https://www.nature.com/articles/nphys1994

Yang PR 85 808. https://link.aps.org/doi/10.1103/PhysRev.85.808

Zhang & Sejnowski 2000, PNAS. https://pdodds.w3.uvm.edu/files/papers/others/2000/zhang2000a.pdf